

Université du Québec  
**Institut National de la Recherche Scientifique**  
Énergie Matériaux Télécommunications

## **Reconfigurable Antennas using Frequency Selective Surfaces**

By

**Jinxin Li**

A dissertation submitted in partial fulfillment of the requirements for the degree of  
Doctor of Philosophy (Ph. D.) in Telecommunications

### **Jury d'évaluation**

External examiner	Prof. Cevdet Akyel École Polytechnique de Montréal
External examiner	Prof. Chan-Wang Park Université de Québec à Rimouski (UQAR)
Internal examiner	Prof. Serioja O. Tatu INRS-EMT
Research Director	Prof. Tayeb A. Denidni INRS-EMT
Research co-director	Prof. Qingsheng Zeng Nanjing University of Aeronautics and Astronautics



## **ACKNOWLEDGEMENT**

First and foremost, I would like to express my sincere and profound gratitude to my supervisor Prof. Tayeb A. Denidni for his support, help and continuous encouragement throughout my PhD period. I really appreciate his continual guidance, profound insights and helpful suggestions on my research, which have been very important factor for the completion of my work.

I would like to pass my sincere thanks to my co-supervisor Dr. Qingsheng Zeng for his help and useful advices during my research endeavour.

I also gratefully thank all technical colleagues at Institute National de la Recherche Scientifique—Énergie, Matériaux et Télécommunications (INRS-EMT) and Poly-Grames Research Center for their generous help with the fabrication of my antenna prototypes. Special thanks go to my colleagues Arun Kesavan, Javad Pourahmadazar, Abdolmehdi Dadgarpour, Behnam Zarghooni, Zhenjiang Zhao and Mohamad Mantash.

The most and for most, my biggest and deepest appreciations go to my mother and my father for their encouragement, understanding and all their continuous unforgettable support during whole of my study, which gave me all the strength needed to successfully finish my PhD career.

Last but not the least, I would like to thank my boyfriend for his kind care, patience, encouragement and support through the period of time.

Finally special thanks to those who helped me in developing this thesis.



## ABSTRACT

Nowadays, because of the requirements of miniaturization and multifunction in the modern communication systems, more and more electronic devices are integrated into a single platform. By using this method, the communication quality can be improved significantly. However, another serious problem of interference has been introduced. As a solution for resolving this issue to enhance the performance of communication systems, radiation pattern reconfigurable antennas have received much attention. The conventional methods for designing radiation pattern reconfigurable antennas based on the phased antenna arrays incur large loss, and are complicated and expensive to be applied in practice. For this issues, frequency selective surfaces (FSSs) work as space filters to electromagnetic (EM) waves, which can be either transmitted or reflected in the operating frequency band. Therefore, radiation pattern reconfigurable antennas are realized by using frequency selective surface (FSS) in this thesis. This approach offers more antenna functionality, less cost and a significant save in terms of size and space. Thus, research in this field is very important and is one of the most popular fields nowadays.

In this dissertation, first and foremost, a novel dual-band beam-sweeping antenna based on two independent cylindrical active frequency selective surfaces (AFSS) have been proposed. As the AFSS unit cell characteristic is the primary influential parameter that affects the sweeping radiation pattern functionality. Hence, two AFSS unit-cells with integrated pin-diodes have been proposed at two different frequency bands, 2.45 GHz and 5.2 GHz. When a dual-band omnidirectional monopole antenna is surrounded by two cylindrical AFSS screens, the proposed design has shown that it can effectively realize beam-sweeping which covers all azimuth angles at 2.45 GHz and 5.2 GHz simultaneously. The size of antenna system can be reduced greatly in comparison with the case where the two cylindrical FSS screens work independently from each other when they are loaded in the same antenna system.

Secondly, a beam-switching antenna with high gain and flexible control of beam numbers has been proposed based on FSS. The proposed antenna is composed of an omnidirectional monopole antenna as a radiating source surrounded by a hexagon FSS screen and six metallic sheets. By changing the states of the pin-diodes in the hexagon FSS screen, the proposed antenna can not only sweep the beam six directions with gain enhancement in the azimuth plane, but also it can flexibly operates at multiple beam modes at 5.2 GHz.

Then, a beam-tilting antenna with negative refractive index metamaterial (NRIM) loading has also been designed. The proposed antenna is composed of a double-feed dielectric resonator antenna (DRA) and  $1 \times 4$  NRIM array, which is fixed over and in the middle of the DRA. This beam-tilting antenna can steer the main beam by  $\pm 38^\circ$  in the xoz-plane over 5 to 5.5 GHz band. The reflection coefficient of the antenna is better than -10 dB in the band from 5 to 5.5 GHz.

In the final design, a three layers quasi-yagi antenna has been designed with multi- beam directions in both elevation and azimuth plane at 5.2 GHz. There are four elements of quasi-Yagi antenna and eight pin-diodes as switches inserted them in the middle layer. The top and bottom layers include the parasitic elements each of which are inserted into pin-diodes. By controlling the pin-diodes in the different layers, the antenna can realize beam switching in the azimuth plane in four directions and beam tilting in the elevation plane.

# TABLE OF CONTENTS

<b>1</b>	<b>INTRODUCTION.....</b>	<b>1</b>
1.1	BACKGROUND AND MOTIVATION.....	1
1.2	RESEARCH STATUS OF RADIATION PATTERN RECONFIGURABLE ANTENNA.....	3
1.2.1	<i>Mechanical controlling method .....</i>	3
1.2.2	<i>Electrical controlling method .....</i>	4
1.2.3	<i>Optical controlling method .....</i>	7
1.2.4	<i>Changing the material properties method .....</i>	8
1.2.5	<i>Using metamaterial method.....</i>	9
1.3	RESEARCH OBJECTIVES.....	12
1.4	ORGANIZATION OF THE THESIS .....	12
1.5	LIST OF PUBLICATIONS.....	15
<b>2</b>	<b>FREQUENCY SELECTIVE SURFACES.....</b>	<b>17</b>
2.1	APPLICATIONS OF FREQUENCY SELECTIVE SURFACES.....	18
2.2	DESIGN PARAMETERS FOR FREQUENCY SELECTIVE SURFACES .....	19
2.3	RESEARCH STATES OF ACTIVE FREQUENCY SELECTIVE SURFACES .....	20
2.4	INTRODUCTION OF THEORETICAL ANALYSIS METHODS OF FSS.....	22
<b>3</b>	<b>DESIGN OF A DUAL-BAND BEAM SWEEPING ANTENNA USING ACTIVE SURFACE SELECTIVE SURFACES .....</b>	<b>23</b>
3.1	INTRODUCTION .....	23
3.2	ACTIVE FRQUENCY SELECTIVE SURFACES UNIT CELL DESIGN .....	24
3.3	DESIGN AND OPERATION MECHANISM .....	26
3.3.1	<i>Dual-band radiating source design .....</i>	27
3.3.2	<i>Mechanism of the proposed beam-sweeping antenna.....</i>	28
3.4	PARAMETERIC STUDIES AND DISCUSSIONS.....	29
3.5	FABRICATION AND MEASUREMENT RESULTS .....	32
3.6	CONCLUSION .....	42
<b>4</b>	<b>HIGH GAIN WITH FLEXIABLE BEAM NUMBERS ANTENNA DESIGN .....</b>	<b>43</b>
4.1	INTRODUCTION .....	43
4.2	FSS UNIT CELL DESIGN .....	44
4.3	BEAM-SWITCHING ANTENNA DESIGN WITH HIGH GAIN .....	46
4.3.1	<i>The excitation source .....</i>	47
4.3.2	<i>Mechanism of the beam-switching antenna with gain enhancement .....</i>	49

4.4	PARAMETRIC STUDIES.....	50
4.5	FABRICATION AND MEASUREMENT RESULTS .....	54
4.6	CONCLUSION .....	62
<b>5</b>	<b>BEAM-TILTING ANTENNA WITH METAMATERIAL LOADING DESIGN .....</b>	<b>64</b>
5.1	INTRODUCTION .....	64
5.2	BEAM TILTING ANTENNA DESIGN.....	65
5.2.1	<i>NRIM Unit-cell design</i> .....	65
5.2.2	<i>Double-feed dielectric resonator antenna</i> .....	66
5.2.3	<i>The DRA with NRIM Loading</i> .....	67
5.2.4	<i>Beam-tilting Antenna Theory Analysis</i> .....	69
5.3	EXPERIMENTAL RESULTS.....	70
5.4	CONCLUSION .....	73
<b>6</b>	<b>PATTERN-RECONFIGURABLE ANTENNA FOR ELEVATION AND AZIMUTH PLANES..</b>	<b>74</b>
6.1	INTRODUCTION .....	74
6.2	ANTENNA DESIGN AND CONFIGURATION .....	74
6.3	EXPERIMENTAL RESULTS AND DISCUSSION.....	76
6.4	CONCLUSION .....	79
<b>7</b>	<b>CONCLUSION AND FUTURE WORK.....</b>	<b>80</b>
7.1	CONCLUSION .....	80
7.2	FUTURE WORKS .....	81
<b>8</b>	<b>RÉSUMÉ .....</b>	<b>83</b>
8.1	CONTEXTE ET MOTIVATION .....	83
8.2	ANTENNE RECONFIGURABLE EN DIAGRAMME DE RAYONNEMENT .....	85
8.2.1	<i>Méthode de contrôle mécanique</i> .....	85
8.2.2	<i>Méthode de contrôle électrique</i> .....	86
8.2.3	<i>Méthode de contrôle optique</i> .....	90
8.2.4	<i>Changer les propriétés de la méthode matérielle</i> .....	91
8.2.5	<i>Utilisation des métamatériaux</i> .....	92
8.3	SURFACES SELECTIVES EN FREQUENCE .....	97
8.4	APPLICATIONS DES SURFACES SELECTIVES EN FREQUENCE .....	98
8.5	LES OBJECTIFS DE RECHERCHE .....	100
8.6	ORGANISATION DE LA THESE .....	100
8.7	TRAVAUX FUTURS .....	102
<b>9</b>	<b>REFERENCES.....</b>	<b>105</b>

## LIST OF TABLES

TABLE 1.1	COMPARISON OF DIFFERENT RECONFIGURABLE APPROACHES .....	11
TABLE 3.1	FINAL DIMENSIONS OF TWO AFSS UNIT CELLS(UNIT:MM).....	24
TABLE 4.1	FINAL DIMENSIONS OF FSS UNIT CELL (UNIT:MM).....	46
TABLE 4.2	THE SIMULATED AND MEASURED GAIN OF DIFFERENT MODES.....	62
TABLE 5.1	THE EFFECT OF DIFFERENT NRIM LAYERS ON THE ANTENNA PERFORMANCE .....	69
TABLE 6.1	PEAK GAIN OF PROPOSED ANTENNA IN DIFFERENT MODES OF STATE 1 .....	79
TABLEAU 8.1	COMPARAISON DE DIFFERENTES APPROCHES RECONFIGURABLES.....	96



# LIST OF FIGURES

FIGURE 1.1	MECHANICALLY PATTERN RECONFIGURABLE ANTENNA USING METASURFACES [26].....	3
FIGURE 1.2	A COMPACT BEAM-STEERABLE LENS ANTENNA [27].....	4
FIGURE 1.3	A COMPACT PLANAR PATTERN-RECONFIGURABLE [29]. .....	5
FIGURE 1.4	A BEAM-STEERABLE PLANAR ANTENNA USING CIRCULAR DISC AND FOUR PIN-CONTROLLED TAPERED STUBS [31]. .....	5
FIGURE 1.5	RADIATION PATTERN RECONFIGURABLE SQUARE SPIRAL MICROSTRIP ANTENNAS WITH RF MEMS SWITCHES [36].....	6
FIGURE 1.6	A RADIATION PATTERN RECONFIGURABLE SCAN-BEAM SPIRAL ANTENNA [37]. .....	6
FIGURE 1.7	A RADIATION PATTERN RECONFIGURABLE ANTENNA WITH VARACTOR DIODE [42]. .....	7
FIGURE 1.8	PHOTOGRAPH OF FREQUENCY AND BEAM RECONFIGURABLE ANTENNA USING PHOTOCONDUCTING SWITCHES [47]. .....	8
FIGURE 1.9	BASIC GEOMETRY OF THE SCAN ANTENNA BASED ON FERROELECTRIC SUBSTRATE [52]. .....	8
FIGURE 1.10	A BEAM SWITCHING ANTENNA BASED ON ELECTROMAGNETIC BANDGAP (EBG) [58]. .....	10
FIGURE 1.11	A PATTERN RECONFIGURABLE ANTENNA USING A HIGH-IMPEDANCE SURFACE (HIS) [63]. .....	10
FIGURE 1.12	A PATTERN RECONFIGURABLE ANTENNA BASED ON FREQUENCY SELECTIVE SURFACE (FSS) [69]. .....	10
FIGURE 1.13	A RADIATION PATTERN STEERABLE ANTENNAS BASED ON AFSS [73], (A) ANTENNA STRUCTURE AND INSTALLATION. (B) RADIATION PATTERNS OF SINGLE-BEAM MODES AND DUAL-BEAM MODES. ....	11
FIGURE 2.1	THE BASIC STRUCTURES AND THEIR FREQUENCY RESPONSE. ....	17
FIGURE 2.2	THE TYPICAL FSSs ELEMENTS[7]. .....	18
FIGURE 2.3	SCHEMATIC DIAGRAM OF RADOME. ....	19
FIGURE 2.4	A SCHEMATIC DIAGRAM OF FSS AS SUB-REFLECTOR IN ANTENNA SYSTEMS. ....	19
FIGURE 2.5	INTEGRATED MEMS SWITCHES TUNABAL FSS STRUCTURE[81]. .....	21
FIGURE 2.6	TUNABAL FSS STRUCTURE USING (A) PIN-DIODES AND (B) VARACTOR DIODES[82]. .....	22
FIGURE 3.1	GEOMETRY OF AFSS UNIT-CELLS: (A) 2.45 GHz AFSS UNIT-CELL, (B) 5.2 GHz AFSS UNIT-CELL....	24
FIGURE 3.2	SIMULATED TRANSMISSION COEFFICIENTS OF THE AFSS UNIT-CELLS: (A) 2.45 GHz AFSS UNIT-CELL, (B) 5.2 GHz AFSS UNIT-CELL.....	26
FIGURE 3.3	PROPOSED DUAL-BAND BEAM-SWEEPING ANTENNA STRUCTURE: (A) TOP VIEW, (B) SIDE VIEW.....	27
FIGURE 3.4	(A) GEOMETRY OF THE DUAL-BAND ANTENNA, (B) MEASURED RADIATION PATTERNS OF MONOPOLE ANTENNA. ....	28
FIGURE 3.5	SIMULATED AND MEASURED REFLECTION COEFFICIENTS RESULTS OF MONOPOLE ANTENNA. ....	28
FIGURE 3.6	THE EFFECT OF THE W1 ON THE TRANSMISSION COEFFICIENTS OF THE 2.45 GHz AFSS UNIT-CELL: (A) PIN-DIODE ON, (B) PIN-DIODE OFF.....	30
FIGURE 3.7	THE EFFECT OF THE W3 ON THE TRANSMISSION COEFFICIENTS OF THE 5.2 GHz AFSS UNIT-CELL: (A) PIN-DIODE ON, (B) PIN-DIODE OFF.....	31
FIGURE 3.8	SIMULATED GAIN OF PROPOSED BEAM-SWEEPING ANTENNA. ....	32

FIGURE 3.9	PHOTOGRAPH OF THE FABRICATED ANTENNA PROTOTYPE IN ANECHOIC CHAMBER.....	33
FIGURE 3.10	OPERATION METHODS: (A) CASE I, (B) CASE II, (C) AND (D) CASE III.....	34
FIGURE 3.11	MEASURED RADIATION PATTERNS RESULTS IN THE AZIMUTH PLANE OF CASE I: (A) AND (B) 2.45 GHz, (C) 5.2 GHz.....	36
FIGURE 3.12	MEASURED RADIATION PATTERN RESULTS IN THE AZIMUTH PLANE OF CASE II: (A) AND (B) 5.2 GHz, (C) 2.45 GHz .....	38
FIGURE 3.13	MEASURED RADIATION PATTERNS OF CASE III: (A) 1-2-6 AND 8-7-12 PIN-DIODES ON AT 2.45 GHz AND 5.2 GHz, (B) 1-2-3 AND 8-9-10 PIN-DIODES ON AT 2.45 GHz AND 5.2 GHz.....	39
FIGURE 3.14	SIMULATED RESULTS OF RADIATION PATTERNS IN THE AZIMUTH PLANE: (A) 2.45 GHz. (B) 5.2 GHz.. .....	41
FIGURE 3.15	MEASURED AND SIMULATED REFLECTION COEFFICIENTS IN CASE III.....	42
FIGURE 4.1	(A) GEOMETRY OF FSS UNIT-CELL. (B) CONFIGURATION OF FSS UNIT-CELL SIMULATION. (C) E-FIELD DISTRIBUTION AT 2.5 GHz. (D) E-FIELD DISTRIBUTION AT 4.8 GHz. (E) E-FIELD DISTRIBUTION AT 5.2 GHz. (F) E-FIELD DISTRIBUTION AT 5.8 GHz. ....	45
FIGURE 4.2	SIMULATED TRANSMISSION COEFFICIENTS OF FSS UNIT-CELL IN DIFFERENT PIN-DIODE STATES.....	46
FIGURE 4.3	PROPOSED BEAM-SWITCHING WITH HIGH GAIN ANTENNA STRUCTURE: (A) TOP VIEW, (B) SIDE VIEW .	47
FIGURE 4.4	STRUCTURE OF THE MONOPOLE ANTENNA.....	48
FIGURE 4.5	SIMULATION RESULTS OF THE MONOPOLE ANTENNA: (A) REFLECTION COEFFICIENT. (B) NORMALIZED RADIATION PATTERN AT 5.2 GHz. ....	48
FIGURE 4.6	SIMULATION RESULTS OF THE MONOPOLE ANTENNA: (A) REFLECTION COEFFICIENT. (B) NORMALIZED RADIATION PATTERN AT 5.2 GHz. ....	49
FIGURE 4.7	E-FIELD DISTRIBUTION OF THE ANTENNA AT 5.2 GHz: (A) SINGLE-BEAM MODE. (B) TWO-BEAM MODE. (C) THREE-BEAM MODE.....	50
FIGURE 4.8	THE EFFECT OF $D1$ ON THE PROPOSED ANTENNA PERFORMANCES: (A) REFLECTION COEFFICIENTS. (B) GAIN. ....	51
FIGURE 4.9	THE EFFECT OF $D2$ ON THE PROPOSED ANTENNA PERFORMANCES: (A) REFLECTION COEFFICIENTS. (B) GAIN. ....	52
FIGURE 4.10	THE EFFECT OF $B$ ON THE RADIATION PATTERNS OF PROPOSED ANTENNA. ....	53
FIGURE 4.11	THE EFFECT OF $H$ ON THE RADIATION PATTERNS OF PROPOSED ANTENNA. ....	53
FIGURE 4.12	SIMULATED RADIATION PATTERNS OF ANTENNA WITH AND WITHOUT METALLIC SHEETS IN THE AZIMUTH PLANE AT 5.2 GHz.....	54
FIGURE 4.13	PHOTOGRAPH OF THE FABRICATED ANTENNA IN ANECHOIC CHAMBER. ....	55
FIGURE 4.14	MEASURED REFLECTION COEFFICIENT RESULTS OF PROPOSED ANTENNA IN DIFFERENT MODES. ....	56
FIGURE 4.15	FIG.15 MEASURED RADIATION PATTERNS OF A SINGLE-BEAM MODE AT 5.2 GHz: (A), (B) AND (C) IN AZIMUTH PLANE, (D) IN ELEVATION PLANE. ....	58
FIGURE 4.16	SIMULATED AND MEASURED RADIATION PATTERNS OF SINGLE-BEAM MODE WHEN COLUMN 4 OFF AT 5.2 GHz IN AZIMUTH PLANE. ....	60

FIGURE 4.17	SIMULATED AND MEASURED RADIATION PATTERNS OF TWO-BEAM MODE AT 5.2 GHz IN AZIMUTH PLANE: (A) COLUMNS 3 AND 6 OFF. (B) COLUMNS 1 AND 3 OFF. (3) COLUMNS 1 AND 4 OFF.....	61
FIGURE 4.18	SIMULATED AND MEASURED RADIATION PATTERNS OF THREE-BEAM MODE AT 5.2 GHz IN AZIMUTH PLANE WHEN COLUMN 1, 3 AND 5 OFF.....	62
FIGURE 5.1	(A) PROTOTYPE OF PROPOSED NEGATIVE REFRACTIVE INDEX METAMATERIAL (NRIM) UNIT-CELL, AND (B) S-PARAMETERS OF THE PROPOSED NRIM UNIT-CELL.....	66
FIGURE 5.2	(A) REFRACTIVE-INDEX OF PROPOSED THE NRIM UNIT-CELL AS A FUNCTION OF FREQUENCY, AND (B) EXTRACTED PERMITTIVITY AND PERMEABILITY OF THE NRIM UNIT-CELL.....	66
FIGURE 5.3	(A) GEOMETRY OF THE PROPOSED DOUBLE-FEED DRA, AND (B) ITS NORMALIZED RADIATION PATTERN IN THE XOZ-PLANE.....	67
FIGURE 5.4	3D CONFIGURATION OF DOUBLE-FEED DRA WITH $1 \times 4$ PROPOSED NRIM ARRAY LOADING. (A) FRONT VIEW, AND (B) SIDE VIEW. (UNIT: MM). .....	67
FIGURE 5.5	RADIATION PATTERN OF DRA WITH AND WITHOUT NRIM LAYERS LOADING EXCITED BY PORT 1 AT 5.2 GHz. ....	68
FIGURE 5.6	ELECTRIC FIELD DISTRIBUTION IN THE XOZ-PLANE WHEN PORT 1 EXCITED AT 5.2 GHz. ....	69
FIGURE 5.7	PROPOSED BEAM-TILTING ANTENNA FABRICATED AND ASSEMBLED, (A) SIDE VIEW, AND (B) TOP VIEW.. ....	70
FIGURE 5.8	MEASURED REFLECTION COEFFICIENT OF PROPOSED ANTENNA IN DIFFERENT STATES. ....	71
FIGURE 5.9	MEASURED RADIATION PATTERN WITH DIFFERENT INPUT EXCITED AT 5.2 GHz, (A) WITH AND WITHOUT NRIM LOADING IN XOZ-PLANE, AND (B) WITH AND WITHOUT NRIM LOADING IN YOZ-PLANE. ....	71
FIGURE 5.10	MEASURED AND SIMULATED RADIATION PATTERN OF THE PROPOSED ANTENNA WITH DIFFERENT INPUT PORT EXCITED AT: (A) 5.1 GHz, (B) 5.2 GHz, AND (C) 5.3 GHz.....	72
FIGURE 5.11	SIMULATED AND MEASURED GAIN OF THE ANTENNA WITHOUT AND WITH NRIM STRUCTURES. ....	73
FIGURE 6.1	GEOMETRY OF PROPOSED ANTENNA. (A) TOP VIEW. (B) BOTTOM VIEW AND (C) SIDE VIEW.....	75
FIGURE 6.2	PHOTOGRAPH OF FABRICATED ANTENNA.....	77
FIGURE 6.3	MEASURED AND SIMULATED S11 OF PROPOSED ANTENNA IN STATE 1 UP MODE.....	77
FIGURE 6.4	MEASURED NORMALIZED RADIATION PATTERNS AT 5.2 GHz IN DIFFERENT STATES. (A) AZIMUTH PLANE. (B) ELEVATION PLANE. ....	78
FIGURE 6.5	SIMULATED 3D RADIATION PATTERNS OF STATE 1 DOWN MODE AND STATE 2 UP MODE AT 5.2 GHz... 79	79
FIGURE 8.1	ANTENNE RECONFIGURABLE A STRUCTURE MECANIQUE UTILISANT LA METASURFACE [26]. ....	87
FIGURE 8.2	UNE ANTENNE DE LENTILLE ORIENTABLE A FAISCEAU COMPACT [27].....	87
FIGURE 8.3	UN MODELE PLAN COMPACT-RECONFIGURABLE [29]. ....	87
FIGURE 8.4	ANTENNE PLANAIRE ORIENTABLE PAR FAISCEAU UTILISANT UN DISQUE CIRCULAIRE ET DES STUBS EFFILES CONTROLES PAR QUATRE BROCHES [31]. ....	88
FIGURE 8.5	ANTENNES MICRORUBAN SPIRALES RECONFIGURABLES A MOTIF DE RAYONNEMENT AVEC COMMUTATEURS RF MEMS [36]. ....	89

FIGURE 8.6 UN DIAGRAMME DE RAYONNEMENT RECONFIGURABLE ANTENNE A SPIRALE DE FAISCEAU DE BALAYAGE [37].....	89
FIGURE 8.7 ANTENNE RECONFIGURABLE A DIAGRAMME DE RAYONNEMENT AVEC DIODE VARACTOR [42]. .....	90
FIGURE 8.8 PHOTOGRAPHIE DE L'ANTENNE RECONFIGURABLE EN FREQUENCE ET EN DIAGRAMMES DE RAYONNEMENT A L'AIDE DE COMMUTATEURS PHOTOCONDUCTEURS [47]. .....	92
FIGURE 8.9 GEOMETRIE DE BASE DE L'ANTENNE DE BALAYAGE A BASE DE SUBSTRAT FERROELECTRIQUE [52].....	92
FIGURE 8.10 ANTENNE DE FAISCEAU COMMUTABLE BASEE SUR LA BANDE INTERDITE ELECTROMAGNETIQUE (EBG) [58]. .....	93
FIGURE 8.11 ANTENNE RECONFIGURABLE EN DIAGRAMME DE RAYONNEMENT UTILISANT UNE SURFACE A HAUTE IMPEDANCE (HIS) [63].....	94
FIGURE 8.12 UNE ANTENNE RECONFIGURABLE EN DIAGRAMME DE RAYONNEMENT BASEE SUR LA SURFACE SELECTIVE DE FREQUENCE (FSS) [69].....	94
FIGURE 8.13 ANTENNES ORIENTABLES A DIAGRAMME DE RAYONNEMENT BASE SUR L'AFSS [73], (A) STRUCTURE DE L'ANTENNE ET INSTALLATION. (B) SCHEMAS DE RAYONNEMENT DES MODES A FAISCEAU UNIQUE ET DES MODES A DOUBLE FAISCEAU. ....	95
FIGURE 8.14 LES STRUCTURES DE BASE ET LEUR REPONSE EN FREQUENCE.....	97
FIGURE 8.15 LES ELEMENTS TYPIQUES DES FSSs.....	98
FIGURE 8.16 SCHEMA DE PRINCIPE DU RADOME.....	99
FIGURE 8.17 DIAGRAMME SCHEMATIQUE DU FSS EN TANT QUE SOUS-REFLECTEUR DANS LES SYSTEMES D'ANTENNES.....	99

# **1 INTRODUCTION**

## **1.1 Background and motivation**

Wireless communication systems have become one of the fastest growing areas. The new generation of mobile communications, wireless LAN, satellite positioning system, a variety of military and civil radars have become more and more important in our daily live. As one of the most important elements in wireless communication systems, the operating characteristics of an antenna directly affect system performances [1-2]. The rapid development of modern wireless communication systems has put forward higher requirements such as multifunction, high-capacity and ultra-wideband, which directly leads to an increasing number of subsystems on the same platform while the number of antennas is also correspondingly increased. As a result, there are several problems arise such as large volume, high costs and electromagnetic compatibility. As it has become more and more difficult to meet these requirements using traditional antennas whose performances are fixed in many applications, a variety of new antennas are being gradually developed. A reconfigurable antenna is one of these antennas, which not only meets the development requirements of wireless communications, but also have simple structures and small sizes [3-4].

A reconfigurable antenna is referred to any radiation structure which is controlled by means of electrical, light, mechanical approaches to change one or some of its fundamental operating characteristics. The key principle in designing reconfigurable antennas is based on the theory of conventional antennas. Their desired radiation characteristics are shifted by adjusting the radiator structure, controlling the current distribution, or changing the electrical parameters of the antenna [5]. Reconfigurable antennas are able to independently tune their operating frequency, bandwidth, polarization, and radiation-pattern to accommodate changing operation requirements [6].

According to the reconstruction performance, reconfigurable antennas can be classified into frequency reconfigurable antennas, polarized reconfigurable antennas, radiation pattern reconfigurable antennas, and multi-performance reconfigurable antennas [7]. The frequency reconfigurable antennas have ability to tune the working frequency band, which can filter out the interfering signals, or tune the antenna to account for the new environments [8-11]. For the

polarized reconfigurable antennas, polarization of the antenna can be reconfigured to separate desired signals and filter the unwanted signals [12-14]. In addition, the radiation pattern reconfiguration antennas can change the direction of main beam to send EM signals to the desired direction effectively [15-16]. These antennas can significantly decrease interfering signals and improve the system capacity. Multi-performance reconfigurable antennas are two or three kinds of antennas with variable performance, such as frequency and radiation pattern reconfigurable antennas, frequency and polarization reconfigurable antennas, radiation pattern and polarization reconfigurable antennas [17-19]. In this thesis, our main research is focused on designing new radiation pattern reconfigurable antennas.

Radiation-pattern reconfigurable antennas can bring several improvements and enhancements for modern wireless communication systems. Firstly, using the radiation pattern reconfigurable antenna, aligning the main radiation direction of the antenna with the useful signal direction can increase signal-to-noise ratio, improve system performance and reduce power consumption [7]. Secondly, as multi-input multi-output (MIMO) technology has able to increase capacity of system, it mostly will be used in 5G communication systems. MIMO systems need to integrate multiple antennas in a limited space, hence, it requires a weak coupling between antenna elements. Radiation-pattern reconfigurable antennas can effectively reduce the mutual coupling between elements in MIMO systems [20-21]. Thirdly, to fulfill the requirements of miniaturization and multifunction in modern communication systems, more and more electronic devices are integrated into a single platform. Although this method can significantly improve the communication quality, it can also lead to serious problems of interference. Radiation pattern reconfigurable antennas can reduce the interference coming from undesired radiation to enhance the communication performance [22].

In summary, radiation pattern reconfigurable antennas can reduce the size, cost and design complexity of a wireless communication system, which greatly improves the overall performance of a wireless communication system. The outstanding advantages of these antennas for wireless modern communication systems have motivated us to establish a comprehensive research in this field. Therefore, this project aims to design, analyze, and prototype novel dual-band radiation-pattern reconfigurable antennas for wireless modern communication systems.

## 1.2 Research status of radiation pattern reconfigurable antenna

In recent years, more and more researchers have focused their interests on radiation-pattern reconfigurable antennas. One of the most traditional methods to design radiation pattern reconfigurable antennas is to use phased arrays [23-24], in which to control the radiation pattern of antenna is realized by changing the phase of the phase shifter. However, the complex feeding network of phased antenna array leads to the problems of high costs and complex design processes. Compared to phased antenna arrays, radiation pattern reconfigurable antennas have a simple structure and a relatively easy design process has attracted researchers' significant interest. According to the different implementation methods, radiation pattern reconfigurable antennas can be classified into mechanical controlling method, electrical controlling method, optical controlling method, changing the material property method or using metamaterial method.

### 1.2.1 Mechanical controlling method

Mechanical steering is achieved by repositioning and moving the antenna to reach the intended characteristics. However, the applications of the mechanical approach are limited by its low speed and complex system installation [25-27]. In [26], Hai Liang Zhu et al. have proposed a radiation pattern reconfigurable antenna that is composed of a planar semi-circular metasurface placed directly at the top of a planar circular patch antenna, shown in Fig. 1.1. By rotating the metasurface around the centre of the patch antenna, the antenna beam can be continuously steered. The main-beam direction of the antenna steered to an angle of  $32^\circ$  from the boresight direction. In [27], Jorge R. Costa et al. have designed a steerable beam antenna composed of a dielectric lens that pivots in front of a single stationary moderate gain feed, shown in Fig. 1.2. This antenna can steer the main beam in the elevation and full azimuth plane mechanically.

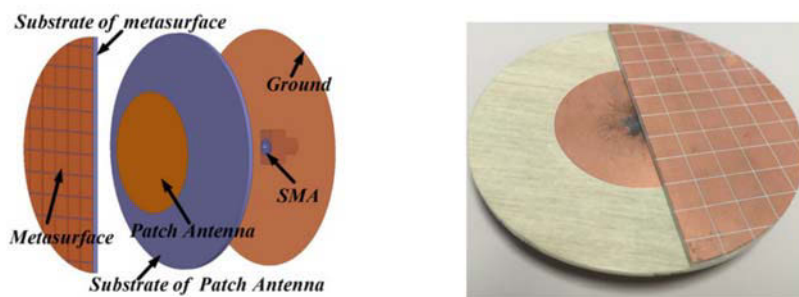


Figure 1.1 Mechanically pattern reconfigurable antenna using metasurfaces [26].



**Figure 1.2      A compact beam-steerable lens antenna [27].**

### 1.2.2 Electrical controlling method

Electrical controlling methods to design reconfigurable antennas uses RF switching components and variable reactance devices. RF switches can be used to connect / disconnect a part of the antenna structure or change the distribution of current to achieve different performances of antennas. Microwave switching components mainly include pin-diodes and radio frequency micro-electromechanical systems (RF-MEMS) switches. For variable reactance devices, they are mainly varactor diodes. In the literature, many radiation pattern reconfigurable antennas are controlled by pin-diodes [28-34]. Pin-diodes have small insertion loss, fast switching speed and low DC bias voltage. They can control large current microwave signal conduction and cut off. In [29], Tamer Aboufoul et al. have proposed a compact planar pattern reconfigurable by incorporation of four pin-diode switches and two parasitic elements, as shown in Fig.1.3. The radiation patterns of this antenna could be changed from a nearly omnidirectional into two opposite end-fire patterns. In [31], M. S. Alam et al. have designed a planar beam-steerable antenna, which includes a central circular disc surrounded by four PIN-controlled tapered microstrip stubs, as shown in Fig.1.4. Using Pin-diodes, the stubs change their status from grounded to open-ended mode to provide pattern reconfigurability in four directions.

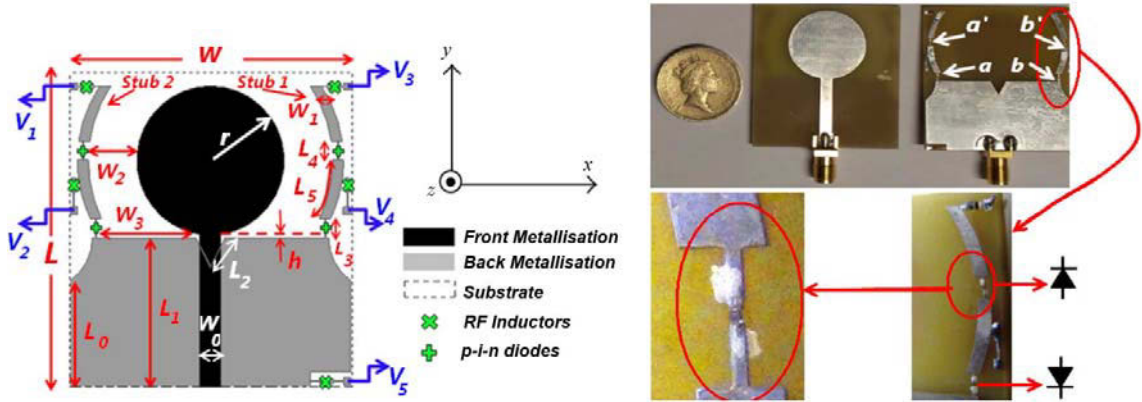


**Figure 1.3** A compact planar pattern-reconfigurable [29].

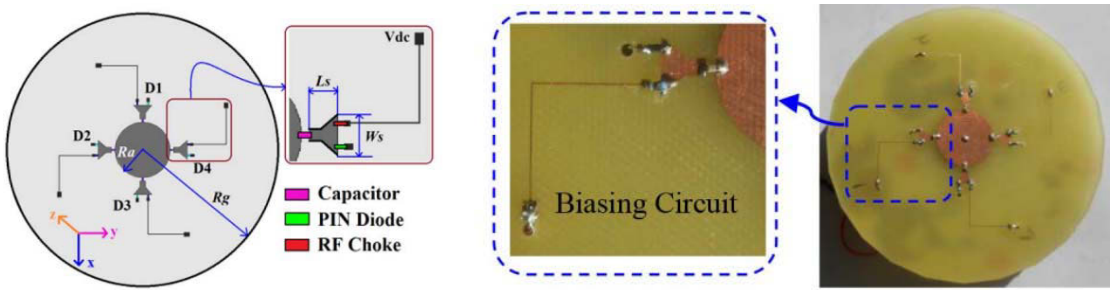


**Figure 1.4** A Beam-Steerable Planar Antenna Using Circular Disc and Four PIN-Controlled Tapered Stubs [31].

RF-MEMS switches are a new type of RF devices. As early as 1998, E. R. Brown proposed the use of RF-MEMS switches to design a reconfigurable antenna [35]. More and more studies have been reported in [36-41]. One of the major advantages of RF-MEMS switches is their good isolation and low-loss property. They can be used at microwave frequencies with good linearity. However, a disadvantage of MEMS switches is their slower response compared to pin-diodes, and the bias voltage is higher than pin-diodes [20]. In [36], Greg H. Huff et al. have designed a radiation pattern reconfigurable microstrip antenna with microelectromechanical system (MEMS) switches. Two MEMS switches are used to reconfigure the radiation patterns of a resonant square spiral microstrip antenna between endfire and broadside modes over a common impedance bandwidth. The designed and fabricated antennas are shown in Fig.1.5. The antenna shown in Fig. 1.6 is a reconfigurable rectangular spiral antenna with a set of RF-MEMS switches, which is fed through a coaxial cable at its center point. The structure consists of five sections that

are connected with four RF-MEMS switches. Based on the status of the integrated RF-MEMS, the antenna can change its radiation beam direction [37].

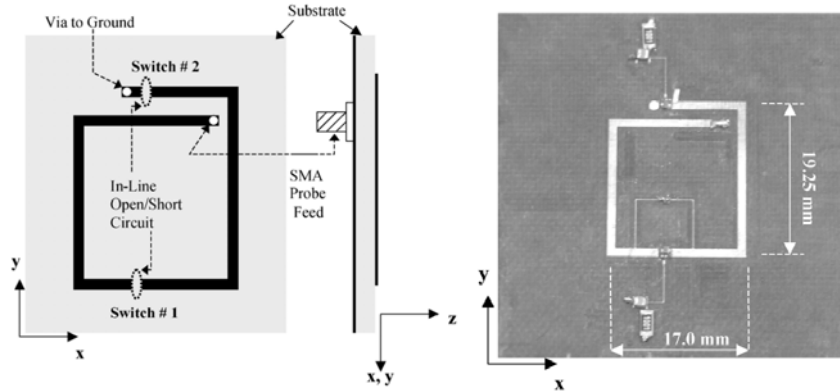


**Figure 1.5** Radiation pattern reconfigurable square spiral microstrip antennas with RF MEMS Switches [36].

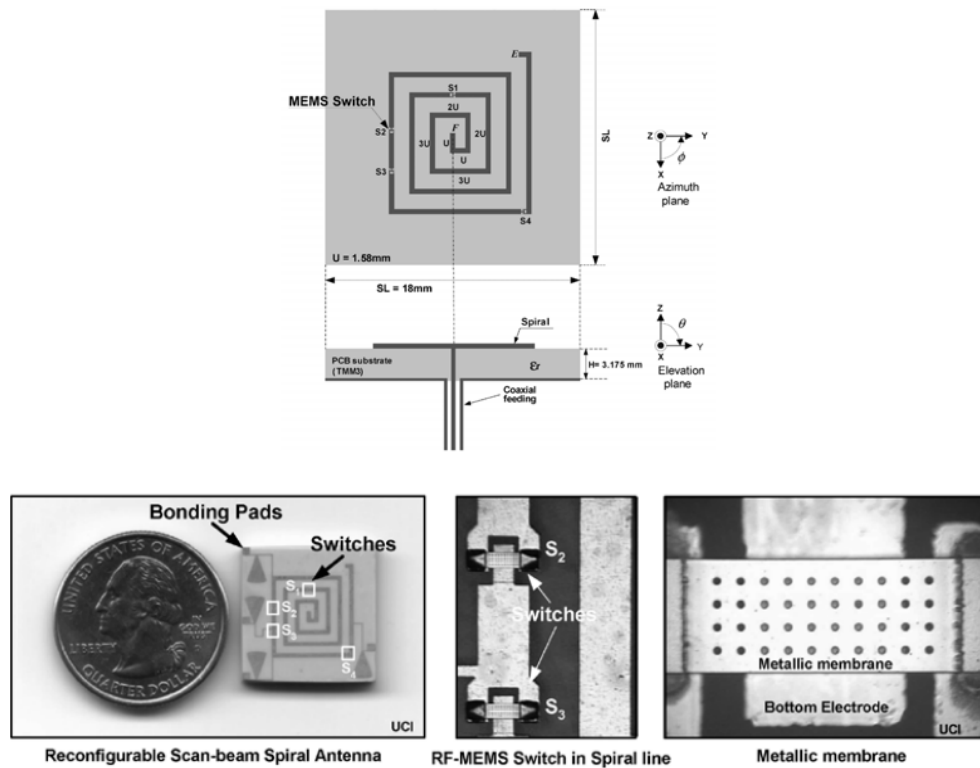


**Figure 1.6** A radiation pattern reconfigurable scan-beam spiral antenna [37].

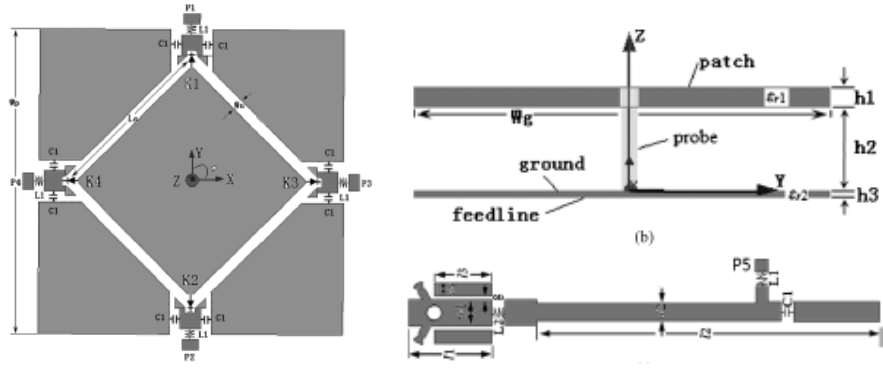


**Figure 1.7      A radiation pattern reconfigurable antenna with varactor diode [42].**

Varactor diode is a commonly used in microwave solid-state device, the capacitance between the two poles changes with the DC bias voltage change. Varactor diode can be used to continuously adjust the operating frequency of antennas to achieve continuous adjustable antenna radiation performances [42-45]. Another reconfigurable antenna, shown in Fig.1.7, has been presented in [42], it is based on a two-element dipole array model. The two dipoles of the array are folded to form a square and the phases of the magnetic dipoles are adjusted by the loaded varactor diodes. The radiation patterns of this antenna are reconfigured in two orthogonal planes.

### 1.2.3 Optical controlling method

Thirdly, optical controlled reconfigurable antennas are based primarily on photoconducting switches. The laser light is used to tune a photoconducting switch. Compared to the traditional microwave switching devices, photoconducting switches do not require additional DC bias wire, thereby reducing the radiation effects on the antenna. In addition, they do not need to consider the isolation between the positive and negative DC bias voltage, which reduces the complexity of antenna structures. However, the most challenges of this reconfigurable technology are integration and power consumption because laser generation needs laser diodes and fiber optics. Photoconducting switches have commonly been used to design frequency reconfigurable antennas [46-50]. C. J. Panagamuwa et al. have designed a frequency and beam reconfigurable antenna using phototconducting switches, which is shown in Fig.1.8. From this, we find that two silicon photo switches are placed on small gaps in both dipole arms equidistant from the centre feed. Light from two infrared laser diodes is channelled through fiber optic cables and applied on the switches. With the gaps in the dipole bridged, the antenna resonates at lower frequencies.

Therefore, the lengths of the two arms of antenna were effectively changed by using a laser to control the photoconducting switches, the frequency and beam reconfigurable antenna was achieved [47].

#### 1.2.4 Changing the material properties method

Changing the material properties is another interesting method to design radiation-pattern and frequency reconfigurable antenna [51-53]. Liquid crystals (LC), ferroelectric and ferromagnetic materials are some kind of these materials, which have been used as means of reconfiguration. By applying DC voltage or magnetic field on these materials, their electrical properties of them are modified, leading to alter the EM responses of the structures. In [51] and [52], a fixed-frequency beam scanning antenna has been designed by using a ferroelectric substrate, as shown in Fig.1.9. By changing the DC bias voltage on the substrate, the permittivity of the ferroelectric material is changed. Hence, electrically phase constant of the propagation wave is changed and the direction of the main beam could be changed. However, the higher cross polarization level in the ferromagnetic material limits its applications as radiators in the antenna engineering.

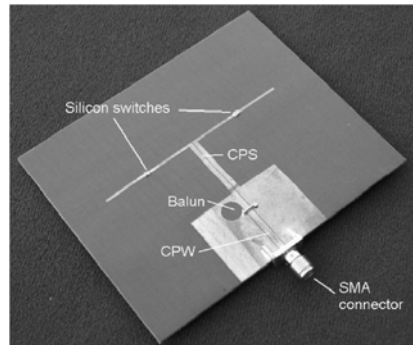


**Figure 1.8      Photograph of frequency and beam reconfigurable antenna using photoconducting switches [47].**

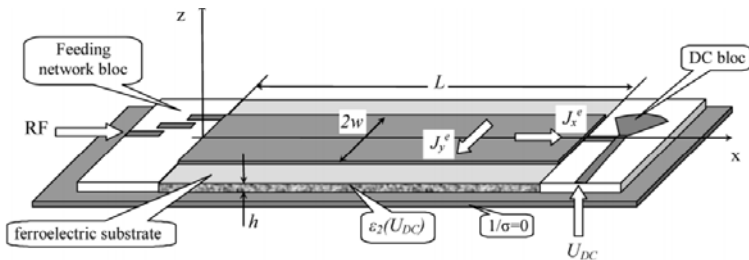


**Figure 1.9      Basic geometry of the scan antenna based on ferroelectric substrate [52].**

### **1.2.5 Using metamaterial method**

In recent years, metamaterials has increasingly attracted researchers' attention to develop new antennas and RF devices [54-56]. Depending on the way that they treat with the incident electromagnetic waves, metamaterials can be realized as Electromagnetic Bandgap structures (EBG), Artificial Magnetic Conductor (AMC), High Impedance Surface (HIS) and Frequency Selective Surfaces (FSS). They are constructed of an array of periodic elements arranged in one, two or three dimensional pattern. There have been many structures such metamaterials that are used to design radiation pattern reconfigurable antennas because of their specific performances on electromagnetic waves [57-75].

In [58], M.A. Habit et al. have proposed a switching beam antenna based on electromagnetic bandgap (EBG) periodic structures. This antenna operates at 1.8GHz with a gain of 10dBi, and it switches in six different beams with  $60^\circ$  of beam-width and covered  $360^\circ$  in the azimuth plane, which is shown in Fig.1.10. Fig.1.11 shows a pattern reconfigurable antenna with four open circuit switches over a high-impedance surface (HIS) proposed in [63]. By switching different switch combinations, beam steering is achieved. From references [64-75], the designs of radiation pattern reconfigurable antennas were based on frequency selective surfaces (FSS). In [69], Arezou Edalati et al. have proposed a reconfigurable antenna using an active cylindrical FSS, as shown in Fig.1.12. The FSS structure consists of metallic discontinuous strips with Pin-diodes in their discontinuities. An omnidirectional electromagnetically coupled coaxial dipole (ECCD) array is surrounded by cylindrically FSS. By controlling the state of diodes in FSS, a directive radiation pattern can be swept in the entire azimuth plane. In [73], Liang Zhang et al. have designed a beam steerable antenna system using active frequency selective surfaces (AFSS), as shown in Fig.1.13. The varactors are mounted on this AFSS to achieve continuous tuning. The reflection band changes with the reverse voltage added on the varactor diodes continuously. The beam of this antenna could sweep in the whole azimuth plane for both the single-beam modes and the dual-beam modes.

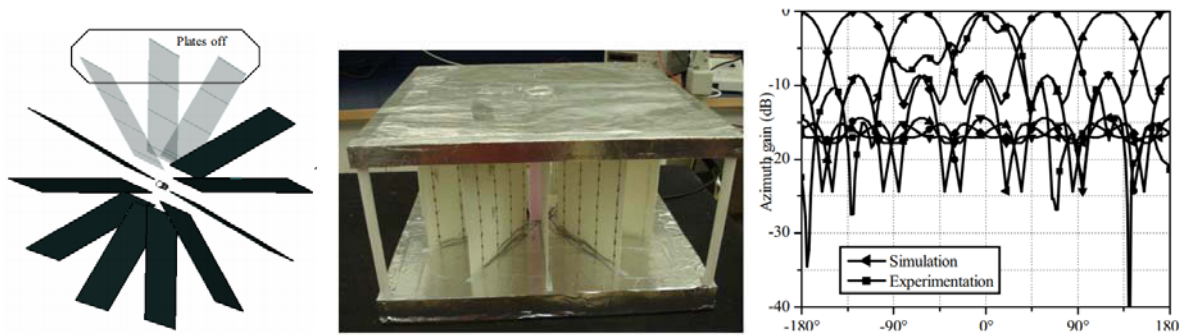


**Figure 1.10** A beam switching antenna based on electromagnetic bandgap (EBG) [58].

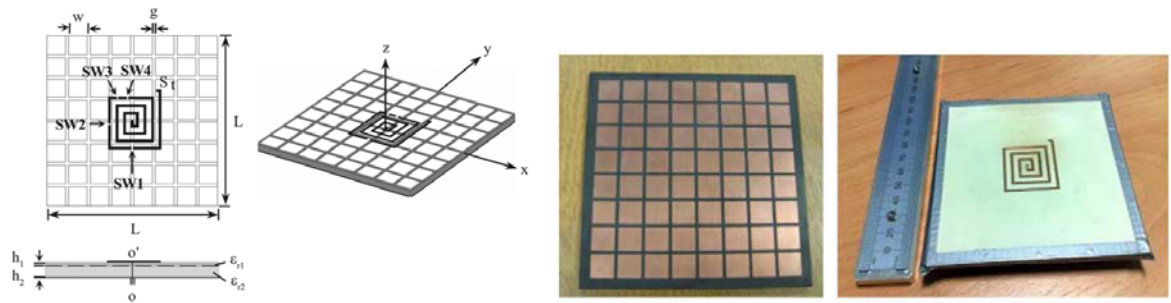


**Figure 1.11** A pattern reconfigurable antenna using a high-impedance surface (HIS) [63].

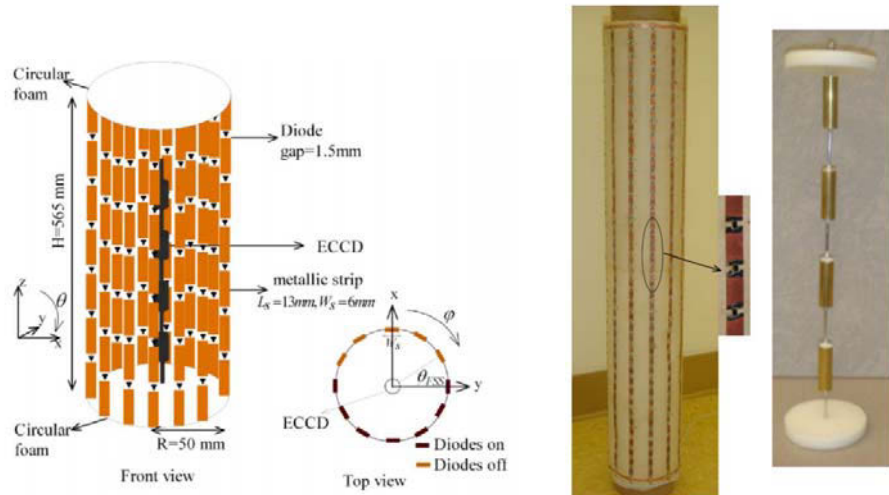
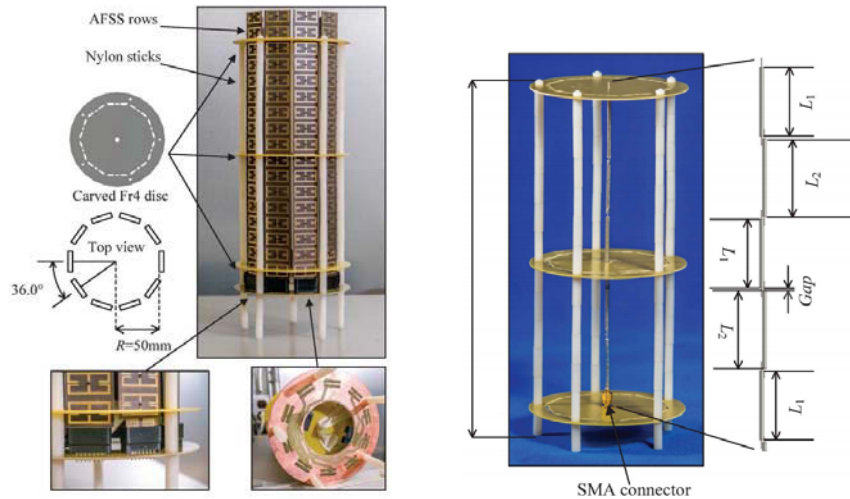
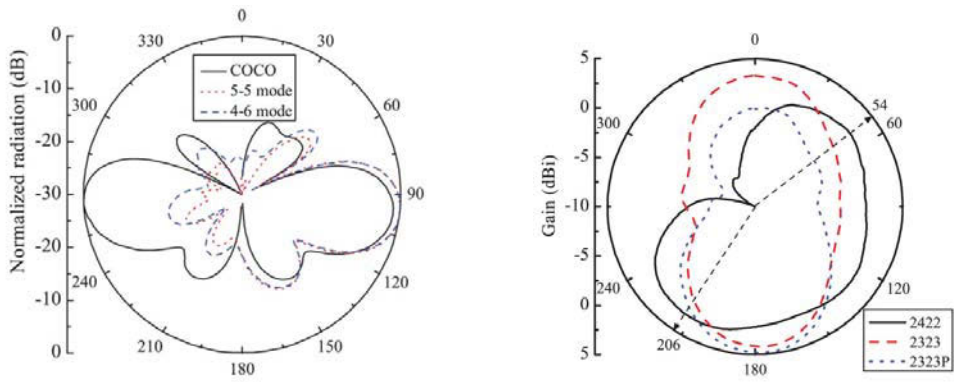


**Figure 1.12** A pattern reconfigurable antenna based on frequency selective surface (FSS) [69].



(a)



(b)

**Figure 1.13** A radiation pattern steerable antennas based on AFSS [73], (a) Antenna structure and installation. (b) Radiation patterns of single-beam modes and dual-beam modes.

**Table 1.1** Comparison of different reconfigurable approaches.

Design Methods	Advantages	Disadvantages
Mechanical	Continuously steering, low insertion loss	Low speed and complex system installation
Pin-diode	Fast speed, low cost	More insertion losses, isolation reducing with the frequency increasing, need to design the DC bias circuit

RF-MEMS	High isolation, low insertion losses, low power consumption	Slow speed, high bias voltage, high cost
Varactor	Continuously adjustable, low insertion losses, low power consumption	Requires a stable bias voltage
Photoconducting switches	Do not need additional DC bias wires	High cost and difficult integration
Changing the material properties	More designing freedom	High bias voltage, more losses, high cross polarization
Using metamaterial	Fast speed, small size, more designing freedom, low power consumption	Need to design the DC bias circuit

In summary, the mentioned reconfiguration approaches above are compared in Tab. 1-1. Based on the data listed in this table, it can be concluded that implementing a reconfigurable structure using metamaterial technology makes the antenna performances better in terms of loss, speed, power consumption and freedom degree for design.

### 1.3 Research objectives

The main objective of the research is to develop a compact, low-profile, low cost antenna which has the functionality to switch the direction of the main beam in the azimuth and elevation planes without severely affecting its performance. In the design process, the number of active elements needs is kept as minimum as possible to decrease the antenna cost and also to enhance its radiation performance in terms of gain.

### 1.4 Organization of the thesis

This thesis is divided into 8 chapters including the abstract and the reference. The contents of the dissertation chapters are listed below.

Chapter 1 firstly introduces the background and motivation of research on radiation pattern reconfigurable antennas. Research status of radiation pattern reconfigurable antenna are also presented. Moreover, the most commonly used reconfiguration approaches are also described and compared to each other in this chapter.

Following the research survey presented in the first chapter, comprehensive studies on frequency selective surfaces are presented in Chapter 2.

Chapter 3 describes a compact dual-band beam-sweeping antenna which consists of two independent cylindrical active frequency selective surfaces (AFSS) and a dual-band omnidirectional monopole antenna. The unit-cells of the two proposed AFSS screens are designed. The transmission and reflection characteristics of the unit-cell of the two AFSS are also investigated, respectively, at their own operating frequency. Then the operation mechanism of the dual-band beam switching antenna and parametric studies are introduced and discussed in this chapter. At last, the simulation and measurement results of the proposed design are depicted, indicating that it can effectively realize beam-sweeping at 2.45 GHz and 5.2 GHz covering all azimuth angles simultaneously. The size of the proposed antenna system is reduced greatly by using this method.

Chapter 4 presents a beam-switching antenna with high gain and flexible control of beam numbers based on FSS. This presented high gain antenna is composed of an omnidirectional monopole antenna as radiating source surrounded by a hexagon FSS screen and six metallic sheets. The design of the FSS unit-cell used in this desgin is presented in this part. The transmission and reflection characteristics of FSS unit-cell are also investigated at 5.2 GHz. Then the operation mechanism of this high gain beam swiching antenna and parametric studies are described and discussed. At last, the simulation and measurement results of the proposed design are depicted. By switching the states of the pin-diodes in the hexagon FSS screen, the proposed antenna not only sweeps six directions with high gain in the azimuth plane, but also flexibly operates at multiple beam modes, including two-beam mode and three-beam mode with low power at 5.2 GHz. Moreover, the result shows that the maximum gain of this proposed antenna has been enhanced by 7 dB when six metallic sheets are applied to the design.

Chapter 5 proposes a beam-tilting antenna with negative refractive index metamaterial (NRIM) loading. The proposed antenna is composed of a double-feed dielectric resonator antenna (DRA)

and  $1 \times 4$  NRIM array which are fixed over and in the middle of the DRA. The NRIM unit cell and double feed dielectric resonator antenna are designed. Then, the working mechanism of the beam tilting antenna is discussed and the simulation and experimental results are shown in this chapter. From these results, this designed antenna can steer the main beam by  $\pm 38^\circ$  in the  $xoz$ -plane over 5 to 5.5 GHz band. In the operating frequency band, the reflection coefficient is better than -10 dB. Moreover, the measured results are in a good agreement with simulated ones.

In chapter 6, a three layers pattern reconfigurable quasi-yagi antenna is proposed. This design achieved multi beam directions in both elevation and azimuth planes at 5.2 GHz. There are four elements of quasi-Yagi antenna and eight pin-diodes as switches inserted in the middle layer. The parasitic elements are included in the top and bottom layers, into which pin-diodes are inserted. By controlling the pin-diodes in the middle layer, the antenna can realize beam switching in the azimuth plane in four directions. Moreover, beam tilting in the elevation plane is achieved by activating the pin-diodes in the top and bottom layers to reconfigure the lengths of the parasitic elements. The performance is very advantageous for modern wireless communication.

In chapter 7, the accomplishments of this thesis is summarized, and the future work is proposed in the research orientation.

A French summary of this thesis is presented in Chapter 8.

## 1.5 List of publications

### *Journals*

- [1]. **J. Li**, Q. Zeng, R. Liu and T. A. Denidni, "A Compact Dual-Band Beam-Sweeping Antenna Based on Active Frequency Selective Surfaces," *IEEE Trans. Antennas Propag.*, vol. 65, no. 4, pp. 1542-1549, April 2017.
- [2]. **J. Li**, Q. Zeng, R. Liu and T. A. Denidni, "Beam-Tilting Antenna With Negative Refractive Index Metamaterial Loading," *IEEE Antennas Wireless Propag. Lett.*, vol. 16, pp. 2030-2033, 2017.
- [3]. **J. Li**, Q. Zeng, R. Liu and T. A. Denidni, "A Gain Enhancement and Flexible Control of Beam Numbers Antenna Based on Frequency Selective Surfaces," *IEEE Access*, vol. 6, pp. 6082-6091, 2018.
- [4]. **J. Li**, Q. Zeng and T. A. Denidni, "Pattern-reconfigurable antenna for elevation and azimuth planes." *Microwave and optical technology letters*. Submitted

### *Conference*

- [5]. **J. Li**, Q. Zeng and T. A. Denidni, "A beam switching antenna with gain enhancement," *2017 IEEE International Symposium on Antennas and Propagation & USNC/URSI National Radio Science Meeting*, San Diego, CA, 2017, pp. 1981-1982.
- [6]. **J. Li**, T. A. Denidni and Q. Zeng, "A dual-band reconfigurable radiation pattern antenna based on active frequency selective surfaces," *2016 IEEE International Symposium on Antennas and Propagation (APSURSI)*, Fajardo, 2016, pp. 1245-1246.
- [7]. **Jinxin Li**, T. A. Denidni, Ruizhi Liu and Qingsheng Zeng, "Beam-tilting antenna with metamaterial loading," *2016 Progress in Electromagnetic Research Symposium (PIERS)*, Shanghai, 2016, pp. 4830-4830.
- [8]. **J. Li**, T. A. Denidni and Q. Zeng, "A compact gain-enhancement patch antenna based on near-zero-index metamaterial superstrate," *2016 17th International Symposium on Antenna Technology and Applied Electromagnetics (ANTEM)*, Montreal, QC, 2016, pp. 1-2.

- [9]. **J. Li**, T. A. Denidni and Q. Zeng, "High gain reconfigurable millimeter-wave dielectric resonator antenna," *2015 IEEE International Symposium on Antennas and Propagation & USNC/URSI National Radio Science Meeting*, Vancouver, BC, 2015, pp. 444-445.
- [10]. **J. Li**, T. A. Denidni and Q. Zeng, "Beam switching antenna based on active frequency selective surfaces," *2015 IEEE MTT-S International Conference on Numerical Electromagnetic and Multiphysics Modeling and Optimization (NEMO)*, Ottawa, ON, 2015, pp. 1-3.
- [11]. **Jinxin Li**, T. A. Denidni, Qingsheng Zeng and Wenmei Zhang, "Active frequency selective surfaces for beam switching applications," *2015 IEEE 6th International Symposium on Microwave Antenna Propagation and EMC Technologies (MAPE)*, Shanghai, 2015, pp. 816-818.
- [12]. **J. Li**, Q. Zeng and T. A. Denidni, "Pattern Reconfigurable Antenna Loaded with Frequency Selective Surface and Artificial Dielectric Medium," *2018 IEEE International Symposium on Antennas and Propagation & USNC/URSI National Radio Science Meeting*, accepted.

## 2 FREQUENCY SELECTIVE SURFACES

Frequency selective surfaces (FSSs) are a two-dimensional or three-dimensional periodic structure, which is usually composed of an infinite array of metal patches or an array of apertures in a metal sheet based on a dielectric substrate. FSSs have originally been developed as a kind of spatial filter because of their responses to the electromagnetic (EM) waves. FSSs can transmit nearly all EM waves over a specific bandwidth while reflecting nearly all energy through another frequency bandwidth. According to the filter characteristics, FSSs can be divided into low-pass, high-pass, band-stop and bandpass four types. The basic structures and their frequency response are shown in Fig. 2.1. The orange color in the figure shows the metal material. From Fig. 2.1, the metal grid provides high-pass filter characteristics on the electromagnetic field and the patches provide low-pass filter characteristics, while the metal and the apertures have band-stop and band-pass filtering characteristics, respectively [76-78].

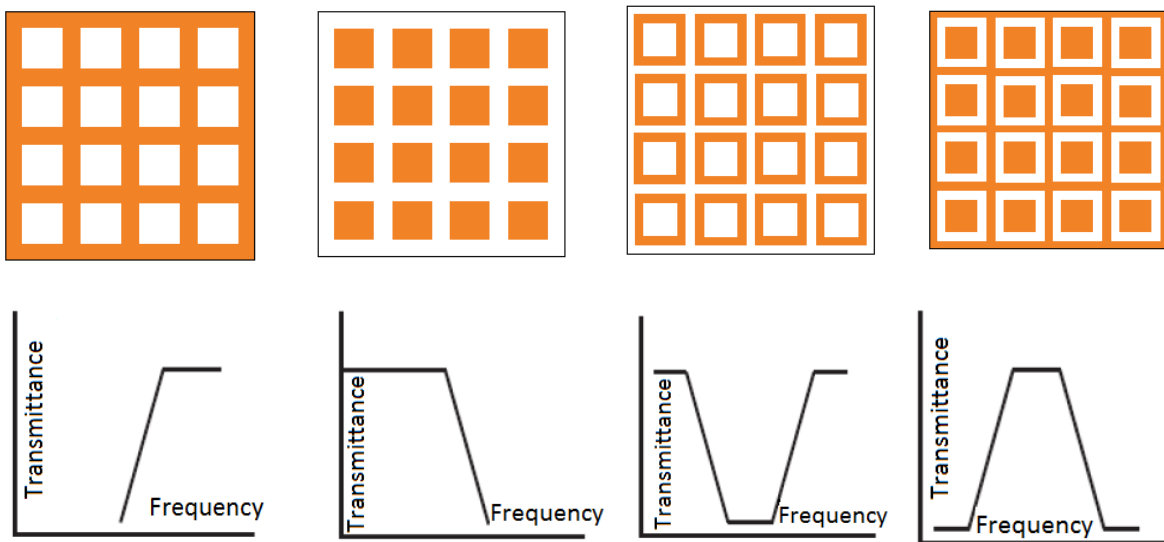


**Figure 2.1** The basic structures and their frequency response.

There are many different shapes of FSS elements. Generally, these elements may be broadly classified into four categories: center connected, loop elements, solid interior elements and combination elements, shown in Fig. 2.2 [7]. The first group is center connected elements, some typical elements of the first group are a straight element, three-legged element, anchor element and Jerusalem cross. The second group is loop elements, the typical elements of which include

three- and four-legged loaded elements, square and hexagonal loops. The third group is solid interior elements which usually includes such as square patch, hexagon patch, circle patch and triangle patch. The fourth group is combination elements which are constructed by a combination of the other three group members. By tailoring or combining other elements, the different types of combination elements are designed to meet the demands of desired application.

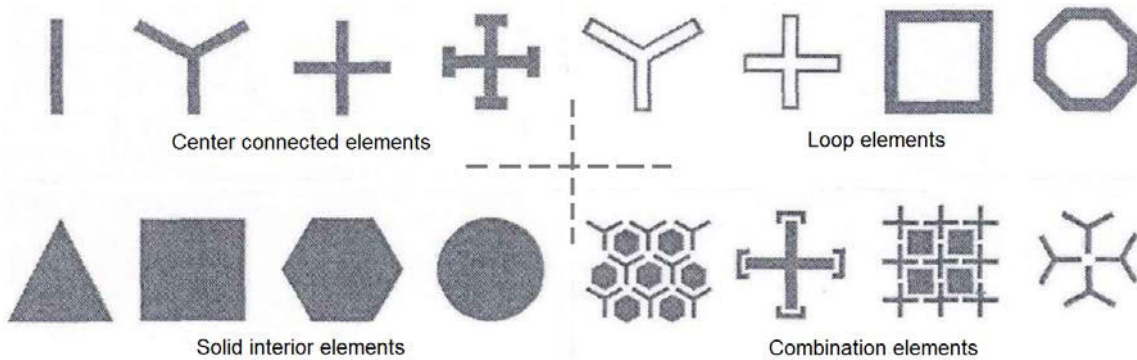


**Figure 2.2** The typical FSSs elements[7].

## 2.1 Applications of frequency selective surfaces

The first FSS prototype as a partially reflector surface has been reported in 1919 by Marconi and Franklin. However, until to the mid-1960s, FSSs were deeply investigated theoretical, and experimental, and were widely used in many fields [76].

One example of FSS applications is the shielding on the door of a microwave oven that allows us to see the food inside without being radiated by the electromagnetic waves of the microwave oven because the shielding is made of FSSs. The FSSs reflect microwave energy and allows visible light to pass through. In addition, there are many places using FSSs in civil applications , such as anti-collision systems for autonomous vehicles, electromagnetic shielding devices in public places such as hospitals and airports, robotic navigation systems, band gap structures of photonic crystals, etc.

Another important application is that the FSSs can be used in the military domain as radomes, which can decrease the radar cross section (RCS) of communication antennas and hide them from the enemy. Radomes work by allowing only the operational frequencies to pass through and rejecting the other frequencies that lie outside this band [76], whose schematic diagram is shown in Fig.2.3.

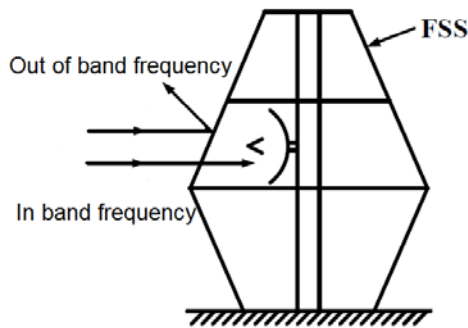


**Figure 2.3** Schematic diagram of radome.

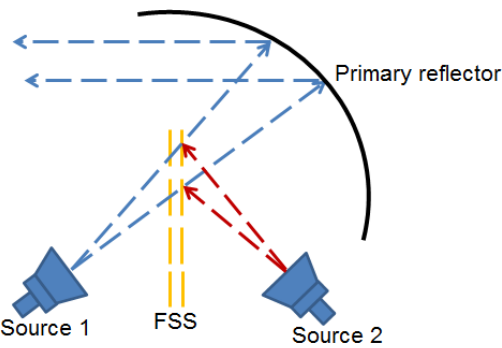


**Figure 2.4** A schematic diagram of FSS as sub-reflector in antenna systems.

There is another very typical application in the microwave antenna field. In order to improve the utilization efficiency of antennas, the FSSs have also been used as a sub-reflector in antenna systems to achieve multi-frequency operation [76]. As shown Fig.2.4, the FSSs are designed as a sub-reflectors placed between two different frequency feeds in a reflector antenna system. The FSS is transparent for feed 1 in the first operating band, while it operates as a sub-reflector in the second working frequency band for feed 2. Therefore, by using only one main reflector at two different operating frequencies, not only the size and cost of antenna systems are reduced but also the efficiencies of antennas has been improved [76].

## 2.2 Design parameters for frequency selective surfaces

The main design parameters of the FSS are the center frequency, transmittance and 3 dB bandwidth. A good FSS structure should have stable transmission characteristics with different angles of incidence and polarization. There are many factors affecting the FSS transmission

characteristics, including the unit cell structure, arrangement way and period, the thickness of the dielectric, dielectric constant, dielectric loss, number of layers.

Firstly, the FSS unit cell is the main factor affecting the center frequency of FSS, which directly determines the performance of the FSS. For some simple structures of unit cell, the center frequencies can be estimated. For example, for a dipole structure, a half wave resonance occurs when the length of unit cell is an integer multiple of the half wavelength of the incident wave. In addition, the better the symmetry of any unit cell, the better the polarization stability and the angular stability [76].

Secondly, the periodic structure and the arrangement way of FSS are also important parameters could affect the final transmission/reflection response of the FSS. Therefore, depending on the application features, both structures and arrangement way of FSS must be carefully chosen to meet all demands. The distance of elements and the geometrical position of adjacent elements significantly affect the center frequency, bandwidth, angular sensitivity, and cross polarization level.

Thirdly, the FSS screens have to be supported by dielectric substrate in practice because of mechanical reasons. In general, the resonant frequency of the dielectric drifts to the high frequency when the incident angle increases, while the FSS resonance frequency shifts to the low frequencies when the incident angle increases. Therefore, bonding the FSS in one side to dielectric or embedding it with dielectric on both sides significantly changes its transmission responses and can improve the structural stability of the angle [76]. In addition, dielectric loaded FSS structures have a wider available bandwidth. The thickness of dielectric also has influence on the FSS response with changing the incident angle and polarization. To achieve an angular stable resonant slot, the thickness of dielectric on both sides of the FSS must be a multiple of a quarter wavelength. When the FSS is loaded with one side dielectric, its thickness has to be a multiple of a half-wavelength to eliminate the mismatch loss [76].

### 2.3 Research states of active frequency selective surfaces

Once the passive FSS is manufactured, the electromagnetic characteristics such as the resonance frequency and the working bandwidth cannot be changed. The FSS radome in the working

frequency band cannot flexibly adapt to change according to the external electromagnetic environment, while the active FSS can solve this problem. Therefore, active FSS has become a popular research topic. Active FSS is also known as tunable FSS, controllable FSS and reconfigurable FSS. Based on a variety of different principles, active frequency selective surfaces are realized commonly using electronically controlled elements and materials in the microwave field. Controllable dielectric materials in the microwave and millimeter-wave bands have a wide range of applications, such as liquid crystal and ferrite materials are excellent controllable materials [79]. At present, there are many active frequency selective surface studies based on such controllable dielectric materials. Another type of active frequency selective surface is based on electronic control components to achieve the purpose of electronic control, including MEMS switches, PIN diode switches, as well as varactor diodes. MEMS switches have good high frequency characteristics, such as advantages of high integration, small size, low loss and low harmonics. Frequency selective surface current paths can be controlled using RF MEMS switches [80, 81], as an example shown in Fig.2.5. However, MEMS switches have not been widely marketed for manufacture as the cost is high and therefore designing active frequency selective surfaces based on MEMS switches is limited.

Pin-diodes have two different states which can be turned on and off in the high frequency band, so pin-diodes are often used as microwave band switches. Varactor diodes are very similar to pin-diodes, which capacitances are controlled by controlling the reverse bias voltage on them. Due to the maturity of pin-diodes and varactor diodes, the tunable frequency selective surface can be realized by the switching characteristics of pin-diodes and varactor diodes [82-87], as shown in Fig.2.6.

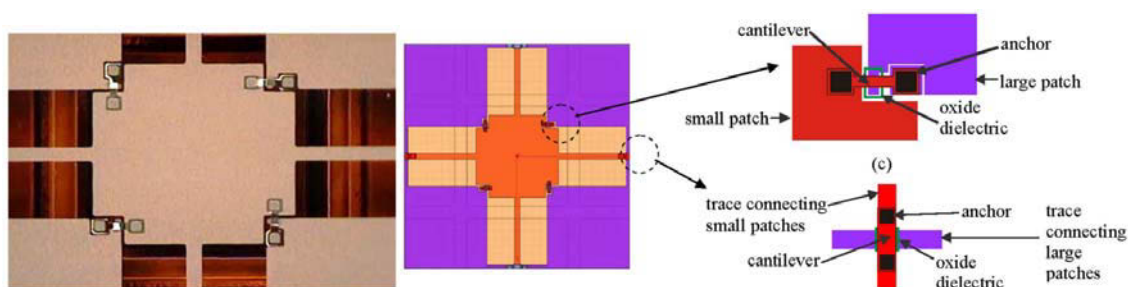


**Figure 2.5** Integrated MEMS switches tunable FSS structure[81].

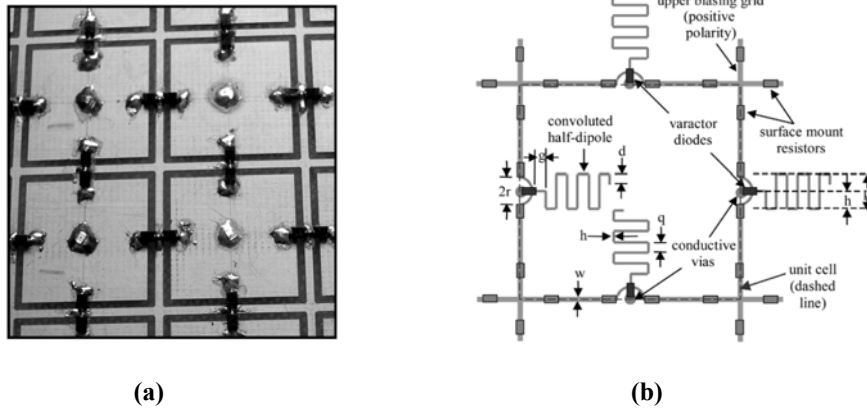


**Figure 2.6** Tunable FSS structure using (a) pin-diodes and (b) varactor diodes[82].

## 2.4 Introduction of theoretical analysis methods of FSS

The continuous improvement of FSS theoretical analysis methods has promoted the development of FSS. Theoretical analysis method is the basis of FSS characteristic analysis and engineering application. It mainly includes two major categories: equivalent circuit method and full wave analysis method.

The equivalent circuit method is based on the assumption of quasi-static field. FSS structural elements are equivalent to inductive and capacitive elements based on the theory of transmission lines. By using the inductance calculation formula of infinite metal strip and the capacitance calculation formula between adjacent strips, the equivalent circuit parameters can be achieved. Hence, the FSS transmission / reflection characteristics are achieved. The equivalent circuit method can directly reflect the filtering mechanism of the FSS structure and quickly obtain the resonance characteristics of the FSS. Especially in the beginning of design, the design process can be speed up by adopting this method. The limitations of this method lie in that the equivalent circuit parameters of the irregular and complex FSS structures are not easily obtained. The equivalent circuit parameters obtained by quasi-static approximation method have limited accuracy, hence, exact solutions of FSS scattering parameters cannot be obtained [88-92].

The full wave analysis method applies a strict vector method, which can obtain the amplitude of the FSS transmission coefficient, as well as phase and polarization characteristics of FSS. Full wave analysis method includes finite difference in frequency domain, spectral domain approach, volume integral equation method, periodic moment method and finite element method [93-98].

### **3 DESIGN OF A DUAL-BAND BEAM SWEEPING ANTENNA USING ACTIVE SURFACE SELECTIVE SURFACES**

#### **3.1 Introduction**

Nowdays, to fulfill the requirements of miniaturization and multifunction in the modern communication systems, more and more electronic devices are integrated into a single platform. Although this method can significantly improve the communication quality, it can also lead to serious problems of interference. As a means of reducing the interference coming from undesired radiation and to enhance the communication performance, radiation pattern reconfigurable antennas have intensively been investigated and received much attention. These antennas can significantly decrease interfering signals and improve the system capacity, while occupying the same or even a smaller physical volume in comparison with traditional smart antennas [22].

In the past few decades, various methods for designing radiation pattern reconfigurable antennas were reported. A conventional method for achieving radiation pattern reconfigurability is the introduction of phased antenna arrays [23,24,99]. However, the complex feed networks of phased arrays make the total antenna structure bulky, complicated and expensive to be applied in practice. On the other hand, many considerable advantages of electrical steerable antennas, such as a low-profile and simple structure, easy and inexpensive fabrication, have been reported. The concept of electronically steerable antenna has early been introduced by Harrington [100], which provides an easier way to obtain the variation of radiation pattern. There are three basic types of reconfigurable mechanisms utilized for electronically steerable antennas: pin-diodes [101-103], varactors [73] and RF micro-electromechanical system (MEMS) switches [37]. Recently, active frequency selective surfaces (AFSS) have been used to modify electromagnetic wave propagation, which has drawn significant interest. By employing active components like pin-diodes and varactors, AFSS could achieve a high level of control over electromagnetic wave propagation [67-75,104].

The traditional reconfigurable antennas could change the radiation pattern dynamically only in a single operating band with a large volume due to the configuration of unit-cells of FSS. In this chapter, a compact dual-band beam-sweeping antenna is presented. The radiating source is a

dual-band omnidirectional monopole antenna, which is surrounded by two cylindrical AFSS screens with different operating frequencies. The proposed design can realize dual-band beam-sweeping characteristics in 6 discrete states of radiation patterns, respectively, at 2.45 GHz and 5.2 GHz by switching pin-diodes on two AFSS screens. Both AFSS screens are made up of 6 unit-cells each, dividing the azimuth plane into 6 equal parts of  $60^\circ$ . By switching pin-diodes between the forward biased and reversed biased states in both AFSS screens, six types of radiation pattern could be created and cover the entire azimuth plane at both frequencies. Therefore, the omnidirectional radiation pattern of the dual-band monopole antenna can be converted into a directional one. From the simulated and measured results, the matching conditions of the proposed dual-band beam-sweeping can be guaranteed at 2.45 GHz and 5.2 GHz.

### 3.2 Active frequency selective surfaces unit cell design

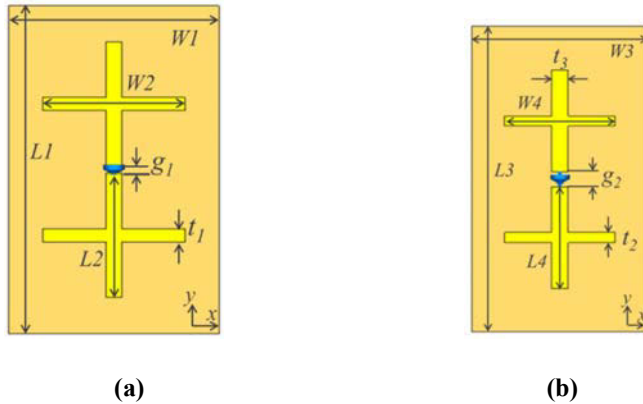


**Figure 3.1** Geometry of AFSS unit-cells: (a) 2.45 GHz AFSS unit-cell, (b) 5.2 GHz AFSS unit-cell.

**Table 3.1** Final dimensions of two AFSS unit cells(unit:mm).

2.45 GHz AFSS Unit cell	Parameters	$W1$	$L1$	$W2$	$L2$	$g_1$	$t_1$	—
	Value	36.6	65	24.7	24.7	1.3	2.3	—
5.2 GHz AFSS Unit cell	Parameters	$W3$	$L3$	$W4$	$L4$	$g_2$	$t_2$	$t_3$
	Value	18.8	30	10	10	1.4	1	1.5

The geometry of the proposed AFSS unit-cells operated at 2.45 GHz and 5.2 GHz are shown in Fig.3.1. Each AFSS unit-cell contains two metallic crosses connected by a pin-diode in serial. The cross structure is chosen here due to its simplicity and symmetrical structures. Moreover, a cross structure can also provide an acceptable angular and polarizations stability. Both proposed AFSS unit-cell structures are printed on the RT/duroid® 5880 substrate with a relative permittivity of  $\epsilon_r = 2.2$  and a thickness of  $h = 0.127$  mm. The dimensions of the 2.45 GHz and 5.2 GHz AFSS unit-cells are shown in Table 3.1. The AFSS unit-cells are simulated using CST Microwave Studio with the unit-cell boundary conditions applied along the  $x$  and  $y$  axis and two ports located along the  $z$  direction, in which the pin-diode is modeled as RLC serial lumped elements. In the forward biased case (state ON), the diode mainly represents a small resistance of  $R_s = 1.8 \Omega$ . When it is reversely biased (state OFF), the diode is equivalent to a capacitance  $C_p = 0.09 \text{ pF}$  and an inductance  $L_p = 0.5 \text{ nH}$  in series [71]. By switching the ON and OFF states of the pin-diodes, two metallic crosses can be either connected or isolated electrically, which leads to the variation of transmitting characteristics of the unit-cells at their own operating frequencies.

Fig. 3.2 (a) shows the simulated transmission coefficients of the 2.45 GHz AFSS unit-cell in both ON and OFF states, clearly indicating that the proposed 2.45 GHz AFSS unit-cell offers a band-stop and band-pass at 2.45 GHz when the pin-diode is ON and OFF, respectively. It is worth mentioning that the 2.45 GHz AFSS unit-cell always transmit the electromagnetic waves at 5.2 GHz no matter which state of the pin-diode is in. The simulated transmission coefficients of the 5.2 GHz AFSS unit-cell with different pin-diode states are illustrated in Fig. 3.2 (b), showing that electromagnetic waves are reflected and transmitted by the AFSS unit-cell at 5.2 GHz when the diode is ON and OFF, respectively.

As can be seen from it, when the diode is ON, electromagnetic waves can be reflected by the AFSS unit-cell. When the diode is OFF, the AFSS unit-cell can transmit electromagnetic waves at 5.2 GHz. Similar to the 2.45 GHz AFSS unit-cell, the 5.2 GHz AFSS unit-cell is always transparent to electromagnetic waves at 2.45 GHz regardless of which state of the pin-diode is in. With the “transparent” characteristics of unit-cells, each AFSS could work independently when placed together in one antenna system.

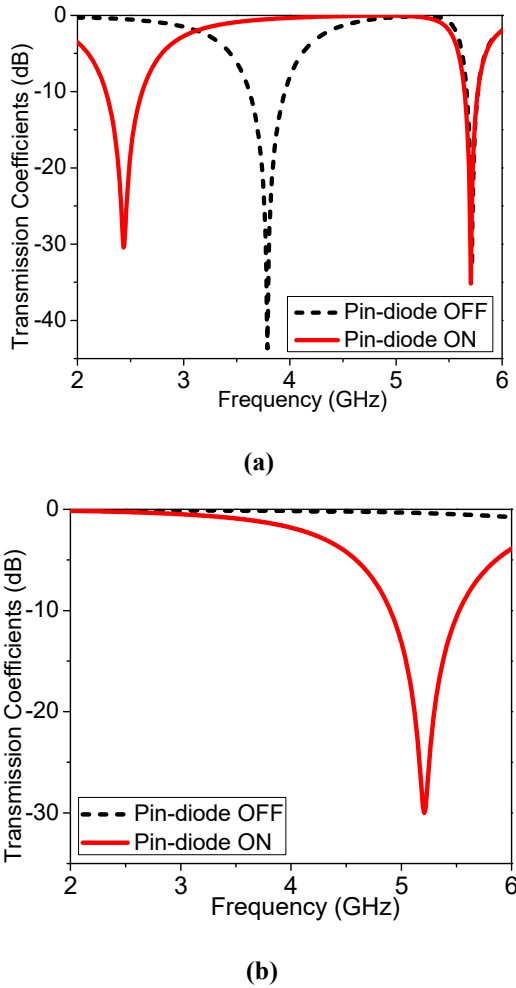


**Figure 3.2** Simulated transmission coefficients of the AFSS unit-cells: (a) 2.45 GHz AFSS unit-cell, (b) 5.2 GHz AFSS unit-cell.

### 3.3 Design and operation mechanism

The proposed dual-band beam-sweeping antenna schematic is shown in Fig. 3.3. For clarity, the outer cylindrical AFSS screen is made transparent in perspective view shown in Fig. 3.3 (b). A dual-band monopole antenna in the center is designed as a radiating source and surrounded by two proposed cylindrical AFSS screens that have a common center. Each cylindrical AFSS screen consists of six AFSS unit-cells, subtending an angle of 60 degree at the center of the cylinder. Consequently, six pin-diodes are required for each AFSS screen, which means twelve pin-diodes are needed for the dual-band beam-sweeping antenna. For simplicity, the biasing circuits are not shown in Fig. 3.3. According to the geometry in Fig.3.3, the radius of the cylinder can be calculated as

$$R1 = \frac{6 \times W1}{2\pi} \quad 3-1$$

$$R2 = \frac{6 \times W3}{2\pi} \quad 3-2$$

where  $R1$  and  $R2$  are the radii of outer and inner cylindrical AFSS screens and the  $W1$  and  $W3$  are the widths of AFSS unit-cells operating at 2.45 GHz and 5.2 GHz.

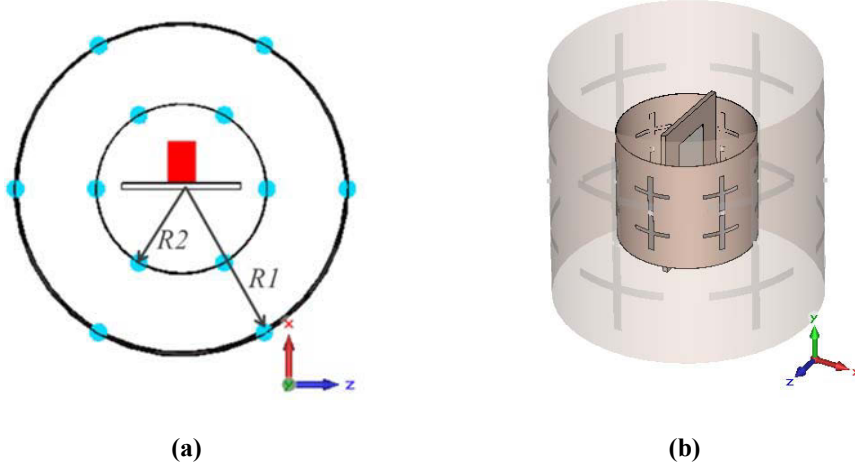


**Figure 3.3** Proposed dual-band beam-sweeping antenna structure: (a) top view, (b) side view.

### 3.3.1 Dual-band radiating source design

A compact monopole antenna for dual-band operation, shown in Fig. 3.4 (a), is in fact a modified version of the monopole antenna reported in [104]. This monopole antenna is selected because of its omnidirectional radiation pattern at 2.45 GHz and 5.2 GHz in the azimuth plane, which makes it ideal to realize beam-sweeping, shown in Fig. 3.4(b). Moreover, this monopole antenna structure is simple, which makes it easy to fabricate.

The monopole antenna consists of two rectangular monopole elements stacked at the top of each other with a small ground plane on the back of the substrate. The main resonators of the antenna are two rectangular elements with different sizes and designed to operate in two bands at 2.45 and 5.2 GHz. The proposed antenna can be fed directly by  $50 \Omega$  microstrip line. The proposed antenna is printed on the RO3006™ substrate with a relative permittivity of  $\epsilon_r = 6.15$  and a thickness of 1.27 mm. The optimized geometry parameters are given as follows:  $b1 = 12$  mm,  $a1 = 12$  mm,  $b2 = 9$  mm,  $a2 = 10$  mm,  $a3 = 4.6$  mm,  $b3 = 7$  mm. The simulated and measured

reflection coefficients and are shown in Fig. 3.5. From it, we can find that the measured results have a good agreement with simulated ones at 5.2 GHz while a slight frequency shift occurs at the low frequency range mostly due to fabrication tolerances.

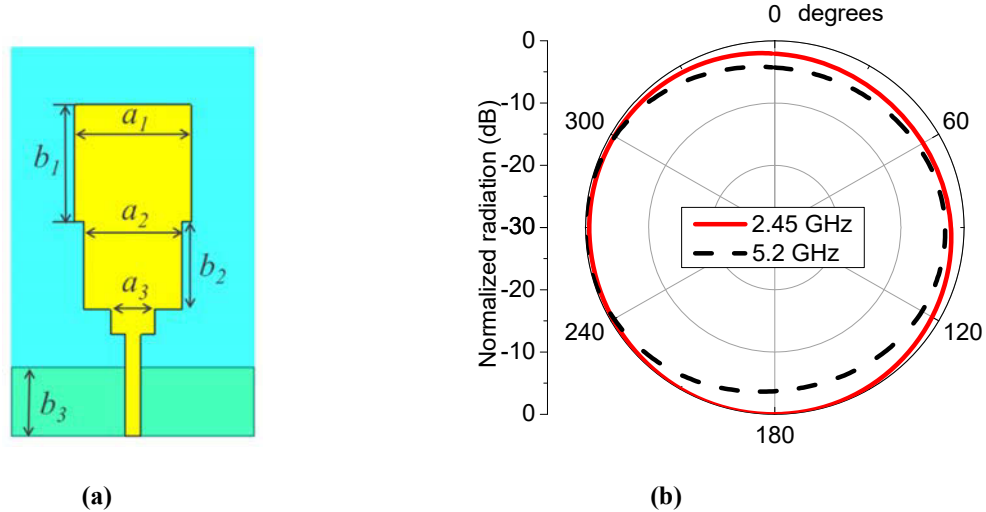


**Figure 3.4** (a) Geometry of the dual-band antenna, (b) measured radiation patterns of monopole antenna.

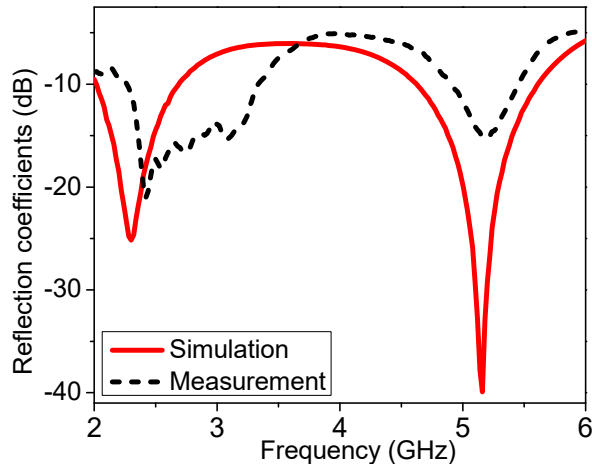


**Figure 3.5** Simulated and measured reflection coefficients results of monopole antenna.

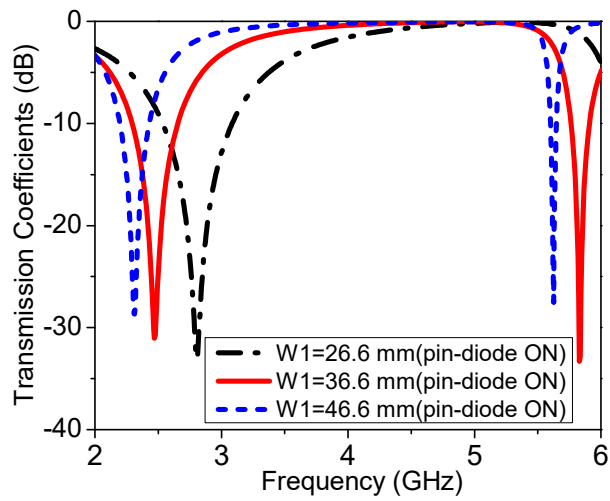
### 3.3.2 Mechanism of the proposed beam-sweeping antenna

The operation mechanism of the dual-band beam-sweeping antenna is stated as follows. For the outer cylindrical AFSS screen, it is divided into six parts. In each step of operation, three adjacent pin-diodes in three AFSS unit-cells are ON and the others are OFF. The AFSS unit-cells

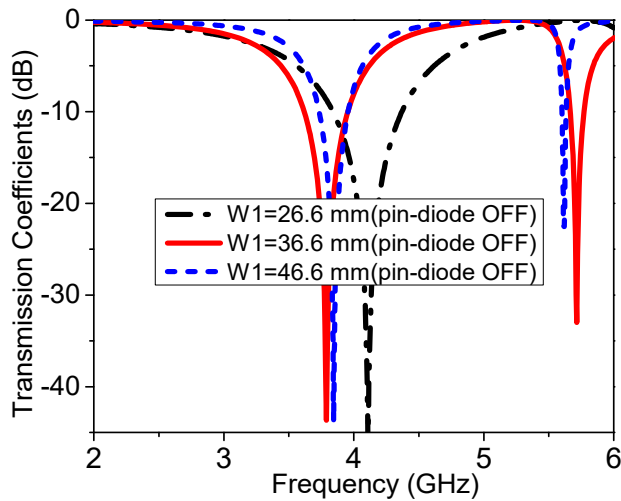
with OFF-state diodes have a high transmission coefficient and almost transparent for incident electromagnetic waves radiated from the monopole antenna in the center and the other parts with ON-state pin-diodes provide a high reflection coefficient acting as a metallic reflector. This means three parts are open and the other three parts are closed to the propagation of electromagnetic waves. Therefore, the omnidirectional radiation pattern of the monopole antenna is converted into a directional one. The inner cylindrical AFSS screen works in the same operating method. As is analyzed in Part 3.2, the outer and inner cylindrical AFSS screens can work independently when they are placed in one antenna system. Therefore, by switching pin-diodes in different AFSS screens between the ON and OFF states, the radiation pattern could scan the entire azimuth plane by six steps at 2.45 GHz and 5.2 GHz at the same time.

### 3.4 Parameteric studies and discussions

To show the effects of the design parameters on the antenna radiation characteristics, parametric studies are presented in this section. Since the parameters  $R1$  and  $R2$  are the major factors that determine the overall dimensions of the cylindrical AFSS screens, which mainly influence the radiation performance and the gain of the antenna, it is necessary to firstly optimize the periodicities  $W1$  and  $W3$ , by which  $R1$  and  $R2$  are defined from Equations 3-1 and 3-2. For simplicity, the DC bias voltage is not taken into account in the following simulations. The values of the parameters  $W1$  and  $W3$  can influence the resonator frequencies of AFSS unit-cells, and hence also influence the radiating characteristics of cylindrical AFSS screens. The effect of  $W1$  on the transmission coefficients of the 2.45 GHz AFSS unit-cell is illustrated in Fig. 3.6 (a) and (b) with the pin-diodes in ON and OFF states, respectively. For the 2.45 GHz AFSS unit-cell, in terms of the reflecting mode (the pin-diode is ON), the resonator frequency at 2.45 GHz is shifted by changing the value of  $W1$ , while the value of  $W1$  does not influence the transmission response at 5.2 GHz. In terms of transmitting mode (the pin-diode is OFF), the transmission coefficients do not change too much at 2.45 GHz and 5.2 GHz when the value of  $W1$  changes. When  $W1 = 36.6$  mm and the pin-diode is ON, the resonator frequency of the 2.45 GHz AFSS unit-cell is 2.45 GHz, as shown in Fig. 3.6 (a).

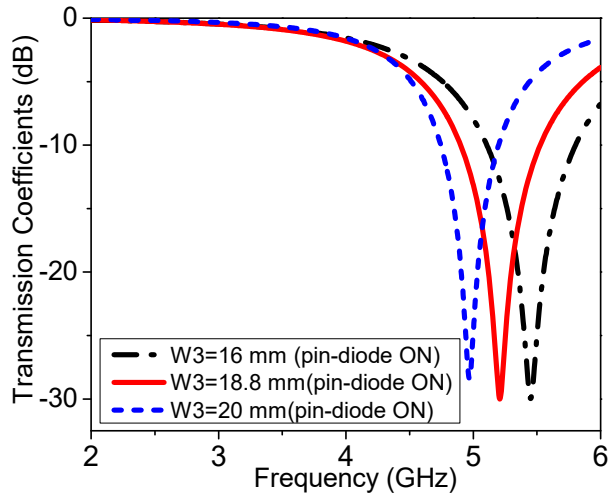


(a)

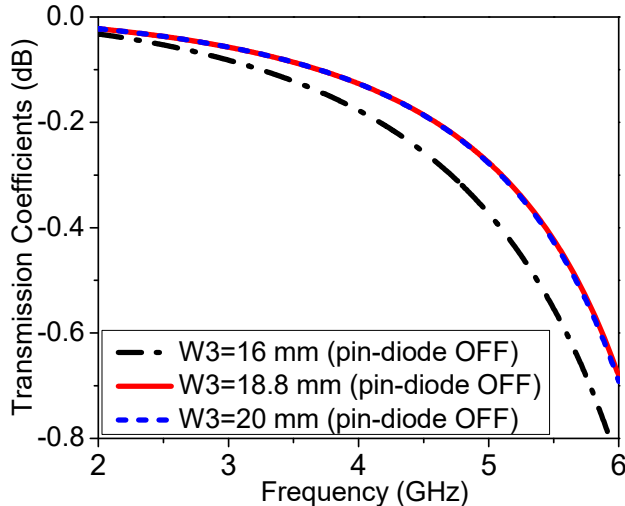


(b)

**Figure 3.6** The effect of the  $W_1$  on the transmission coefficients of the 2.45 GHz AFSS unit-cell: (a) pin-diode ON, (b) pin-diode OFF.



(a)



(b)

**Figure 3.7** The effect of the  $W_3$  on the transmission coefficients of the 5.2 GHz AFSS unit-cell: (a) pin-diode ON, (b) pin-diode OFF.

The effect of the  $W_3$  on the transmission coefficients of the 5.2 GHz AFSS unit-cell is shown in Fig. 3.7 (a) and (b) with the pin-diodes in ON and OFF states, respectively. For the 5.2 GHz AFSS unit-cell, when the pin-diode is ON, the resonator frequency at 5.2 GHz is shifted by changing the value of  $W_3$  but the value of  $W_3$  has no effect on the transmission response at 2.45 GHz. When the pin-diode is OFF, the transmission coefficients change slightly at 2.45 GHz and 5.2 GHz when the value of  $W_3$  is changed. When  $W_3 = 18.8$  mm and the pin-diode is ON, the resonator frequency of the 5.2 GHz AFSS unit-cell is 5.2 GHz, as shown in Fig. 3.7 (a).

Fig. 3.8 illustrates the simulated gain of proposed antenna with different values of  $R1$  and  $R2$ . The maximum gain at 2.45 GHz and 5.2 GHz is found at  $R1 = 35$  mm and  $R2 = 18$  mm. Considering all the analysis results shown in Fig. 3.6 and Fig. 3.7 as well as the gain shown in Fig. 3.8, the optimal values of  $R1$  and  $R2$  for our application are 35 mm and 18 mm, respectively.

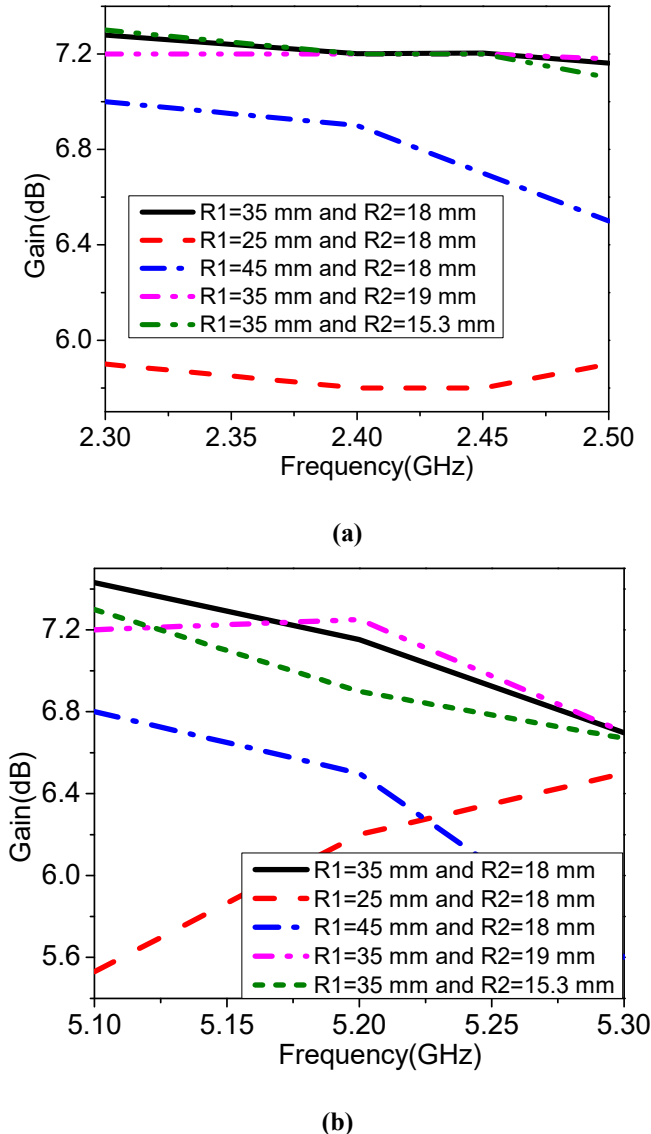
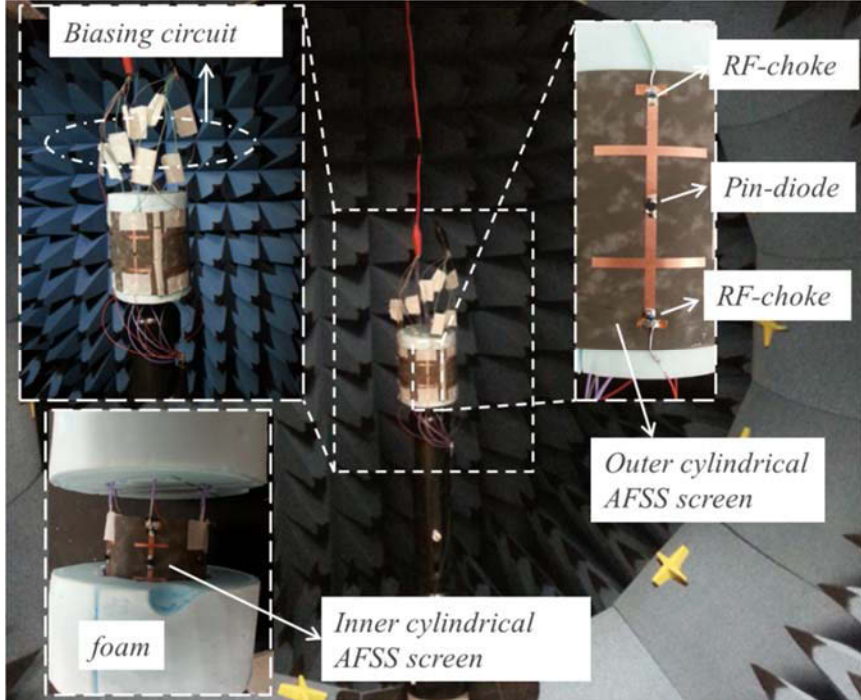


Figure 3.8      Simulated gain of proposed beam-sweeping antenna.

### 3.5 Fabrication and measurement results

To validate the performance of the proposed beam-sweeping antenna, a prototype of the antenna system was fabricated and measured. The fabricated dual-band beam-sweeping antenna is placed

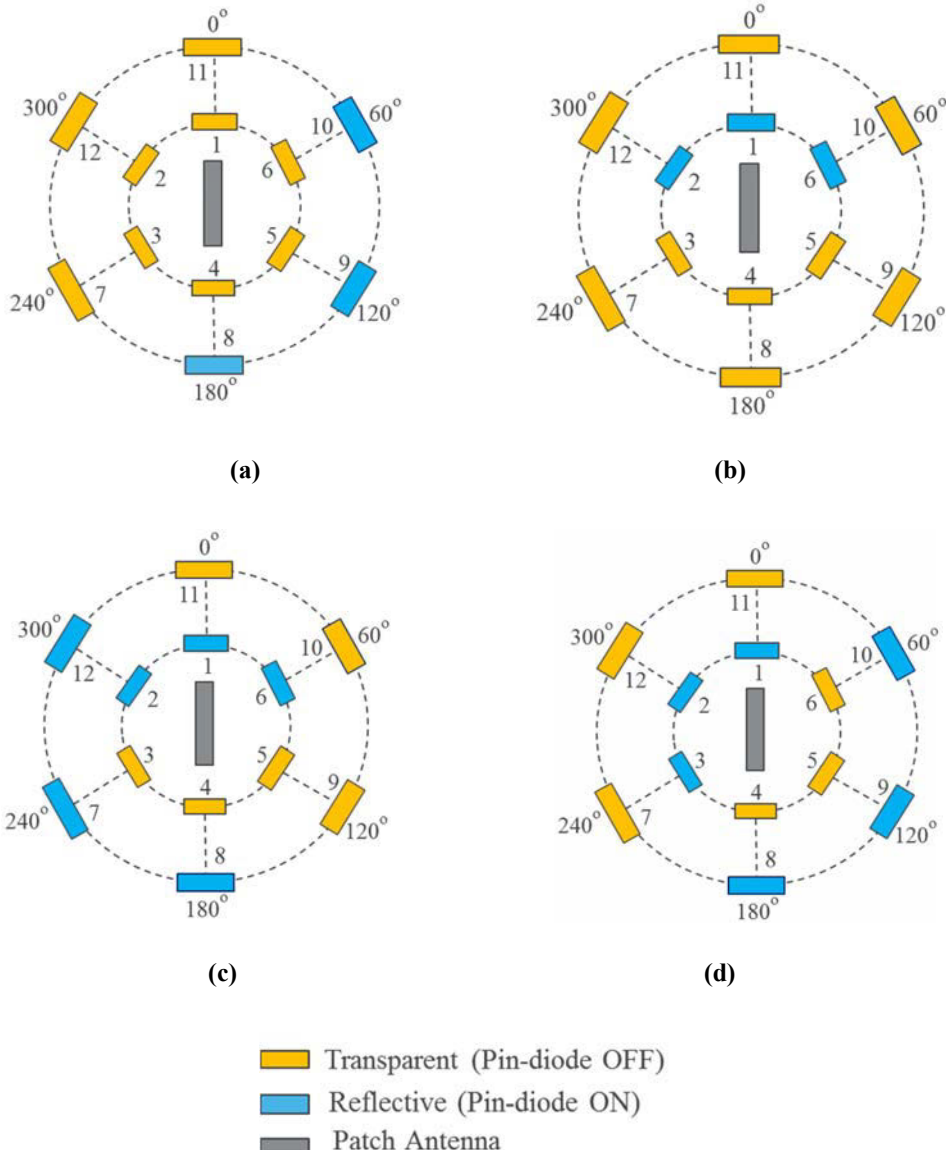
in an anechoic chamber as shown in Fig. 3.9. The two AFSS screens are printed on flexible substrate Rogers RT/duroid® 5880 with a thickness of 0.127 mm. As shown in Fig. 3.9, the inner AFSS screen is inserted into two cylindrical slots in the top and bottom cylindrical foams and the outer AFSS screen is wrapped onto the cylindrical foams.



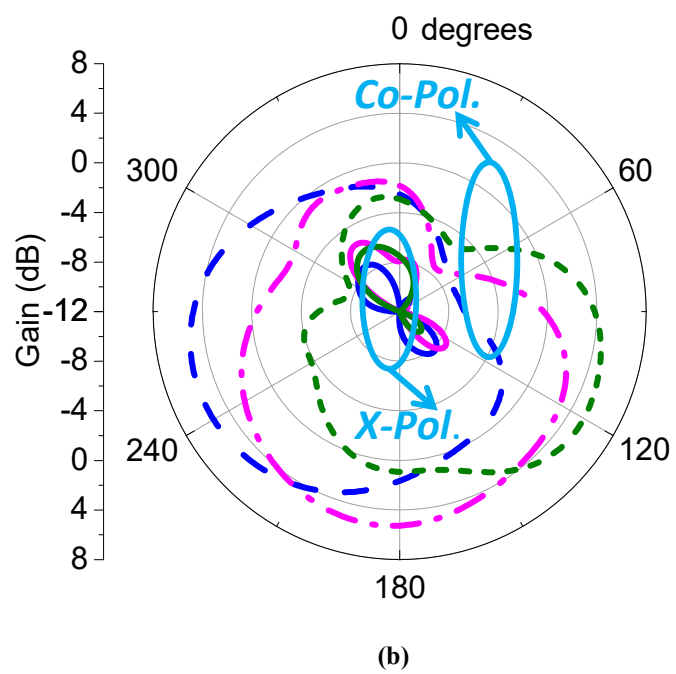
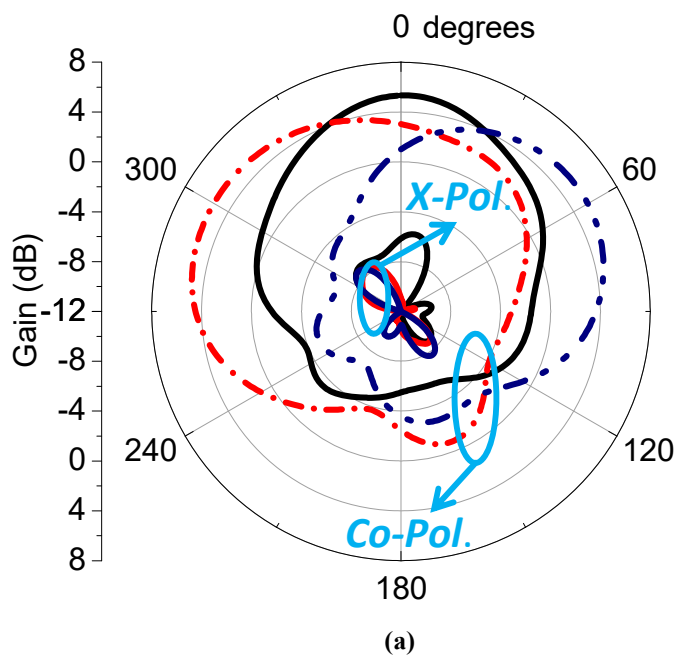
**Figure 3.9** Photograph of the fabricated antenna prototype in anechoic chamber.

At the central of the cylindrical foams, there is a rectangular slot to accommodate the omnidirectional monopole antenna. Twelve high frequency pin-diodes GMP-4201 from Microsemi are inserted into the two AFSS screens [105]. In the simulations, for the forward biased (ON) case, the pin-diode mainly represents as a small resistance  $R_s = 1.8 \Omega$ . When it is reversely biased (OFF), the diode mainly represents as capacitance  $C_p = 0.09 \text{ pF}$  and inductance  $L_p = 0.5 \text{ nH}$  in series. At the top and bottom of each AFSS unit-cell, RF chokes from Murata are used to isolate the RF signal from biasing lines. The values of the RF chokes used in the outer and inner AFSS screens are 47 nH and 18 nH, respectively. Each pin-diode is fed separately with the DC feeding lines from top to bottom. For measurements, the DC voltage is supplied by an external voltage source. When the DC voltage is zero, the pin-diode is OFF. When the DC voltage is 1.1 V, the pin-diode is ON. Three measurement methods are adopted in order to verify

that the proposed antenna can realize beam-sweeping at two different frequencies and that two cylindrical AFSS screens can work independently.



**Figure 3.10** Operation methods: (a) Case I, (b) Case II, (c) and (d) Case III.



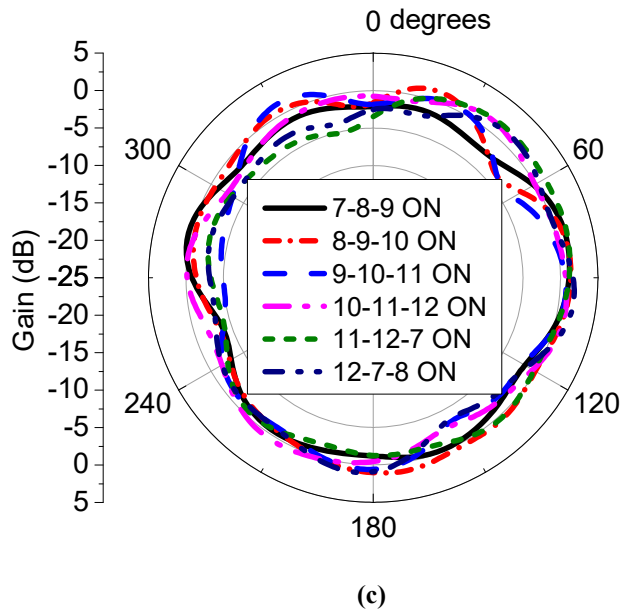
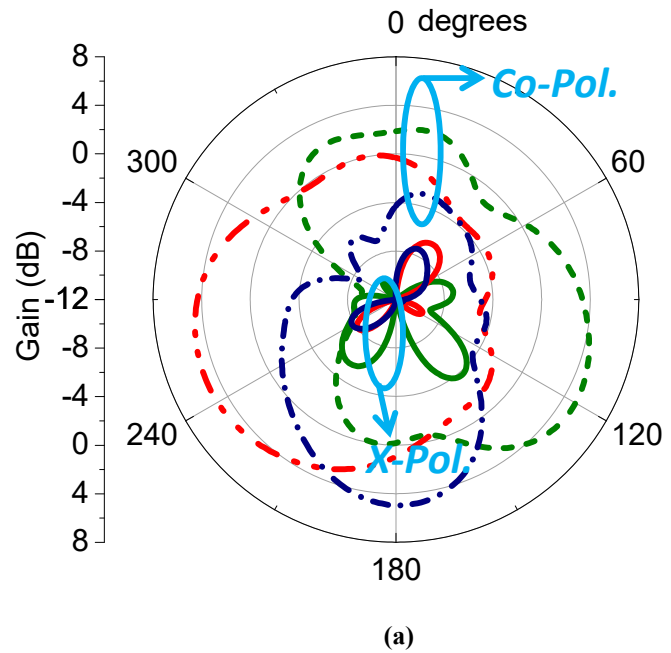
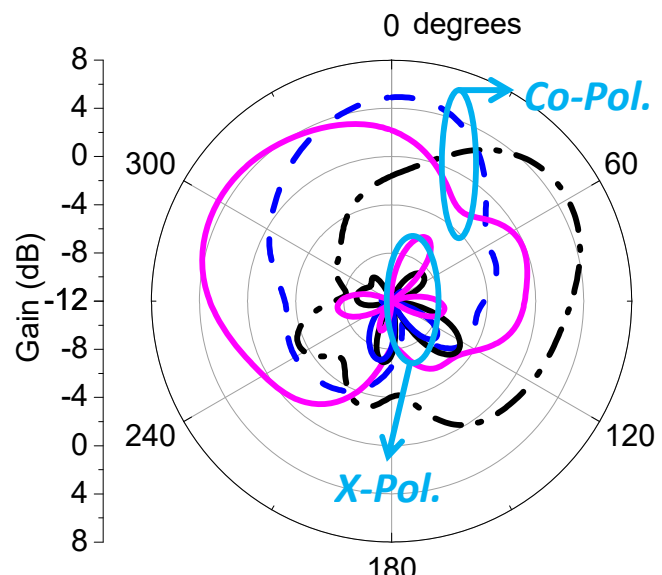


**Figure 3.11** Measured radiation patterns results in the azimuth plane of case I: (a) and (b) 2.45 GHz, (c) 5.2 GHz.

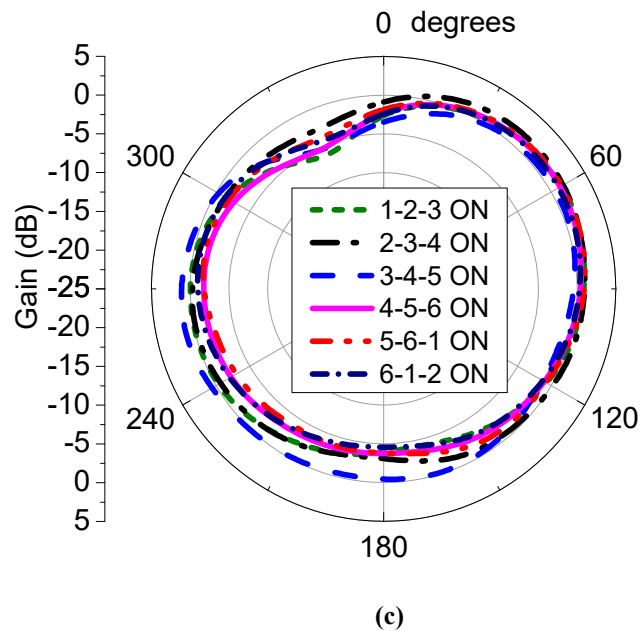
The schematic diagram of Case I is shown in Fig. 3.10 (a) and the number from 1 to 12 represents the pin-diodes embedded on two cylindrical AFSS screens. Zero-DC voltage is supplied to the inner AFSS screen to make sure all the pin-diodes in the inner cylindrical AFSS screen are in OFF-state. For the outer cylindrical AFSS screen, three adjacent pin-diodes are given positive DC voltage and the others are given zero voltage. In this way, by switching the pin-diodes numbered 7-12 following a sequence between the ON and OFF-states, the radiation pattern has the ability to scan the entire azimuth plane in 6 steps at 2.45 GHz. Fig.3.11 shows the measured radiation pattern results in the azimuth plane of Case I. It is clear that six different directional radiation patterns in the azimuth plane are obtained at 2.45 GHz and six omnidirectional radiation patterns occur at 5.2 GHz, which means that the beam switching function is realized at 2.45GHz while the radiation patterns at 5.2 GHz remain the same as the monopole antenna one.



(a)

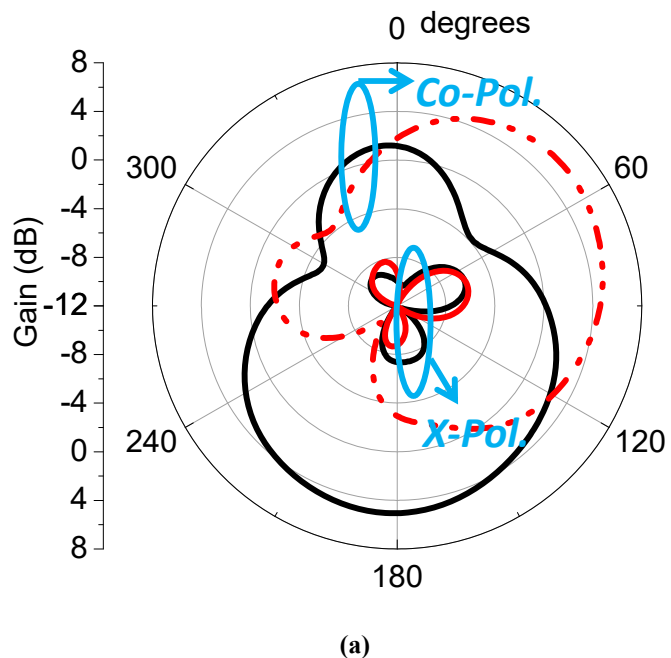


(b)

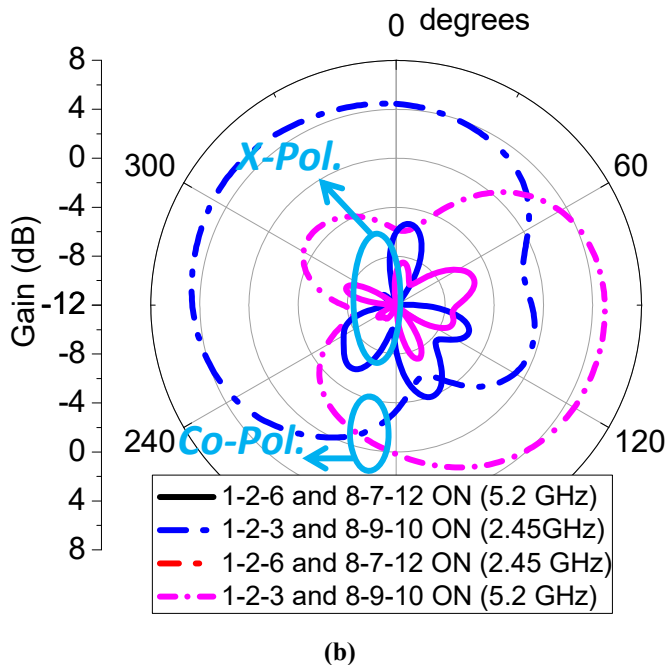


(c)

**Figure 3.12** Measured radiation pattern results in the azimuth plane of case II: (a) and (b) 5.2 GHz, (c) 2.45 GHz.



(a)



(b)

**Figure 3.13** Measured radiation patterns of case III: (a) 1-2-6 and 8-7-12 pin-diodes ON at 2.45 GHz and 5.2 GHz, (b) 1-2-3 and 8-9-10 pin-diodes ON at 2.45 GHz and 5.2 GHz.

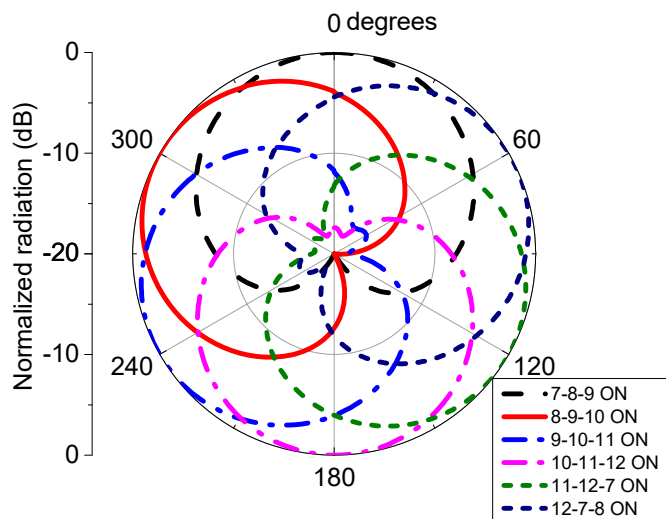
The schematic diagram of Case II is shown in Fig. 3.10 (b). The operating mechanism of Case II is similar to Case I. To make sure all the pin-diodes in outer cylindrical AFSS screen are in OFF state, all the pin-diodes of outer AFSS screen are given zero DC voltage. For the inner cylindrical AFSS screen, three adjacent pin-diodes are on ON state and the others are on OFF state. Then, six radiation patterns are measured at 2.45 GHz and 5.2 GHz, respectively. The measured radiation patterns at 5.2 GHz are shown in Fig. 3.12 (a) and (b), including six different directional radiation patterns. Fig. 3.12 (c) illustrates six similar measured omnidirectional radiation patterns at 2.45 GHz. Hence, beam scanning is realized at 5.2 GHz while the radiation patterns at 2.45 GHz still remain omnidirectional.

The operation methods of Case III are shown in Fig. 3.10 (c) and (d). In order to demonstrate that the proposed antenna is able to scan the entire azimuth plane in 6 steps at 2.45 GHz and 5.2 GHz at the same time, pin-diodes in the outer and inner AFSS screens are supplied with a positive voltage at the same time. In this operation, three adjacent pin-diodes in both cylindrical AFSS screens are given a positive voltage and the others are given zero voltage. In other words, any three adjacent pin-diodes in the outer cylindrical AFSS screen are on OFF state and the others in

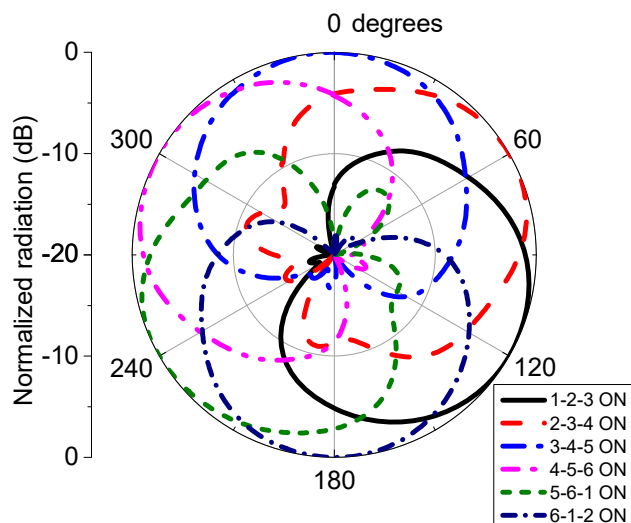
the outer screen on ON state. For the inner AFSS screen, the conditions are set similarly. Therefore, by switching the pin-diodes in different AFSS screens between the ON and OFF states, the radiation pattern has the ability to scan the entire azimuth plane in 6 steps at 2.45 GHz and 5.2 GHz simultaneously.

From the Fig.3.10 (c), the pin-diodes numbered 1, 2 and 6 in the inner AFSS screen are ON and the others in the inner screen are OFF. The pin-diodes numbered 8, 7 and 12 are ON and the others in the outer screen are OFF. Therefore, the beam would aim at the directions of  $60^\circ$  and  $180^\circ$  at 2.45 GHz and 5.2 GHz, respectively. The measured radiation pattern results at two frequencies for the case in Fig.3.10 (c) are shown in Fig.3.13 (a). The measured radiation patterns have a good consistency with the results of theoretical analysis. Fig. 3.13 (b) plots the measured radiation pattern results for the case in Fig. 3.10 (d). Fig. 3.14 plots the simulated results of radiation patterns in the azimuth plane at 2.45 GHz and 5.2 GHz, showing that the measured radiation patterns in Fig. 3.13 have a good agreement with the simulated results. From the measured results in Case III, a clear conclusion can be drawn that these two cylindrical AFSS screens are independent of each other when they are operated in the same antenna system. Hence, the proposed antenna can realize beam-sweeping at 2.45 GHz and 5.2 GHz in  $xz$ -plane simultaneously. In addition, it is noticed that the measured realized gain is smaller than the simulated. The main reason for the difference between the simulated and measured gain could be due to the biasing circuit omitted in the simulation, fabrication tolerances, assembly (such as the size of cylindrical foam and inner cylindrical slots) and measurement errors. Moreover, the actual physical characteristics of the pin-diode enclosure could be another reason for this.

Fig. 3.15 illustrates the simulated and measured reflection coefficients of the proposed antenna in Case III, where a good matching condition is achieved at 2.45 GHz and 5.2 GHz, respectively. From Fig. 3.15, it is seen that the measured results agree well with the simulated ones.



(a)



(b)

**Figure 3.14** Simulated results of radiation patterns in the azimuth plane: (a) 2.45 GHz. (b) 5.2 GHz.

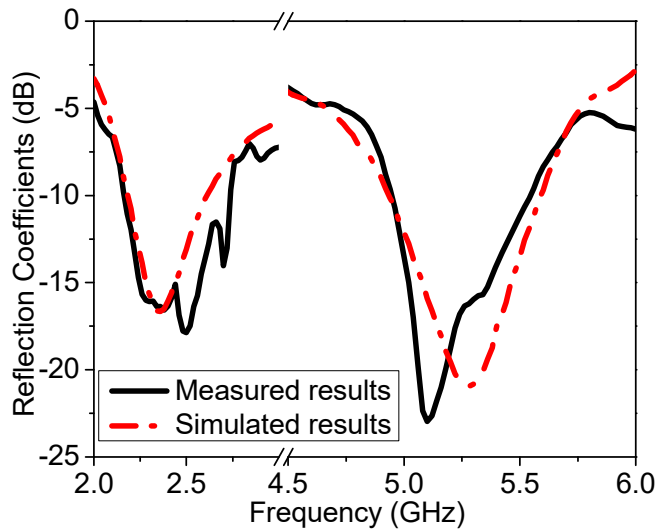


**Figure 3.15** Measured and simulated reflection coefficients in case III.

### 3.6 Conclusion

This chapter has proposed a novel dual-band beam-sweeping antenna based on two frequency independent cylindrical active frequency selective surface (AFSS) screens operated at different frequency bands at 2.45 GHz and 5.2 GHz, respectively. A dual-band omnidirectional monopole antenna has been designed as a radiating source, which is surrounded by two cylindrical AFSS screens. The reflection and transmission characteristics of the proposed two AFSS unit-cells have been investigated. By controlling states of pin-diodes, the transmission and reflection bands of AFSS unit-cells can be changed. Hence, these two cylindrical AFSS screens have been used to implement a sweeping-beam antenna covering all the azimuth angles. The two cylindrical AFSS screens can work independently with each other when they are loaded in the same antenna system. In this way, the size of antenna system can be reduced greatly. Furthermore, the proposed antenna can effectively realize beam-sweeping at 2.45 GHz and 5.2 GHz covering all azimuth angles simultaneously. With a good agreement achieved between the simulated and measured results, the proposed compact dual-band beam-sweeping antenna presents a viable candidate to realize further miniaturization and multifunction of modern communication systems.

## **4 HIGH GAIN WITH FLEXIABLE BEAM NUMBERS ANTENNA DESIGN**

### **4.1 Introduction**

High gain antennas have intensively been investigated because they can be applied in a variety of wireless communication systems, such as cellular base stations, point-to-point and long-range communication links. In general, a high gain antenna has a narrow beamwidth, which means its signal coverage is small. This characteristic can effectively reduce interference. Beam-switching antennas have been proposed whose radiated power is restricted in some prescribed directions rather than transmitting the signal into all the directions. This approach can significantly reduce the effect of interference coming from undesired radiation and improve the system capacity, leading to a good enhancement of the communication system performance [106-110].

During the last decades, various methods for designing beam-switching antennas were reported. The phased antenna arrays as a conventional method have been used to achieve beam-switching antenna, while their complex feed networks made the systems complicated and brought about high cost [23,24,99]. In past several years, more people have been raising their interests in artificial materials/surfaces, such as artificial magnetic conductors (AMCs) [111-113], electromagnetic band-gap (EBG) structures [114-116] and frequency selective surfaces (FSSs) [76, 117]. Recently, applying FSSs to the design of beam-switching antennas has become more popular. FSSs work as space filters to electromagnetic (EM) waves, which can be either transmitted or reflected in the operating frequency band. Furthermore, their transmission or reflection characteristics could be modified in the operating frequency band when they work together with active devices like pin-diodes or varactor diodes. In this way, FSSs could achieve a high level in controlling over EM wave propagation [67-73].

Conventional FSS based beam-switching antennas can change the radiation pattern but do not have a high gain or flexibly control beam number. Liang Zhang et al. [73] have proposed a multi-beam functionality beam steerable antenna system using active frequency selective surfaces. By controlling the bias voltage, both the single-beam mode and the dual-beam mode are achieved; however, the maximum gain is only 7dBi. In chapter 3 we have presented a dual-

band beam switching antenna with FSS at 2.45 GHz and 5.2 GHz. By switching the pin-diodes, the antenna main beam can be switched at two frequencies; however, it could not flexibly control the beam number at operating frequencies.

In this chapter, a gain enhancement and flexible control of beam numbers antenna is proposed. The radiating source is a monopole antenna, which is surrounded by a hexagon FSS screen and six metallic sheets, operates at 5.2 GHz. The transmission characteristics of the proposed FSS unit-cell are investigated for different pin-diode states. The FSS unit-cell with Off-state of pin-diodes has a high transmission coefficient and is almost transparent for incident electromagnetic (EM) waves. The FSS unit-cell with On-state of pin-diodes provides a high reflection coefficient for incident EM waves. The methods of operating at different modes with different beam numbers including single-beam mode and multi-beam modes are discussed. By controlling the states of pin-diodes in different column combinations of the FSS screen, different beam numbers of the proposed antenna can be achieved in the azimuth plane at 5.2 GHz. In addition, six metallic sheets presented in this design are used to shape the radiation pattern for the gain improvement of the proposed antenna. Both simulated and measured results show that the proposed antenna could flexibly control the numbers of beam with good gain. A good matching is also obtained, with this feature, this antenna can be used in WLAN systems at 5.2 GHz.

## 4.2 FSS unit cell design

As the FSS unit-cell is the key element to realize the beam-switching antenna, the design of the FSS unit-cell with reconfigurable transmission coefficients is described in this section. The cross structure is a good candidate due to its simplicity and symmetrical structure, and can provide an acceptable angular and polarization stability. Another reason for applying a cross structure here is that its resonance frequency is lower than strip structure one in a same length, which means the size of the cross FSS unit cell is smaller than the strip unit cell. Thus, two metallic crosses with a pin-diode integrated in the gap are employed in this work. The geometry of the proposed FSS unit-cell is shown in Fig. 4.1 (a), where two RF chokes and biasing circuits are also taken into account in the simulation for the accuracy of simulated results. The RF chokes are used to isolate the RF lines from the DC line during the experiment. This FSS unit-cell is simulated using CST Microwave Studio by locating the unit-cell boundary along the x and y axis with two ports

arranged along the z-direction, shown in Fig. 4.1 (b). The simulated electric field distributions at 2.5 GHz, 4.8 GHz, 5.2 GHz and 5.8 GHz are also shown in Fig. 4.1. The proposed FSS unit-cell structure is printed on RT/duroid® 5880 substrate with a thickness of 0.254 mm and a relative permittivity of 2.2. The final dimensions of the FSS unit-cell are listed in Table 4.1. In the simulation, the pin-diode is modeled with its equivalent RC circuit. For state ON, the diode is modeled as a forward resistance  $R_s = 1.8 \Omega$ . For state OFF, the diode is mainly equal to a capacitance of  $C_p = 0.09 \text{ pF}$  and an inductance of  $L_p = 0.5 \text{ nH}$  in series.

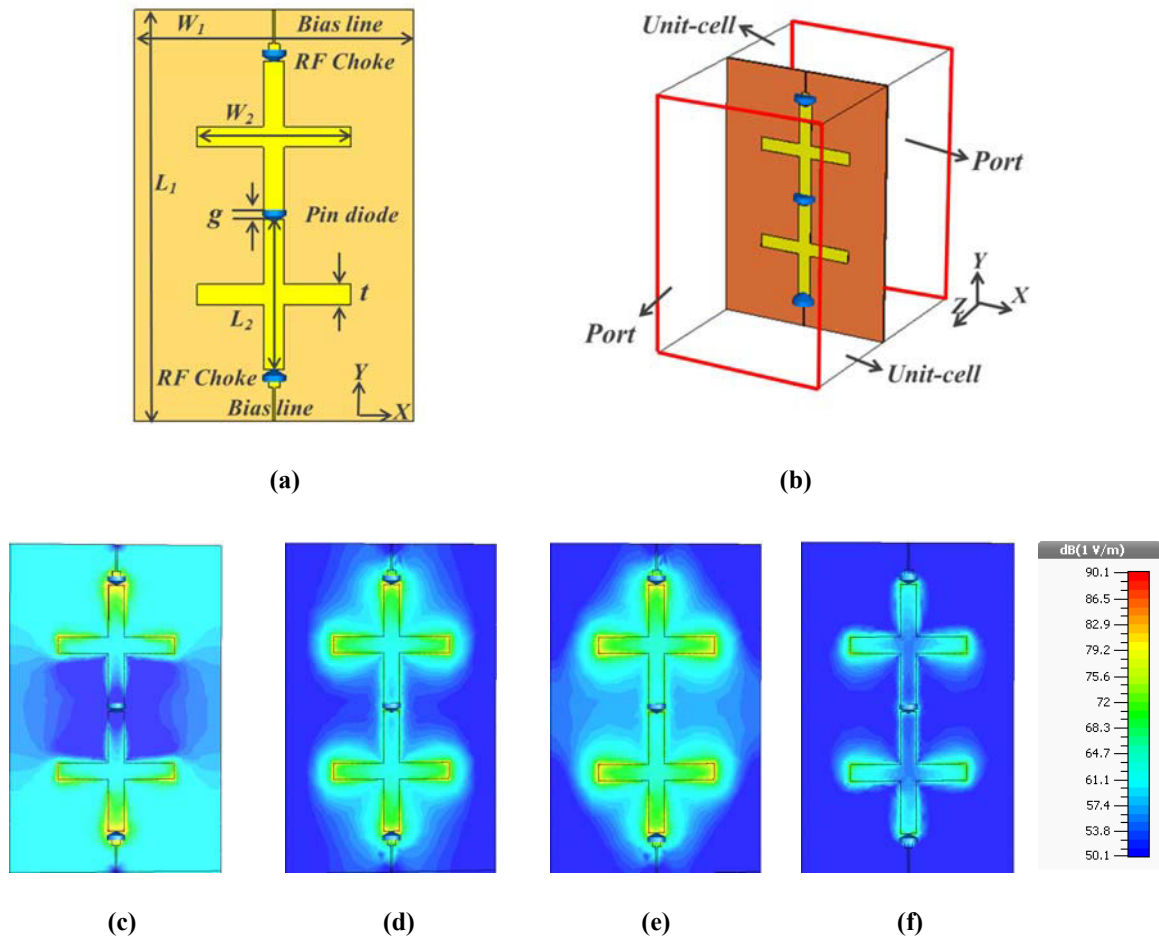


**Figure 4.1** (a) Geometry of FSS unit-cell. (b) Configuration of FSS unit-cell simulation. (c) E-field distribution at 2.5 GHz. (d) E-field distribution at 4.8 GHz. (e) E-field distribution at 5.2 GHz. (f) E-field distribution at 5.8 GHz.

Switching the pin-diode ON and OFF states makes two metallic crosses either connected or isolated electrically. As a result, the transmitting characteristics of the FSS unit-cell can be changed. The simulated transmission coefficients of the FSS unit-cell in different pin-diode states are plotted in Fig. 4.2, illustrating that this FSS unit-cell provides a band-stop and band-pass at 5.2 GHz when the pin-diode is ON and OFF, respectively. This means electromagnetic waves are reflected and transmitted depending on the diode state.

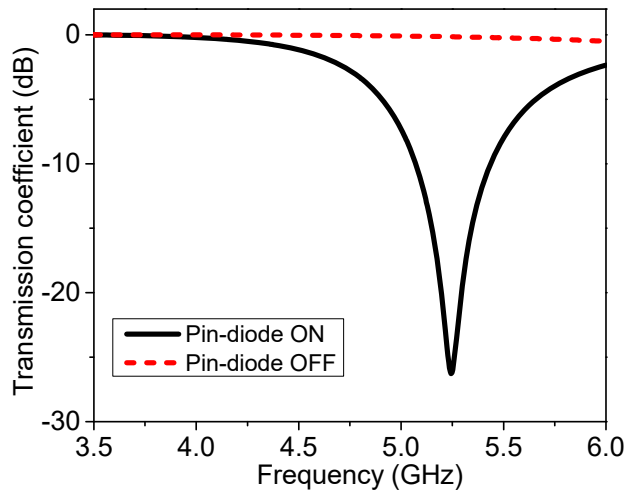


**Figure 4.2** Simulated transmission coefficients of FSS unit-cell in different pin-diode states.

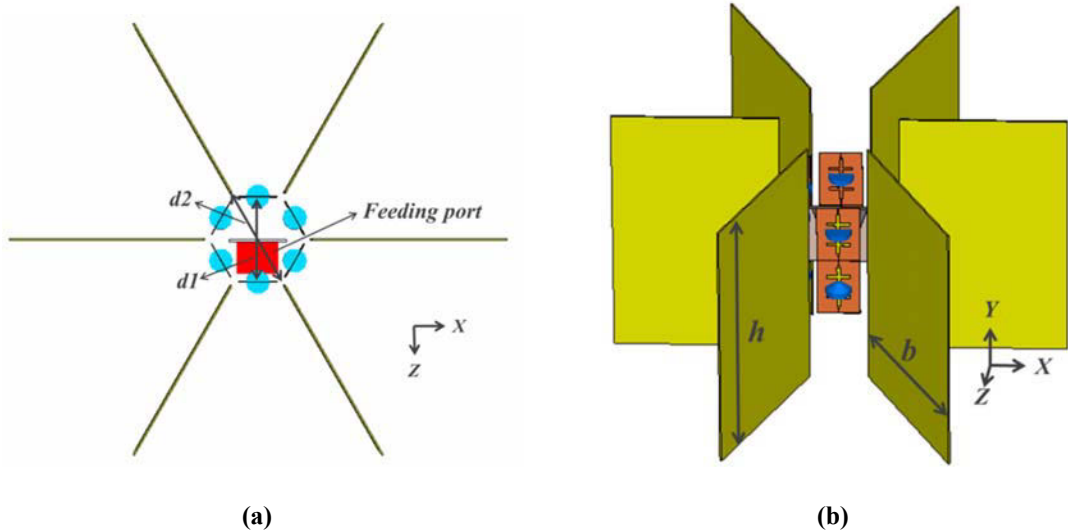
**Table 4.1** Final dimensions of FSS unit cell (unit:mm).

Parameters	$W_1$	$L_1$	$W_2$	$L_2$	$g$	$t$
Value	20	30	11	11	0.5	1.5

### 4.3 Beam-switching antenna design with high gain

The schematic of the proposed beam-switching antenna is shown in Fig. 4.3. This proposed antenna is composed of a monopole antenna as an excitation source, a reconfigurable hexagon FSS screen and six metallic sheets placed around this monopole antenna. This antenna is divided into six equal portions by the hexagon FSS screen together with six metallic sheets. The hexagon FSS screen has 6 columns inside, each includes two FSS unit-cells with two pin-diodes, described in Section 4.2. Through a parametric optimization based on a comprehensive study on

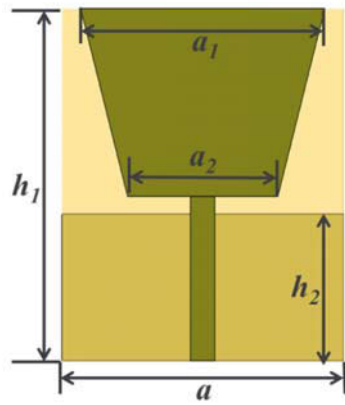
the gain, matching of antenna and 3 dB beamwidth, the final dimensions of the entire antenna structure are given as follows:  $d1 = 41$  mm,  $d2 = 56$  mm,  $h = 130$  mm and  $b = 100$  mm.



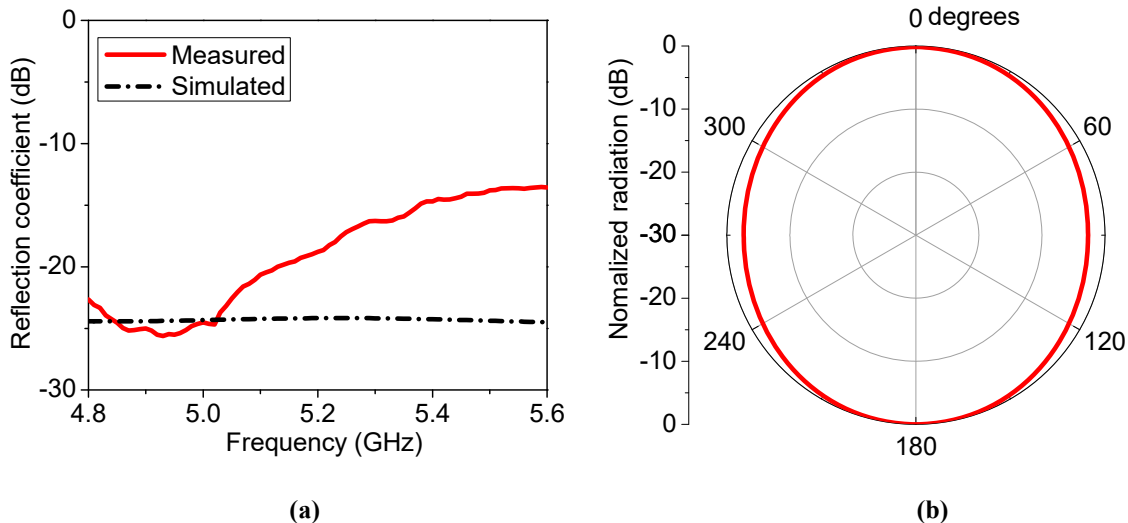
**Figure 4.3** Proposed beam-switching with high gain antenna structure: (a) Top view, (b) Side view.

#### 4.3.1 The excitation source

In this work, an omnidirectional monopole antenna operating at 5.2 GHz is employed as an excitation source, as shown in Fig. 4.4, which is similar to the antenna reported in [118]. The difference between them lies in the substrate. This monopole antenna is composed of an inverted trapezoid element as a main resonator and a small ground plane on the bottom of the substrate, which is fed by a microstrip line. It is selected here for its simple structure, low loss, light weight, easy fabrication, and ability to provide an omnidirectional radiation pattern in the azimuth plane at 5.2 GHz, which is required to realize beam-switching. This monopole antenna is constructed on RO4350B substrate with a relative dielectric constant of 3.66 and a thickness of 1.5 mm, with its geometry parameters given as follows:  $a1 = 26$  mm,  $a2 = 16$  mm,  $a = 30$  mm,  $h1 = 30$  mm, and  $h2 = 12.5$  mm.

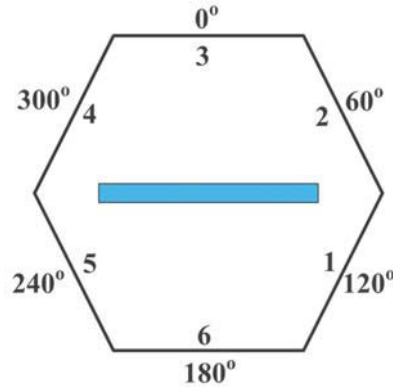


**Figure 4.4** Structure of the monopole antenna.



**Figure 4.5** Simulation results of the monopole antenna: (a) Reflection coefficient. (b) Normalized radiation pattern at 5.2 GHz.

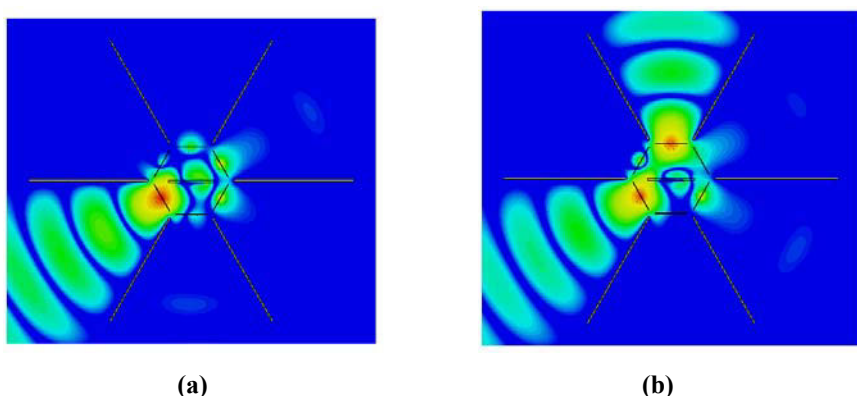
The simulated and measured reflection coefficient and normalized radiation pattern are shown in Fig. 4.5 (a) and Fig. 4.5 (b), respectively. It is clear that this monopole antenna has a wide bandwidth and performs a good impedance matching at 5.2 GHz. Moreover, an omnidirectional radiation pattern is achieved at 5.2 GHz.

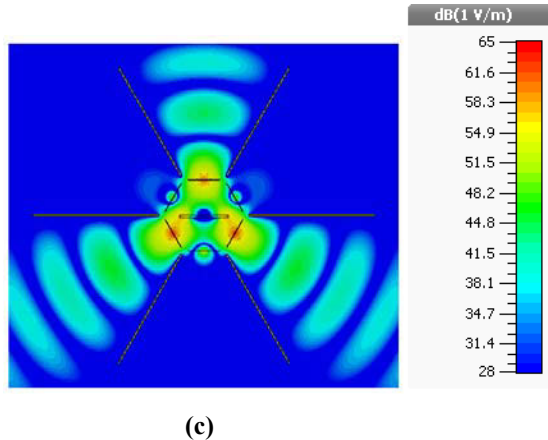


**Figure 4.6** Simulation results of the monopole antenna: (a) Reflection coefficient. (b) Normalized radiation pattern at 5.2 GHz.

#### 4.3.2 Mechanism of the beam-switching antenna with gain enhancement

As the proposed beam-switching antenna is divided into six equal portions by the hexagon FSS screen and six metallic sheets, a schematic diagram of the proposed antenna is shown in Fig. 4.6. The number from 1 to 6 represents the six columns of the hexagon FSS screen and the blue rectangle in the center represents the monopole antenna. To realize the beam-switching antenna with flexible beam numbers, the following operation mechanism is taken. For the single-beam mode, in each step of operation, the pin-diodes in one column are in OFF state and the other pin-diodes in the rest columns are in ON state. As analyzed in Section 4.2, the FSS unit-cell with OFF-state diodes has a high transmission coefficient and the unit-cell with ON-state pin-diodes provide a high reflection coefficient. Hence, the electromagnetic waves radiated from the central monopole antenna can transmit through the OFF-state column and are blocked by the ON-state columns. In this way, by switching pin-diodes between ON and OFF-states in each FSS column, the radiation pattern is able to scan the azimuth plane in the 6 steps at 5.2 GHz.





(c)

**Figure 4.7** E-field distribution of the antenna at 5.2 GHz: (a) Single-beam mode. (b) Two-beam mode. (c) Three-beam mode.

Moreover, multi-beam modes can also be achieved by changing the states of the pin-diodes in different column combinations. When the pin-diodes in any two columns are in OFF states and the pin-diodes in the rest columns are in ON states, two beams radiation pattern can be achieved. Using the same operation method, three beams can be also obtained. Thus, the proposed antenna can flexibly operate at single-beam mode and multi-beam modes. Fig. 4.7 depicts the simulated E-field distribution of single-beam mode, two-beam mode and three-beam mode at 5.2 GHz in xz-plane, which agrees well with the design principle. In addition, six metallic sheets are loaded vertically surrounding the outside of the monopole antenna in this design, which is used to shape the radiation pattern for improving the gain of the proposed antenna. Consequently, the proposed antenna can flexibly control beam numbers.

#### 4.4 Parametric studies

Parametric studies are described in this section. The reflection coefficient of the antenna is mostly affected by the parameters  $d1$  and  $d2$  shown in Fig. 4.3 and they also have a minor effect on the gain of the proposed antenna. The parameter  $d1$  is the distance between two opposite FSS unit-cells in the hexagon FSS screen and the parameter  $d2$  is the distance between two opposite metallic sheet. The effect of the parameters  $d1$  and  $d2$  on the reflection coefficients and gain of the antenna are illustrated in Fig. 4.8 and Fig. 4.9, respectively. Fig. 4.8 (a) shows that the matching of the antenna becomes worse when increasing  $d1$ , while Fig. 4.8 (b) clearly shows that the maximum gain is achieved when  $d1$  is set as 41mm ( $0.7 \lambda$ ) at 5.2 GHz. Hence, the optimal value of  $d1$  for our application is 41mm. From Fig. 4.9, it can be seen that the reflection

coefficient of the antenna can be modified by changing the value of  $d_2$ . The maximum gain is achieved when  $d_2$  is given 56 mm with good matching at 5.2 GHz. Hence, the optimal value of  $d_2$  for our application is 56 mm.

Since the parameters of length ( $b$ ) and height ( $h$ ) of the metallic sheet mainly influence the 3 dB beamwidth and the antenna gain, it is necessary to investigate them separately. Fig.4.10 shows the radiation pattern of the antenna in the  $xz$ -plane at 5.2 GHz with different lengths of the metallic sheet. The results clearly show that the 3 dB radiation beamwidth reduces when increasing the  $b$  value.

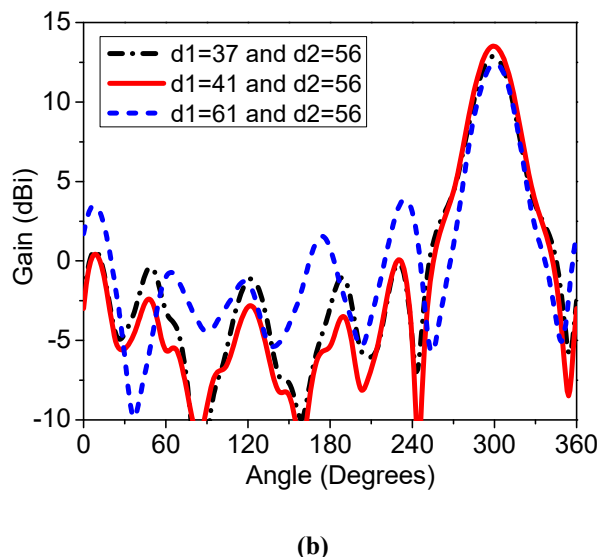
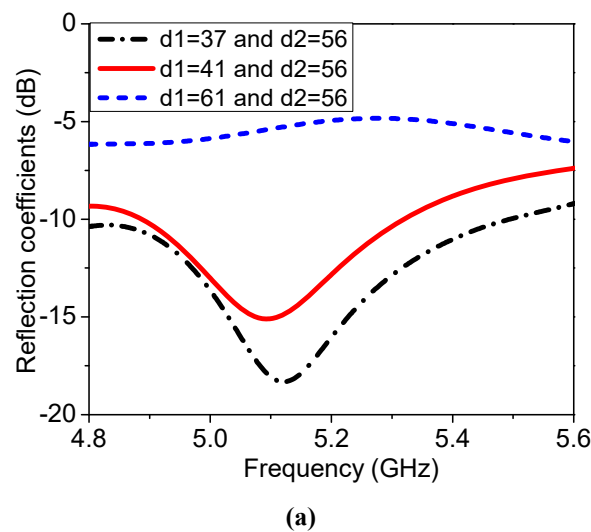
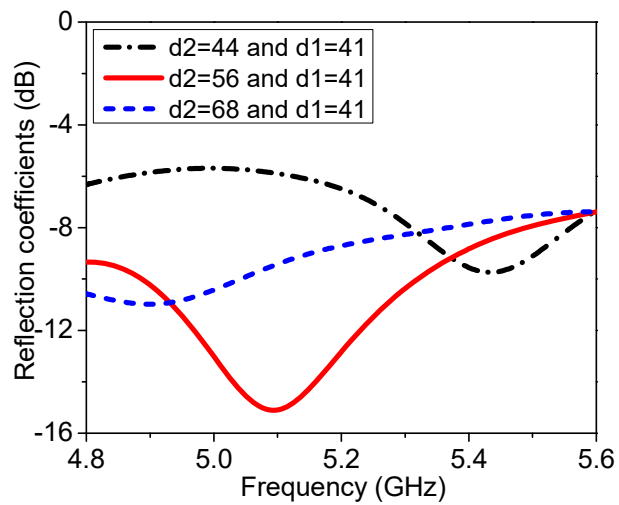
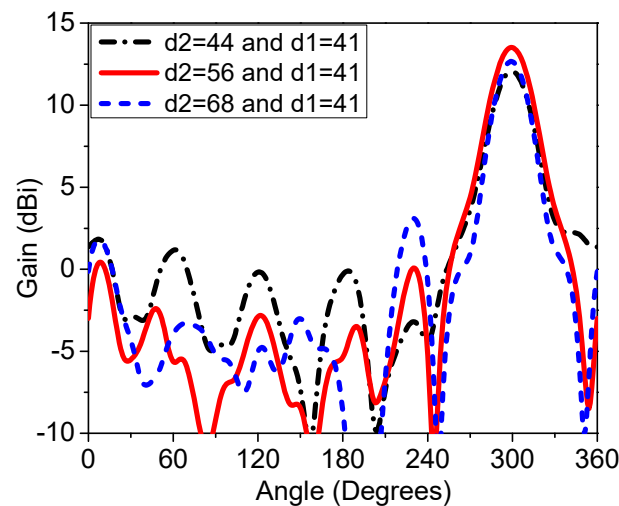


**Figure 4.8** The effect of  $d_1$  on the proposed antenna performances: (a) Reflection coefficients. (b) Gain.



(a)



(b)

Figure 4.9 The effect of  $d_2$  on the proposed antenna performances: (a) Reflection coefficients. (b) Gain.

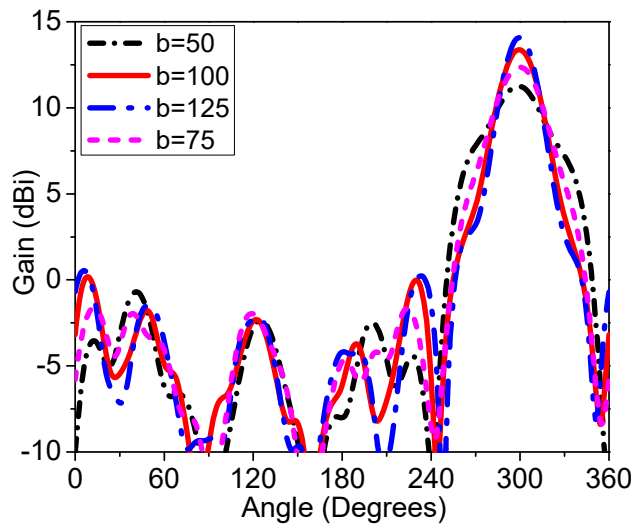


**Figure 4.10** The effect of  $b$  on the radiation patterns of proposed antenna.

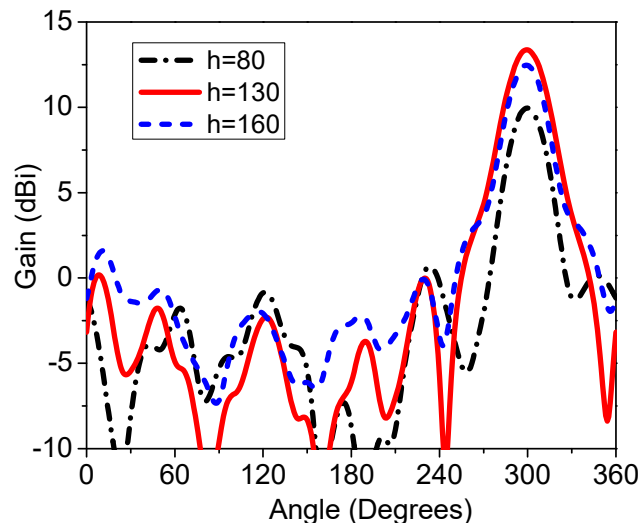


**Figure 4.11** The effect of  $h$  on the radiation patterns of proposed antenna.

The reason is that the radiating aperture in xz-plane increases with increasing the value of  $b$ . Hence, taking into account the whole size of antenna, the beamwidth and gain, the value of  $b$  is chosen as 100 mm, leading to a beamwidth of 30 degrees with gain of 13.5 dBi at 5.2 GHz. As indicated above, the height of the metallic sheet mainly affects the gain of the antenna. The effect of the variation of  $h$  on the radiation patterns of the antenna is illustrated in Fig. 4.11. These results clearly indicate that the maximum gain is obtained in xz-plane at 5.2 GHz, when the height  $h$  is 130 mm. With all the analysis results in this section, the final antenna dimensions are

given in Section 4.3. Moreover, the radiation patterns of the beam-switching antenna with and without metallic sheets in  $xz$ -plane at 5.2 GHz are shown in Fig.4.12, demonstrating that the 7 dB gain enhancement is achieved by comparing the gain values of the beam-switching antennas with and without metallic sheets.

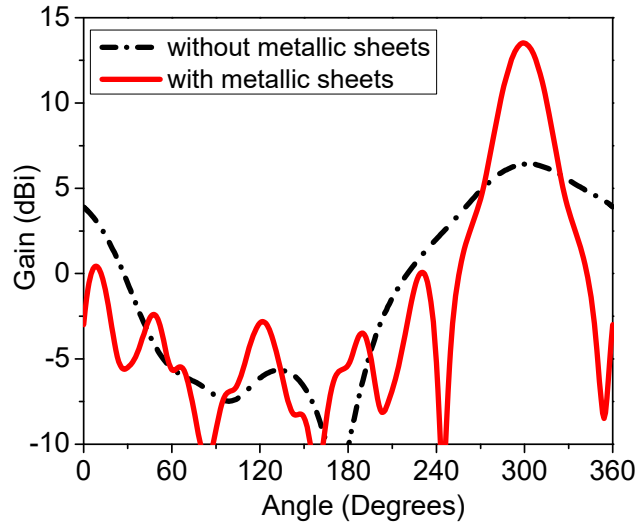
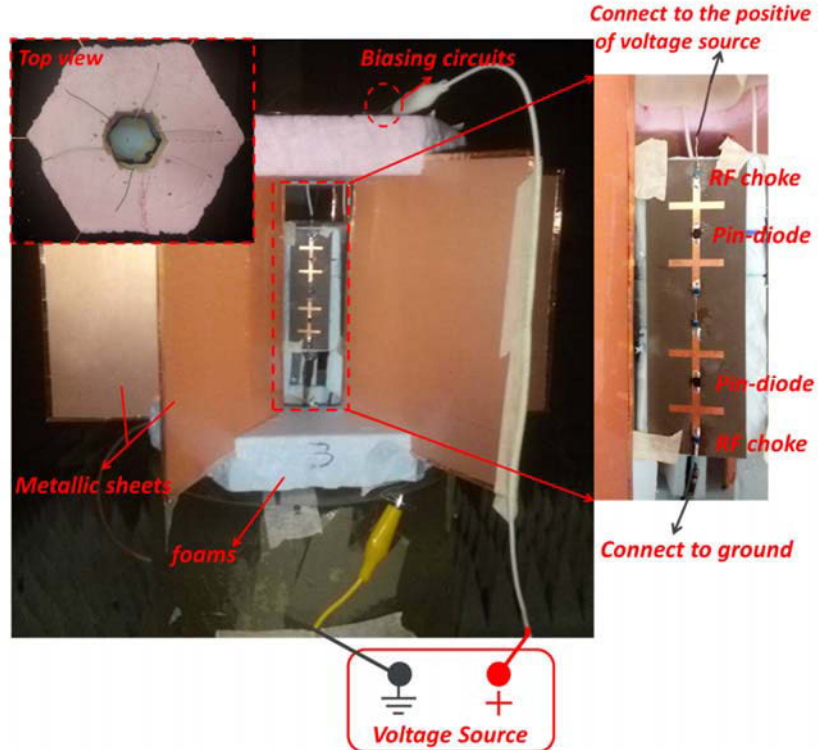


**Figure 4.12** Simulated radiation patterns of antenna with and without metallic sheets in the azimuth plane at 5.2 GHz.

## 4.5 Fabrication and measurement results

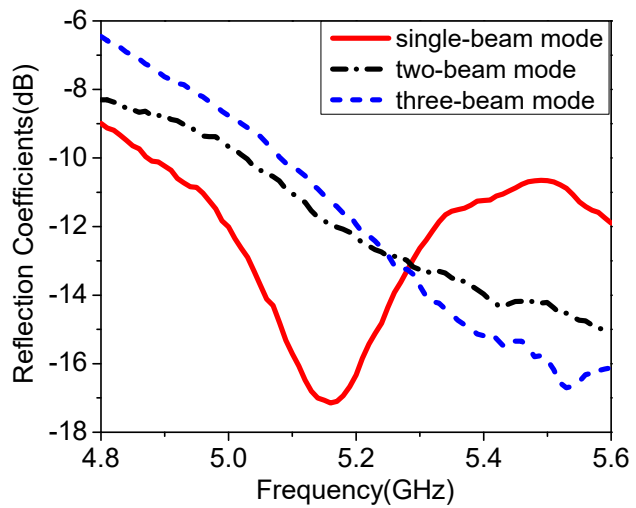
To validate the performance of the proposed concept, an experiment prototype was fabricated and its performances were measured. The photograph of the fabricated prototype antenna in an anechoic chamber is given in Fig. 4.13. The hexagon FSS screen is printed on substrate RT/duroid® 5880 with a permittivity of 2.2 and thickness of 0.254 mm. As shown in Fig. 4.13, six FSS unit-cells are wrapped onto the hexagon foam. Furthermore, there is a centered rectangular aperture in the hexagon foam to accommodate the monopole antenna which is fed through a coaxial cable from the bottom of the structure. Twelve high frequency pin-diodes GMP-4201 from Microsemi are inserted into the FSS screen [105]. RF chocks with 18 nH from Murata are employed in the FSS screen to isolate the RF signal from biasing lines. The pin-diodes in each column of the FSS screen are fed with DC feeding lines from the top and bottom. The DC voltage is supplied by an external voltage source during the measurements. The pin-diodes in one column of the FSS screen are in OFF state, when the DC voltage is supplied zero

to this column. When the DC voltage is given 2.15 V to one column of the FSS screen, the pin-diodes in this column are in ON state.

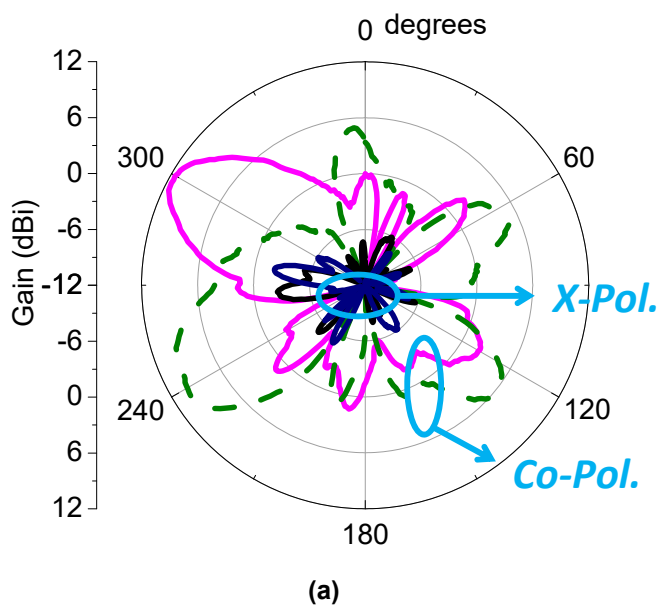


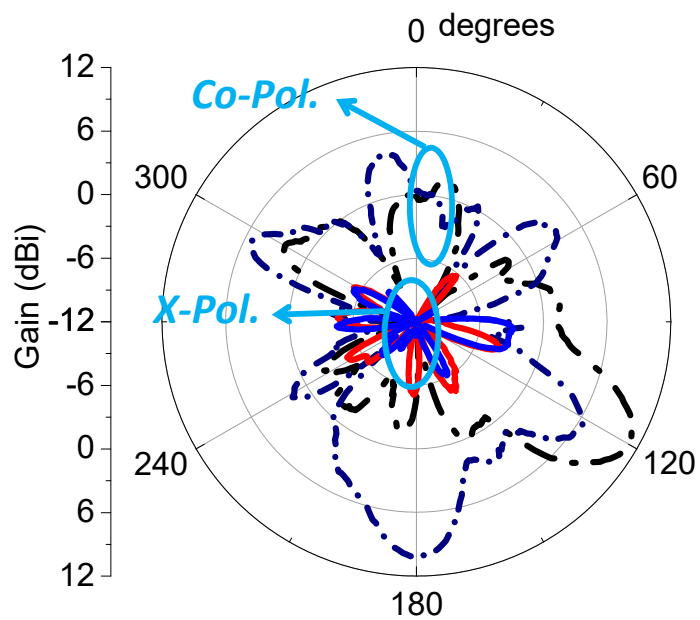
**Figure 4.13      Photograph of the fabricated antenna in anechoic chamber.**

To validate the proposed antenna concept with flexible controlling beam numbers, the measurement methods are divided into three modes including single-beam mode, two-beam mode and three-beam mode. For the single-beam mode measurement, one column is supplied zero DC voltage and the others are given positive voltage, which means that the pin-diodes in zero voltage column are in OFF states and the pin-diodes in positive voltage columns are in ON states. Therefore, from the analysis in Section 4.3.2, the radiation pattern of the proposed antenna can be switched in six directions in the azimuth plane at 5.2 GHz by supplying the zero voltage to each column in turn. For the multi-beam modes (two-beam and three-beam modes), when any two or three columns of the FSS screen are given zero voltage and the others are supplied positive voltage, the two beams and three beams radiation patterns of the proposed antenna can be achieved.

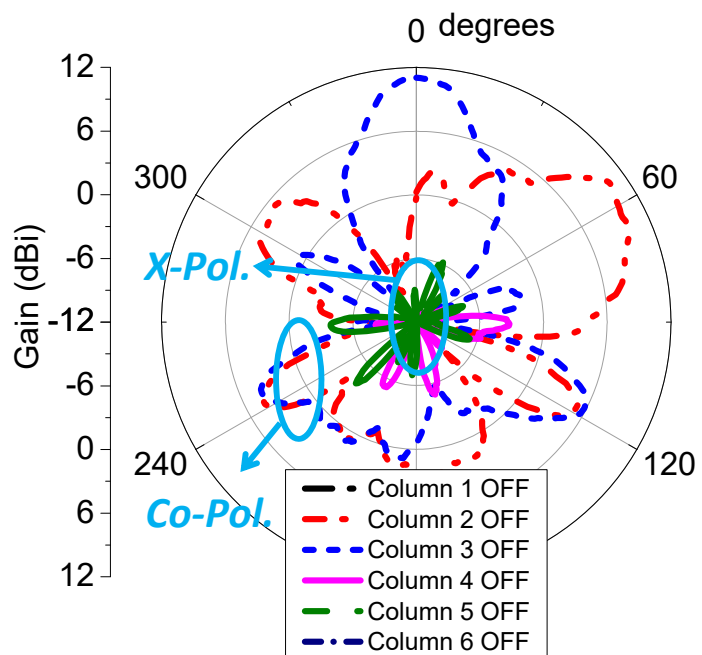


**Figure 4.14** Measured reflection coefficient results of proposed antenna in different modes.





(b)



(c)

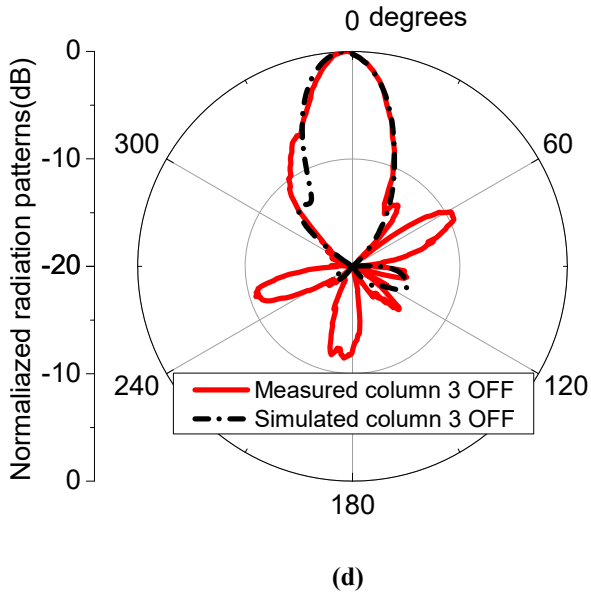


**Figure 4.15** Fig.15 Measured radiation patterns of a single-beam mode at 5.2 GHz: (a), (b) and (c) in azimuth plane, (d) in elevation plane.

The reflection coefficient is measured using Agilent 8722ES vector network analyzer. The measured reflection coefficients of the single-beam mode and multi-beam modes are shown in Fig. 4.14, indicating that there is a good matching over 4.8-5.6 GHz. Furthermore, it can be observed that there is a perfect matching at the resonant frequency of 5.2 GHz and the single-beam mode has a better matching than the multi-beams mode.

The radiation patterns are measured in an anechoic chamber. Fig.4.15 (a), (b) and (c) shows the measured radiation patterns of a single-beam mode in the azimuth plane at 5.2 GHz. The simulated and measured radiation patterns when the pin-diodes in column 3 are in OFF state in elevation plane at 5.2 GHz are shown in Fig.4.15 (d). It is clear that six different directional beams with a 3dB beamwidth of 30 degrees in the azimuth plane are obtained at 5.2 GHz. The 3dB beamwidth of this proposed antenna is much smaller compared to one in [67], which means this proposed antenna has a higher angular resolution for beam-switching application.

The simulated and measured radiation patterns when the pin-diodes in column 4 are in OFF state at 5.2 GHz are shown Fig.4.16. The results clearly show that measured results agree very well with the simulated ones. Fig. 4.17 shows the simulated and measured radiation patterns of two-beam mode at 5.2 GHz in azimuth plane. From the Fig. 4.6 and previous analysis, the beam directions of proposed antenna should be 0 degree and 180 degrees when the pin-diodes in

columns 3 and 6 are OFF. Fig.4.17 (a) depicts the simulated and measured radiation patterns when the pin-diodes in columns 3 and 6 are OFF. From the results, it is seen that the two beams are in the directions of 0 and 180 degrees, respectively, which agrees well with the design principle. Moreover, the experimental results also clearly show that measured result agrees very well with the simulated one. Fig.4.17 (b) and (c) shows the simulated and measured radiation patterns when the pin-diodes in columns 1, 3 are OFF and those in columns 1, 4 are OFF. It is clearly seen that the measured results match well with simulated ones. Additionally, it is noticed that the measured beamwidth of the beam pointing to 120 degrees is narrower than the simulated one. The main reason for this difference could be attributed to the assembly tolerance and errors. The simulated and measured radiation patterns of three-beam mode at 5.2 GHz in azimuth plane are shown in Fig.4. 18, which shows that the directions of the three beams are 0 degree, 120 degrees and 240 degrees, respectively. It also can be seen that the measured radiation pattern of the three-beam mode is in agreement with the simulated ones, except that the measured beamwidth of the beam pointing to 120 degrees, which is narrower than the simulated one because of the assembly tolerance and errors. Hence, from these measured radiation patterns, it is proved that the proposed antenna can flexibly operate at different beam numbers modes including a single-beam, two-beam and three-beam modes.

The gain of the proposed antenna is also measured by the comparison method, and listed together with the simulated gain in Table 4.2. It can be seen that the measured gain is 11.54 dBi, 9 dBi and 7.34 dBi in the single-beam mode, the two-beam mode and three-beam mode, respectively, at 5.2 GHz. It is also found that the measured gain is less than the simulated one. The fabrication tolerance, assembly and measurement errors could be the main reasons for the difference between the simulated and measured gain. Moreover, the actual physical characteristics of the pin-diode enclosure could be another reason for this.

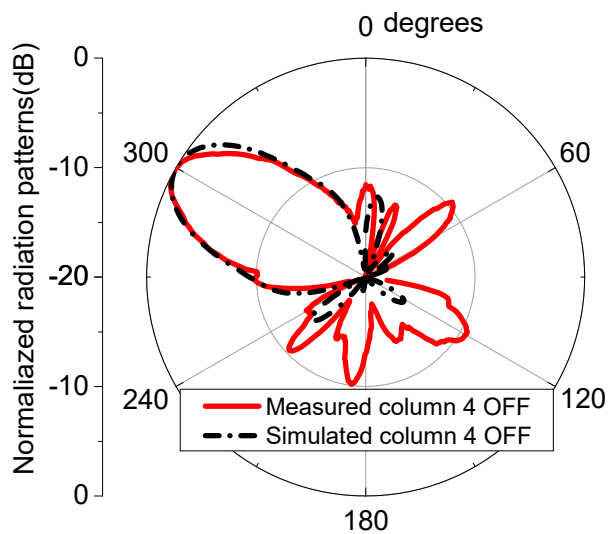
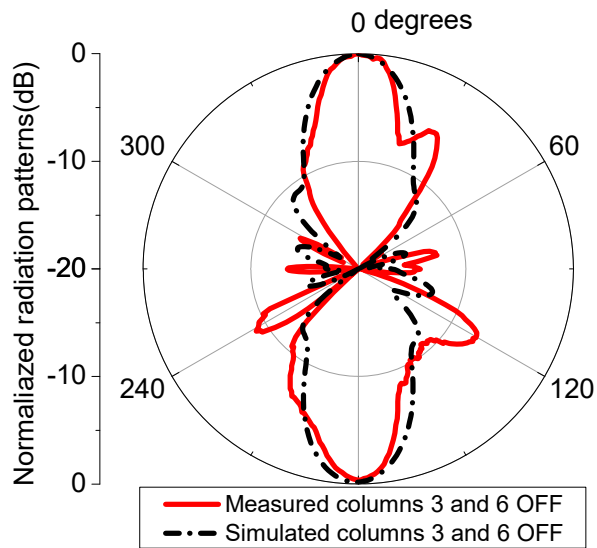
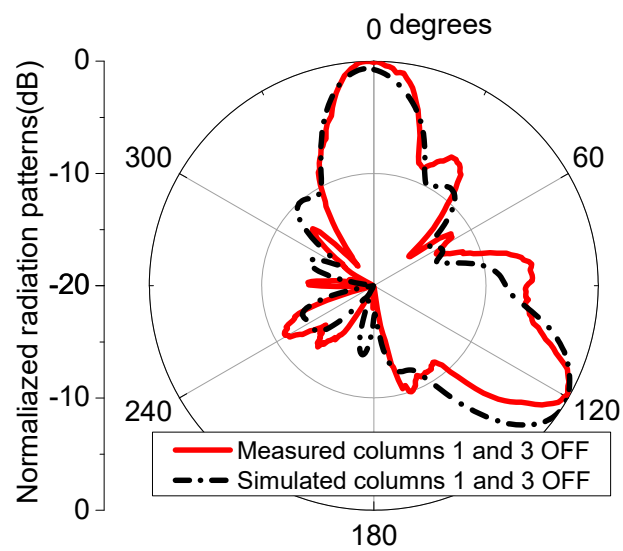


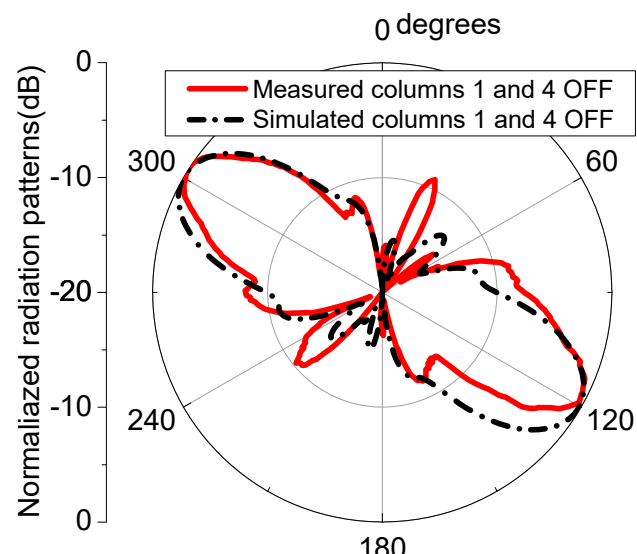
**Figure 4.16** Simulated and measured radiation patterns of single-beam mode when column 4 OFF at 5.2 GHz in azimuth plane.



(a)



(b)



(c)

**Figure 4.17** Simulated and measured radiation patterns of two-beam mode at 5.2 GHz in azimuth plane:  
 (a) Columns 3 and 6 OFF. (b) Columns 1 and 3 OFF. (3) Columns 1 and 4 OFF.

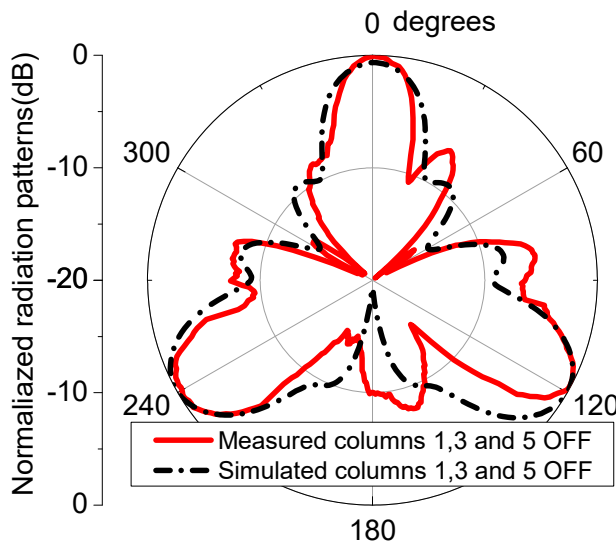


**Figure 4.18** Simulated and measured radiation patterns of three-beam mode at 5.2 GHz in azimuth plane when column 1, 3 and 5 OFF.

**Table 4.2** The simulated and measured gain of different modes.

Gain (dBi)	Single-beam mode	Two-beam mode	Three-beam mode
Simulation	13.5	10.7	9.01
Measurement	11.54	9.0	7.34

## 4.6 Conclusion

This chapter has presented a beam-switching antenna with gain enhancement and flexibly controlling beam numbers based on frequency selective surfaces (FSSs) operated at the resonating frequency of 5.2 GHz. A centered omnidirectional monopole antenna has been designed as a radiating source which is surrounded by a proposed hexagon FSS screen and six metallic sheets. From the experimental results, the proposed antenna with a high gain (11.54 dBi) is effectively operating at 5.2 GHz. The maximum gain of the antenna enhancement of 7 dB has been achieved when the six metallic sheets applied. By changing the states of pin-diodes in different column combinations of the hexagon FSS screen, this proposed antenna has realized a single-beam switching in six directions and multiple beams at 5.2 GHz in the azimuth plane with

low voltage (2.15 V). Furthermore, the measured results have shown a good agreement with the simulated ones. With these features, the proposed antenna is a good candidate for modern communication systems.

## **5 BEAM-TILTING ANTENNA WITH METAMATERIAL LOADING DESIGN**

### **5.1 Introduction**

Radiation pattern reconfigurable antennas have extensively been employed in the wireless communication systems to solve the interference problem. As one kind of radiation pattern reconfigurable antennas, beam-tilting antennas have been investigated as an effective technique to reduce co-channel interference. These antennas can significantly decrease the rate of interfering signals and enhance the system capacity by controlling the beam tilt angle of a beam-tilting antenna, which is a key design parameter [119].

Various methods to design beam-tilting antennas have been reported. Most conventional methods for beam steering purpose include electronic and mechanical techniques. In [120], the H-shaped units with the pin-diodes between them are arranged on both sides of the dipole antenna to direct the power flow in the end-fire direction. Different radiation patterns can be achieved by changing the states of these Pin-diodes. In [103], a microstrip antenna integrated with four Pin-diodes was presented. By changing the states of four Pin-diodes, four different radiation patterns are achieved. The mechanical beam-tilting approaches usually use mechanical installation frame work, which can increase the complexity, size and cost of the design. Recently, metamaterials, as a sort of artificial material, have attracted considerable interest because of their unique EM properties that are distinct from those of natural materials. Metamaterials have been exploited in antenna design and realization for many different applications, such as beam-tilting [119, 121-122], directivity and gain enhancement [123-125, 126-129]. In [121], a bow-tie antenna loading with metamaterial H-shaped unit-cell structures to implement beam-tilting has been presented. The main beam of this antenna can tilt 17 degrees in the E-plane at 7.7 GHz.

In this chapter, a novel beam-tilting antenna loading with the proposed metamaterial unit-cells is presented. The proposed metamaterial unit-cells are used to create a negative refractive index medium, which plays a key role in the beam-tilting mechanism. The proposed beam-tilting antenna consists of a double-feed DRA and  $1 \times 4$  NRIM array fixed by nylon studs over the DRA. The measurement results confirm that the direction of the proposed antenna's maximum beam

can be tilted by  $\pm 38^\circ$  in the xoz-plane. Moreover, the measured reflection coefficient of proposed antenna is better than -10 dB in the band from 5 to 5.5 GHz.

## 5.2 Beam tilting antenna design

### 5.2.1 NRIM Unit-cell design

The proposed NRIM unit-cell, shown in Fig. 5.1 (a), consists of a fractal cross ring resonator structure printed on a Rogers RT/duroid 5880 substrate with the thickness of  $h = 0.254$  mm, permittivity of 2.2, and tangent-loss of 0.0009. In comparison with the fractal ring reported in [118], the NRIM unit-cell in this work has different size, substrate and geometric shape to realize a negative refractive index in the band of 5-5.5 GHz. This structure is chosen because it is symmetric and so can support dual-polarization operation. Furthermore, the fractal structure is compactly designed, which fulfills the requirements of high integration of modern communication systems. The NRIM unit-cell was simulated using CST Microwave Studio with the unit-cell boundary conditions applied along the xz and yz. The two ports are located along the z-direction. After optimization, the final dimensions of the proposed NRIM unit-cell are:  $W = 25$  mm,  $L = 25$  mm,  $W1 = 1.5$  mm,  $L1 = 2.35$  mm,  $W2 = 1.25$  mm,  $L2 = 1.25$  mm,  $W3 = 2.35$  mm,  $L3 = 8.4$  mm,  $t = 0.9$  mm. The transmission and reflection coefficients of the proposed NRIM unit-cell are plotted in Fig. 5.1 (b), clearly showing that the unit-cell has a very low transmission coefficient operated at 5.2 GHz. The simulated S-parameters of the unit-cell are used to extract the effective relative permittivity, permeability and refractive index [130]. The extracted refractive index of the proposed NRIM unit-cell as a function of frequency is shown in Fig. 5.2 (a). It is clear that the proposed unit-cell provides a stable negative refractive index from 5 to 5.5 GHz frequency range. It can be seen that the real part of refractive index of the structure is about -1.4. Fig. 5.2 (b) reveals the extracted effective permittivity and permeability of the NRIM unit-cell.

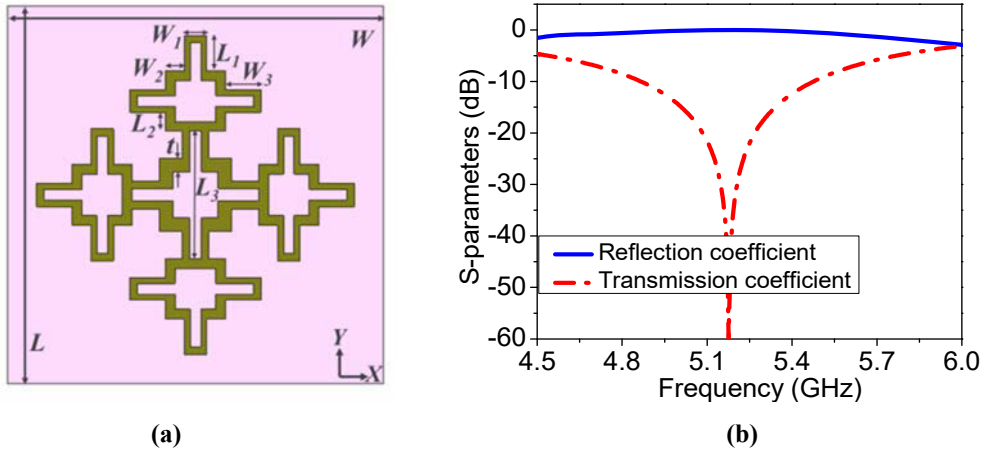


**Figure 5.1** (a) Prototype of proposed negative refractive index metamaterial (NRIM) unit-cell, and (b) S-parameters of the proposed NRIM unit-cell.

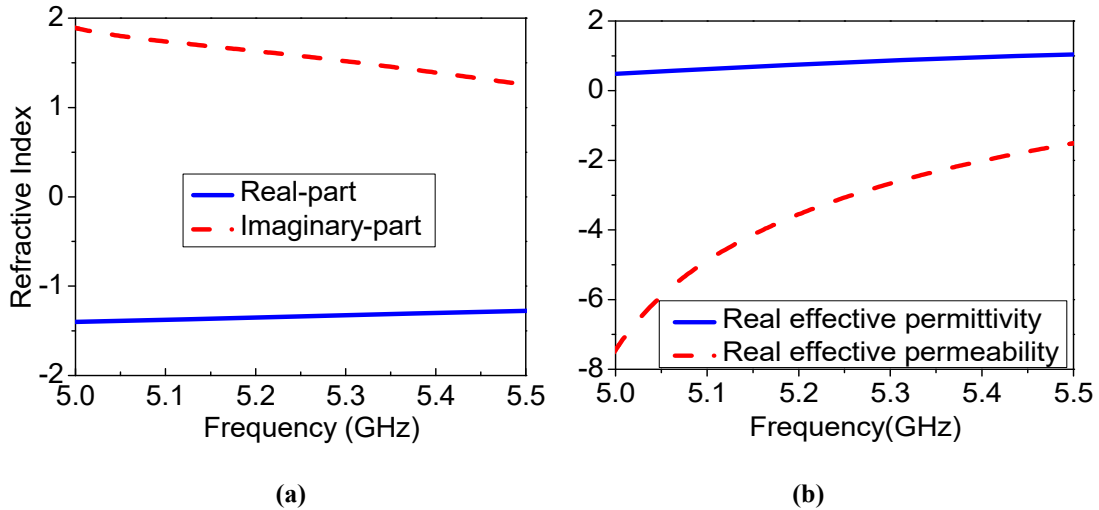


**Figure 5.2** (a) Refractive-index of proposed the NRIM unit-cell as a function of frequency, and (b) Extracted permittivity and permeability of the NRIM unit-cell.

### 5.2.2 Double-feed dielectric resonator antenna

Because of its high-radiation efficiency and low conductor losses, the DRA is selected as the radiation source in this section. The geometry of the proposed double-feed DRA shown in Fig.5.3 (a) essentially consists of two same cylindrical dielectric resonators made of Rogers RT/duroid 6010 with permittivity of 10.7 and tangent-loss of 0.0023. The cylindrical dielectric resonators has a diameter of 14.4 mm and a height of 10.16 mm, which is placed on the ground plane of the Rogers RO4350B substrate with a thickness of 0.762 mm, permittivity of 3.66, and tangent loss of 0.004. Each DRA is fed through a slot by  $50 \Omega$  microstrip line printed on the

bottom of Rogers RO4350B substrate. The energy is coupled into the DRA through the rectangle resonant slot which has a length of 11 mm and a width of 2 mm on the ground plane. The normalized radiation patterns of the DRA fed by different ports in the xoz-plane are shown in Fig. 5.3 (b).

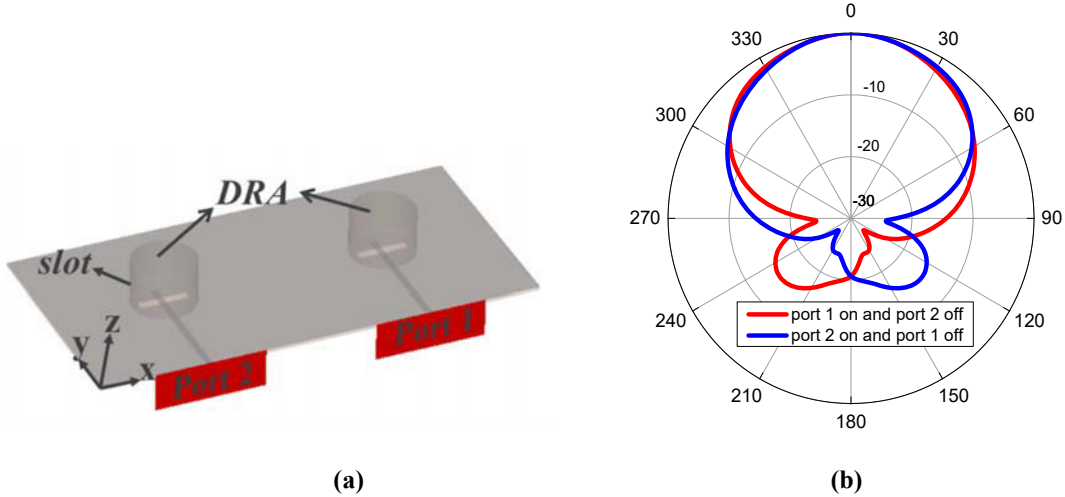


**Figure 5.3** (a) Geometry of the proposed double-feed DRA, and (b) Its normalized radiation pattern in the xoz-plane.

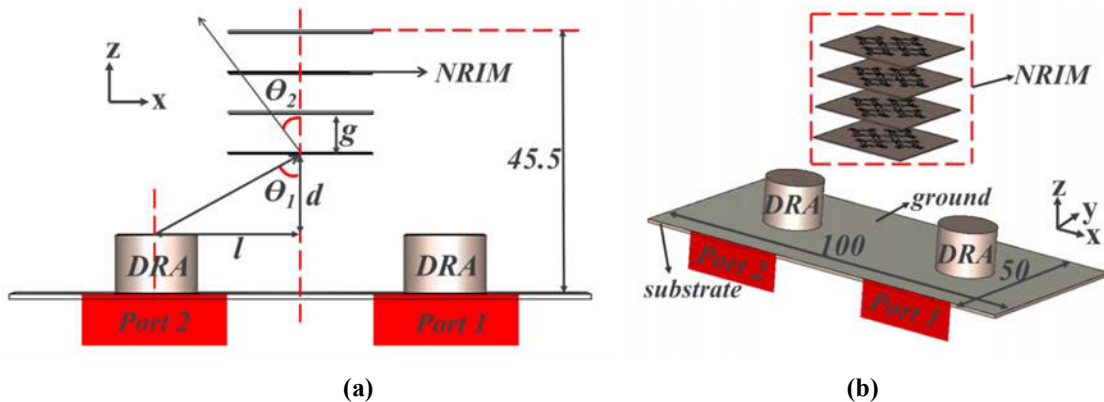


**Figure 5.4** 3D configuration of double-feed DRA with  $1 \times 4$  proposed NRIM array loading. (a) Front view, and (b) Side view. (Unit: mm).

### 5.2.3 The DRA with NRIM Loading

The characteristics of antenna are studied when the  $1 \times 4$  NRIM array is placed on the top of the DRA in z-direction, and fixed in the middle of double-feed DRA, as shown in Fig. 5.4. The key parameters of the combination of the DRA and NRIM have been optimized. As shown in Fig. 5.4 (a), it is clear that the degree of  $\theta_1$  is decided by  $d$  and  $l$ . Hence, the parameters of  $d$  and  $l$

have an influence on the angle of the beam tilting. The parameter of  $g$  represents the distance between the NRIM layers, which has an influence on the gain of the antenna. The final optimized key parameters are given as follows:  $d = 14$ ,  $l = 25$ , and  $g = 7$ . Furthermore, the effects of different number of NRIM layers on the antenna gain, the main beam direction, side-lobe level and 3dB beamwidth are given in Table 5.1. The results indicate that a higher gain is obtained when the layer number increases. The number of layers has little influence on the main beam direction. Additionally, the 3 dB beamwidth decreases with the increase of the number of the NRIM layers. It is found that the better performance of the antenna can be achieved when four NRIM layers are employed. Fig. 5.5 plots the radiation pattern of the double-feed DRA in the xoz-plane with and without the NRIM array loading when port 1 is excited. It demonstrates that the direction of the main beam is tilted by an angle of 38 degrees in the xoz-plane and the gain enhancement of 1 dB is realized owing to the proposed NRIM array. The electric field distribution in the xoz-plane when port 1 is excited at 5.2 GHz is illustrated in Fig 5.6. It is clearly that when the NRIM array is placed over the DRA, the maximum beam direction can tilt to the opposite direction of the proposed NRIM array. The distribution of the electrical field of the antenna with the NRIM structure can be modified. In the other words, the proposed NRIM structure is able to redirect the DRA's main beam. As the NRIM structures can provide a very low transmission coefficient and negative refractive index at specific frequency band (5-5.5 GHz), the radiation pattern of DRA can be tilted 38 degree at this frequency band while the beam can be tilted to another angle at another frequency band.

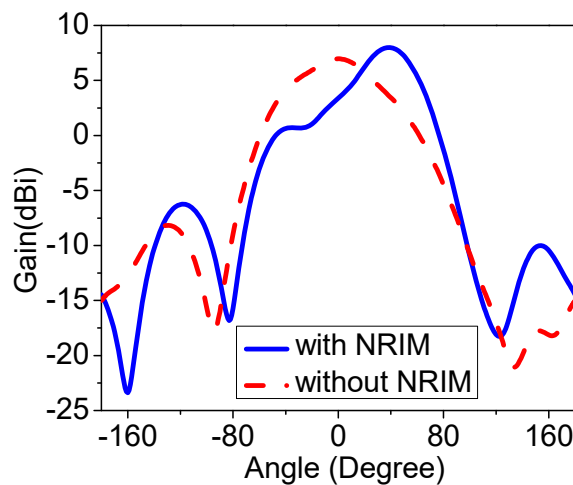


**Figure 5.5** Radiation pattern of DRA with and without NRIM layers loading excited by port 1 at 5.2 GHz.

**Table 5.1** The effect of different NRIM layers on the antenna performance.

Number of NRIM layer	Gain (dBi)	Main beam direction (degree)	Side-lobe level (dB)	3dB-BW (degree)
One layer	7.06	37	-12.6	75
Two layers	7.4	37	-12.8	66
Three layers	7.8	37	-13.6	53
Four layers	8	38	-10.2	49
Five layers	8.2	38	-7.8	46
Six layers	8.37	38	-8.0	44

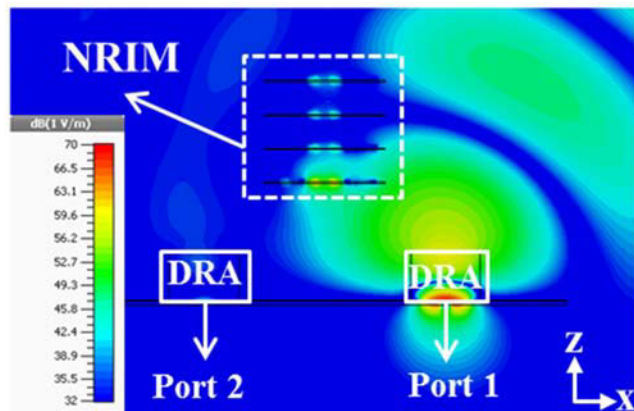


**Figure 5.6** Electric field distribution in the xoz-plane when port 1 excited at 5.2 GHz.

#### 5.2.4 Beam-tilting Antenna Theory Analysis

The mechanism can be explained by applying Snell's law to the boundary of the NRIM array and air,

$$\sin \theta_1 \cdot n_{air} = \sin \theta_2 \cdot n_{NRIM} \quad 5-1$$

Where  $\theta_1$  and  $\theta_2$  in Fig. 5.4 (a) are the incident angles of the EM wave from the air to the NRIM array and from the NRIM array to the air, respectively. The  $n_{NRIM}$  and  $n_{air}$  are the refractive indices of the NRIM array and air, respectively. Based on the diagram of Fig. 5.4 (a) and the

values of the  $n_{NRIM}$ ,  $d$  and  $l$  mentioned in the section 5.2.2 and 5.2.3, the radiation angle calculated by using Equation 5-1 is 38.5 degrees, which agrees with the measured angle.

### 5.3 Experimental results

The proposed beam-tilting antenna is fabricated and assembled, with its photographs shown in Fig. 5.7. The  $1 \times 4$  NRIM array is fixed over the double-feed DRA using nylon studs. Fig. 5.8 plots the measured reflection coefficient of the proposed beam-tilting antenna with and without the NRIM in different input ports. From this figure, it is observed that the proposed antenna performs good impedance matching in the band of 5 - 5.5 GHz, which is suitable for WLAN applications. Besides, the reflection coefficient of the antenna with the NRIM array is better than that without the NRIM.

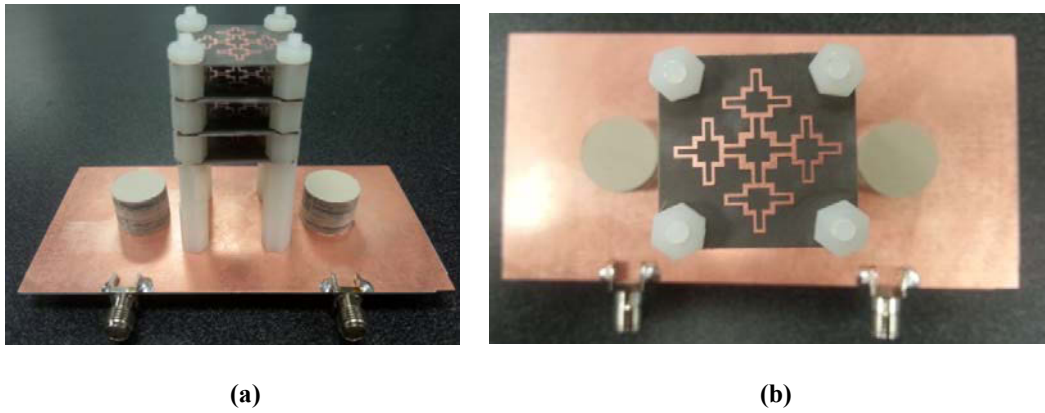


**Figure 5.7** Proposed beam-tilting antenna fabricated and assembled, (a) Side view, and (b) Top view.

The measured radiation patterns of the beam-tilting antenna with and without NRIM array in xoz-plane at 5.2 GHz are shown in Fig. 5.9 (a). As analyzed in Section 5.2, the EM wave emitted from the DRA propagates towards the opposite direction of the NRIM array, which can be clearly observed in Fig. 5.9 (a). When port 2 is excited with port 1 terminated, the blue dash dot line in Fig. 5.9 (a) reveals that the main beam tilts towards  $-38^\circ$  direction. The opposite applies when port 1 is excited with port 2 terminated, the main beam tilted to  $+38^\circ$  direction, as plotted by the black solid line in Fig. 5.9 (a). Hence, it is verified that the proposed NRIM structures are able to tilt the propagation direction of the maximum beam of the DRA. Fig. 5.9 (b) shows the measured radiation patterns in yoz-plane at 5.2 GHz. Fig. 5.10 plots the radiation pattern

measured and simulated in the xoz-plane at 5.1 GHz, 5.2 GHz and 5.3 GHz when port 1 and port 2 are excited, clearly indicating a good agreement between the simulation and measurement results. The simulated and measured gain of the antenna without and with NRIM when port 1 excited at 5.2 GHz are shown in Fig. 5.11. The reason that the measured gain is lower than the simulated one is primarily due to the fabrication and assembly tolerance.

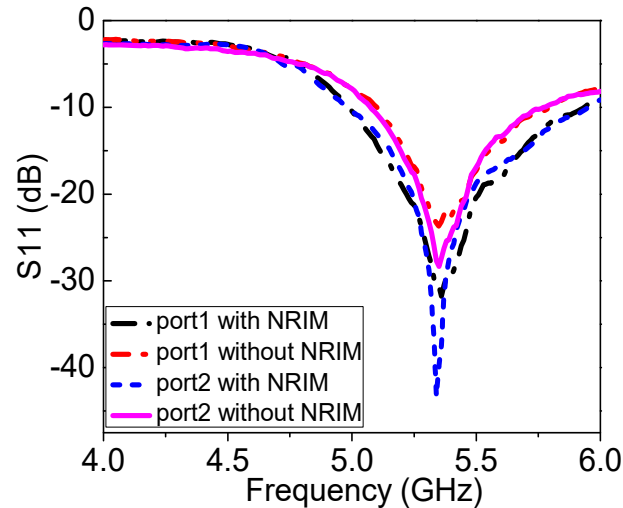


**Figure 5.8** Measured reflection coefficient of proposed antenna in different states.

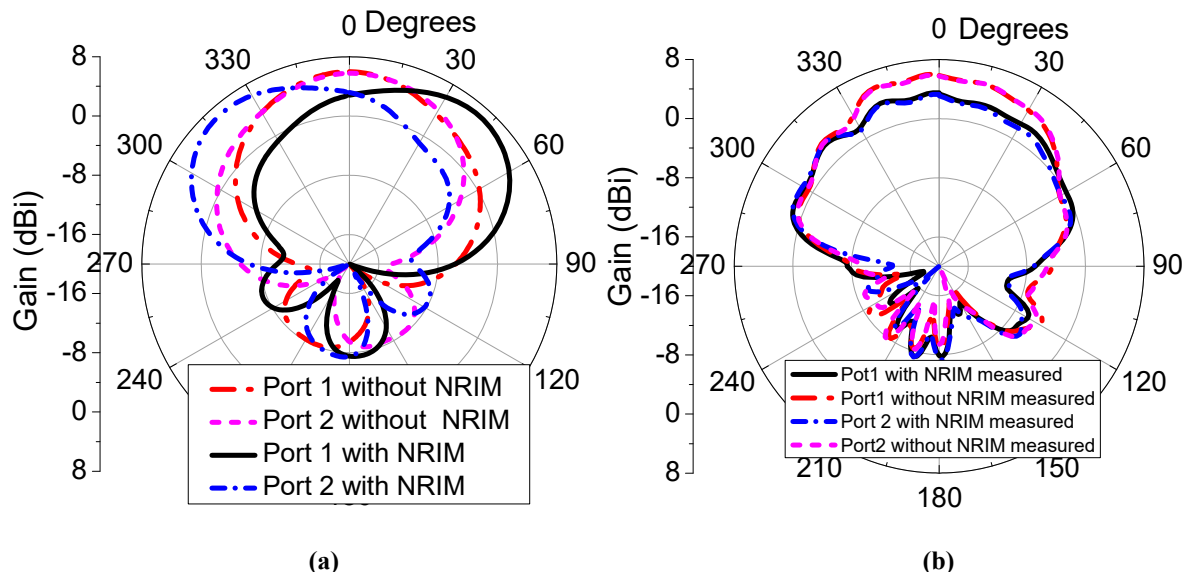


**Figure 5.9** Measured radiation pattern with different input excited at 5.2 GHz, (a) with and without NRIM loading in xoz-plane, and (b) with and without NRIM loading in yoz-plane.

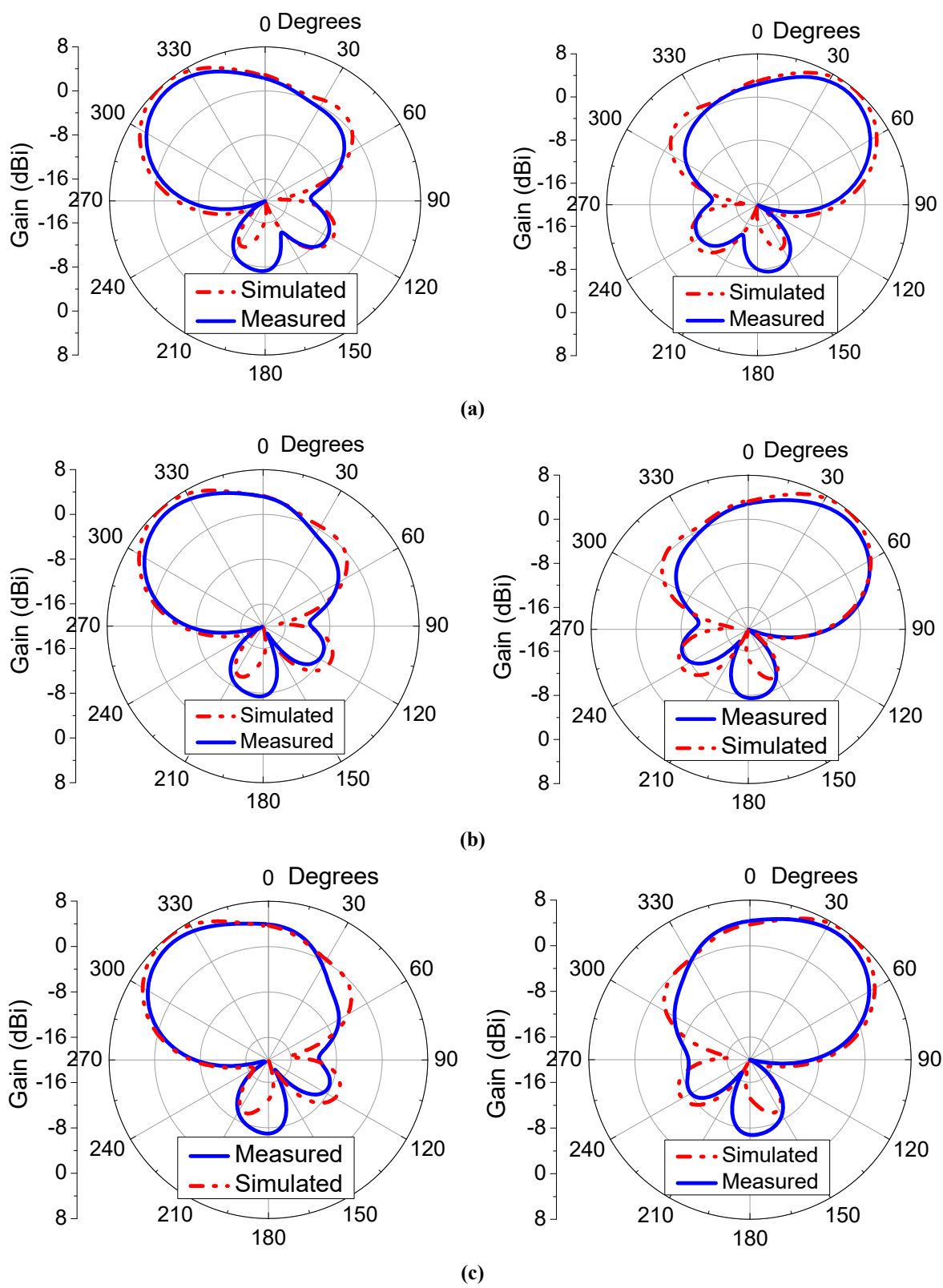


**Figure 5.10** Measured and simulated radiation pattern of the proposed antenna with different input port excited at: (a) 5.1 GHz, (b) 5.2 GHz, and (c) 5.3 GHz.

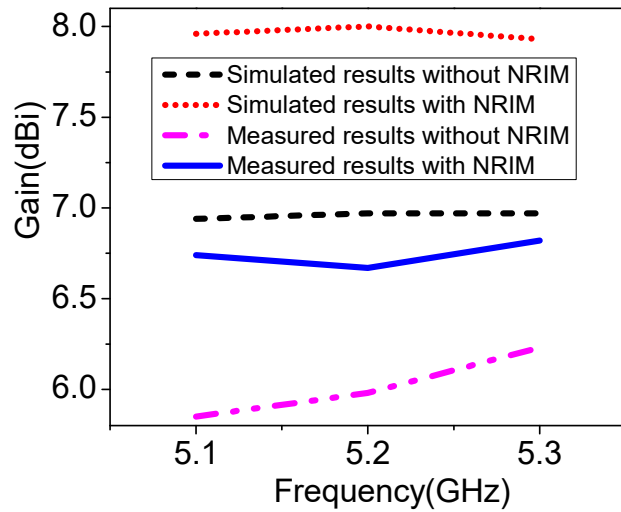


**Figure 5.11** Simulated and measured gain of the antenna without and with NRIM structures.

#### 5.4 Conclusion

In this chapter, a novel negative refractive index metamaterial (NRIM) structure has been proposed, which is used to deflect the direction of the maximum beam of the dielectric resonator antenna. A double-feed DRA with  $1 \times 4$  NRIM array has been fabricated and measured. The measured radiation patterns of the proposed beam-tilting antenna have demonstrated that the main beam can be tilted in the xoz-plane from  $-38^\circ$  to  $+38^\circ$  over a band of 5-5.5 GHz band. In this frequency band, the reflection coefficient of proposed antenna is better than -10 dB. Moreover, the measured results have been in a good agreement with simulated ones. Therefore, the proposed beam-tilting antenna presents a viable candidate for WLAN applications.

## **6 PATTERN-RECONFIGURABLE ANTENNA FOR ELEVATION AND AZIMUTH PLANES**

### **6.1 Introduction**

Radiation pattern reconfigurable antennas have extensively been developed for the wireless communication systems. Radiation-pattern reconfigurable antennas can switch its main radiation beam in several predefined directions, which is an effective technique to reduce co-channel interference and improve the signal-to-noise ratio. Therefore, these antennas can significantly decrease the interfering signals and enhance the capacity of the wireless communication systems. Recently, many methods of designing pattern-reconfigurable antennas have been reported. At present, most of published reconfigurable antennas only focus on switching their radiation patterns in one dimensionally, for example, in the azimuth plane [102, 131-132].

In this chapter, a novel three-layer pattern-reconfigurable antenna based on the quasi-Yagi antenna is introduced. The proposed antenna operates with multi-directions in both elevation and azimuth planes. The main beam of this antenna can be switched in four directions in the azimuth plane. Furthermore, the main beam can be tilted in three directions in the elevation plane by changing the length of the parasitic elements printed on the top and bottom layers. Measurement results are reported to confirm the validity of this design.

### **6.2 Antenna design and configuration**

Fig. 6.1 shows the geometry of the proposed antenna. For the sake of clarity, the bias circuits are not shown in the schematic. The antenna consists of three layers, printed on the Rogers RT/duroid 5880 substrate with a permittivity of 2.2, tangent-loss of 0.0009 and thickness of 1.58 mm. As shown in Fig. 6.1, the reflector elements and director elements are printed in the top and bottom layers, each one is divided into two strips connected through pin-diodes. Hence, sixteen pin-diodes GMP-4201 from Microsemi are applied here to reconfiguring the parasitic elements length.

In the middle layer, there are four elements of quasi-Yagi antenna and eight pin-diodes are inserted to connect the radiating elements. The antenna is fed by a coaxial probe that is

connected to the centre through the ground plane. Moreover, capacitors of 5 pF are mounted on the feedline to avoid DC signal flowing into the RF source of the antenna, as shown in Fig. 6.1. The length of the reflector element is  $1.06 l_d$  and the length of a director is  $0.8 l_d$ , where the  $l_d$  is the length of the printed dipole which is 21.6 mm. They are selected from the fact that the reflector is longer than the director which is smaller than the driven element [133]. The parasitic elements are 9.3 mm away from the driven dipole in the horizontal direction and 8.6 mm in the vertical direction. The dimensions of the proposed antenna are as follows:  $L=80$  mm,  $W=40$  mm,  $w1=18$  mm,  $w2=23$  mm,  $t=1.8$  mm,  $tl=2.2$  mm. The antenna performance analysis is based on the commercial software CST Microwave Studio.

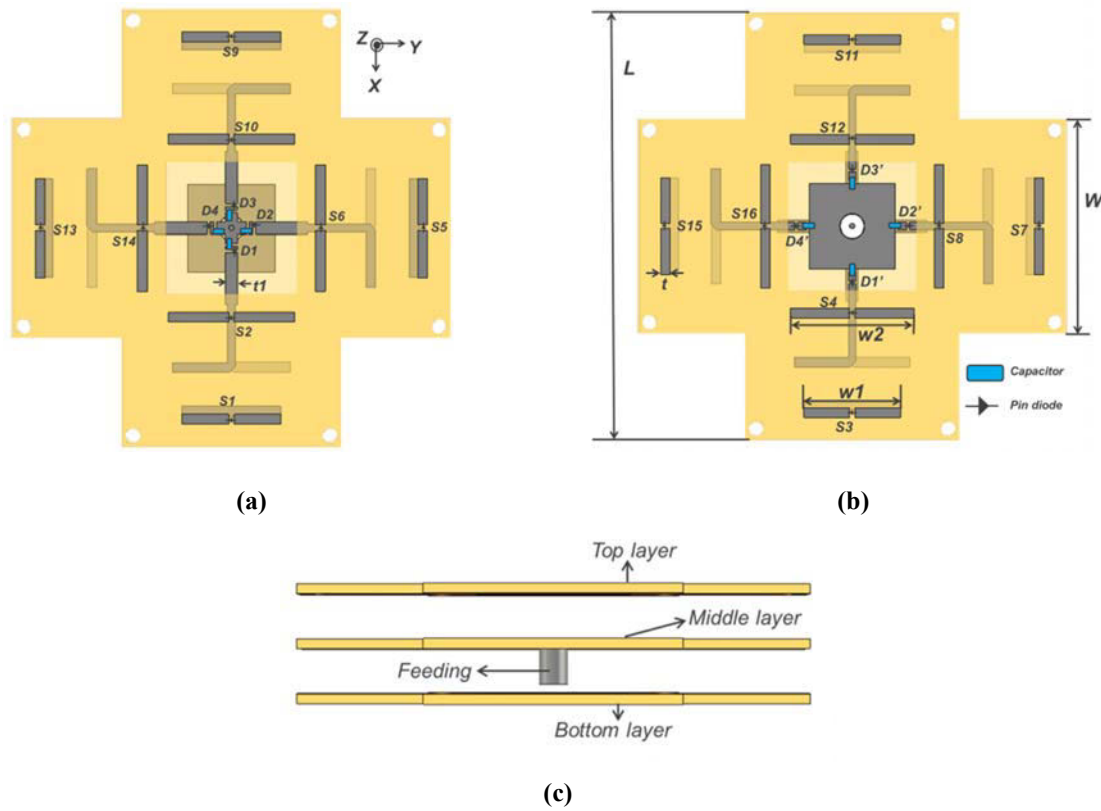


**Figure 6.1** Geometry of proposed antenna. (a) Top view. (b) Bottom view and (c) Side view.

The switches numbered D1–D4 are inserted into the top of the middle layer and D1'–D4' are inserted into the bottom of middle layer. By shifting the pin diodes numbered D1–D4 and D1'–D4', four radiation pattern reconfigurable states are obtained in the azimuth plane. The switches numbered S1–S16 are mounted on the top layer and bottom layer. Three reconfigurable states in the elevation plane are achieved by switching the states of pin diodes numbered S1–S16. Owing

to the symmetrical structure, here, we take one case as an example. When the pin diode D1 and D1' are activated and diodes D2–D4 and D2'–D4' are inactivated (called state 1), the main beam direction of the antenna is positioned at  $\varphi = 0^\circ$ . When the diodes S1 and S4 are activated and S2 and S3 are inactivated (called state 1 up mode), the main beam direction is located at  $\varphi = 0^\circ$  and  $\theta = 46^\circ$ . When the diodes S2 and S3 are activated and S1 and S4 are inactivated (called state 1 down mode), the main beam is positioned at  $\varphi = 0^\circ$  and  $\theta = 132^\circ$ . When the diodes S1 – S4 are inactivated (called state 1 endfire mode), the main beam direction is at  $\varphi = 0^\circ$  and  $\theta = 90^\circ$ .

### 6.3 Experimental results and discussion

The designed antenna was fabricated and measured. The photograph of the proposed antenna is illustrated in Fig. 6.2. As shown in Fig. 6.2, RF chokes from Murata (18 nH) are used to isolate the DC lines from radio frequency signals. In the forward biased case (1.1 V), the diode is ON and represents a small resistance of  $R_s = 1.8 \Omega$ . On the contrary, when it is reversely biased (0 V), the diode is OFF and equivalent to a capacitance  $C_p = 0.09 \text{ pF}$  and an inductance  $L_p = 0.5 \text{ nH}$  in series. Fig. 6.3 depicts the measured and simulated return loss in State 1 up mode. It is clear that the proposed antenna performs good impedance matching at 5.2 GHz. Radiation patterns of the proposed antenna are measured in an anechoic chamber. Fig. 6.4 depicts the measured radiation patterns in different states at 5.2 GHz in the azimuth and elevation planes. It can be seen that the main beam can be switched in four directions in the azimuth plane and be tilted in three directions in the elevation plane. Fig. 6.5 exhibits simulated 3D radiation patterns of state 1 down mode and state 2 up mode at 5.2 GHz. Table 6.1 shows the peak gain of the antenna in different modes of state 1. The coaxial cable feed, assembly, measurement errors and actual physical characteristics of the pin-diode enclosure could be the main reasons for the discrepancy between the simulated and measured patterns and gain. Moreover, the external DC bias lines have some impact on the radiation performance.

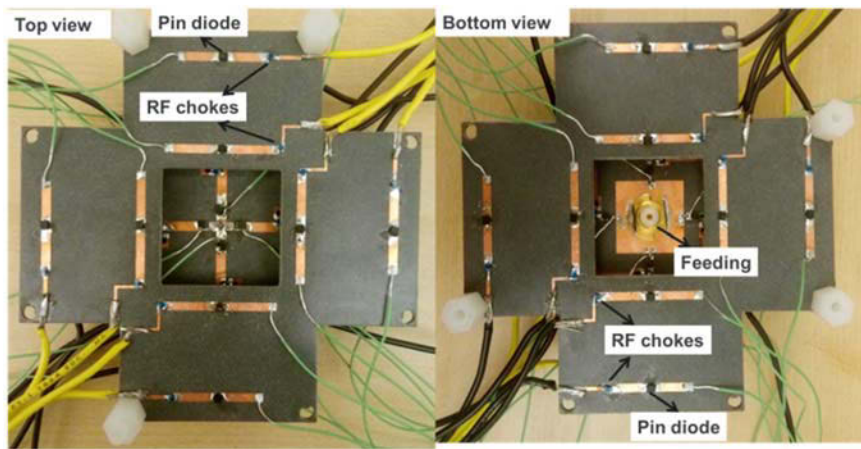


**Figure 6.2** Photograph of fabricated antenna.

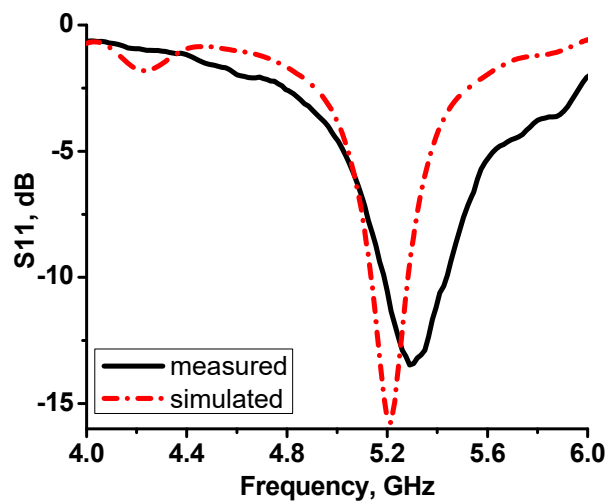
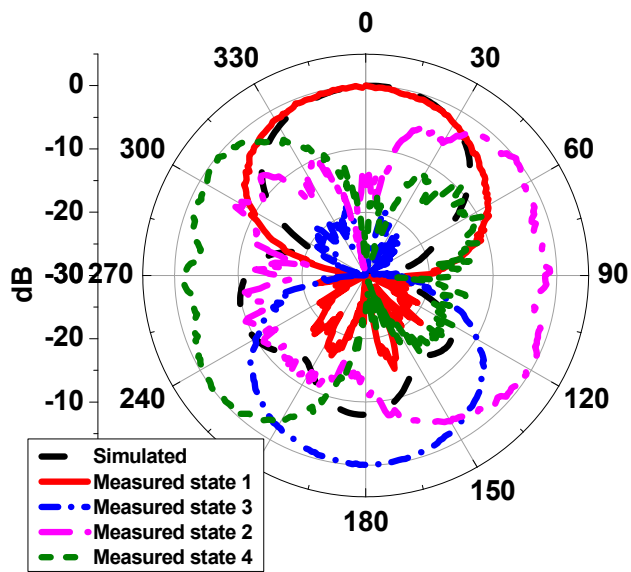
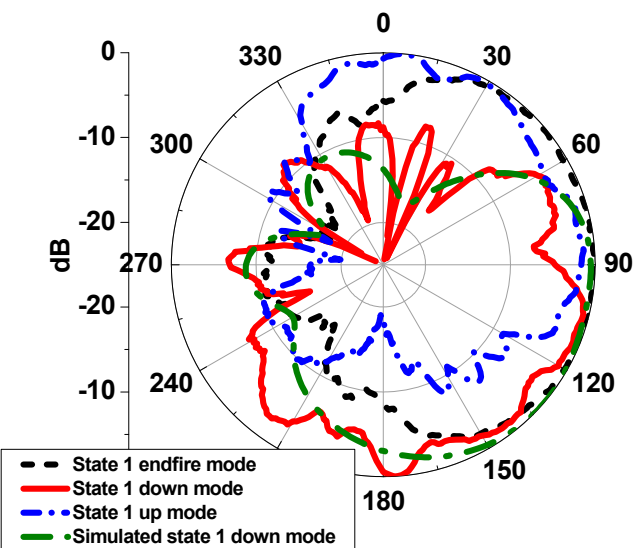


**Figure 6.3** Measured and simulated  $S_{11}$  of proposed antenna in state 1 up mode.



(a)



(b)

**Figure 6.4** Measured normalized radiation patterns at 5.2 GHz in different states. (a) Azimuth plane. (b) Elevation plane.

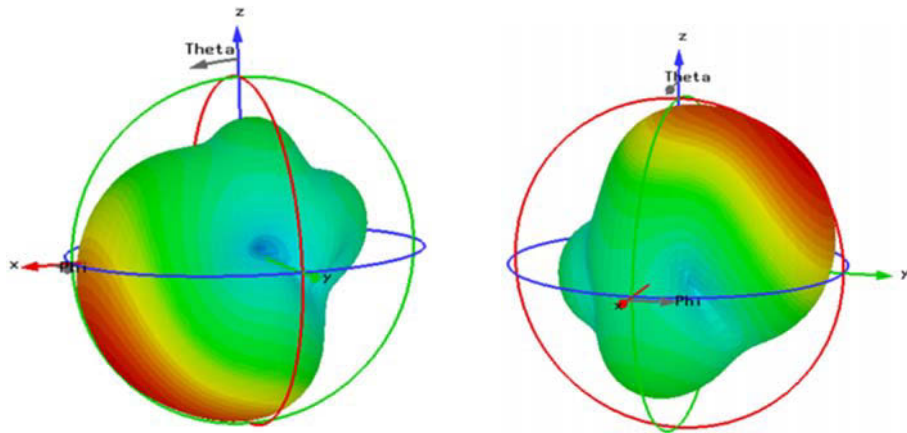


**Figure 6.5** Simulated 3D radiation patterns of state 1 down mode and state 2 up mode at 5.2 GHz.

**Table 6.1** Peak gain of proposed antenna in different modes of state 1.

Gain (dBi)	Up mode	Down mode	Endfire mode
Simulation	7.3	6.7	4.8
Measurement	5.8	5.3	3.8

#### 6.4 Conclusion

In this chapter, a pattern reconfigurable printed quasi-Yagi antenna with multi-directions in both elevation and azimuth plane at 5.2 GHz has been proposed. By activating pin-diodes in the middle layer, the main beam can be switched in four directions in the azimuth plane. By switching the pin-diodes in the top and bottom layers, the beam tilting in three directions has been achieved in the elevation plane. The performance is very advantageous for future wireless communications.

## 7 CONCLUSION AND FUTURE WORK

### 7.1 Conclusion

The modern wireless communication systems put forward more and more new requirements for the antenna, such as the integrating many antennas in a very limited space and requiring an antenna with multi-beams, with high gain characteristic. It is very difficult and even impossible to meet the above requirements with traditional antennas, reconfigurable antennas have become more and more popular as an effective solution to solve the above problems. In this thesis work, the research efforts focus on the reconfigurable antennas. Hence, a comprehensive analysis, development, design and applications of reconfigurable antennas have been presented.

Firstly, a novel compact dual-band beam-sweeping antenna has been successfully proposed. Two frequency independent cylindrical active frequency selective surface (AFSS) screens operated at different frequency bands at 2.45 GHz and 5.2 GHz are used to design this antenna. By controlling states of pin-diodes mounted on AFSS, the proposed antenna can effectively realize beam-sweeping at 2.45 GHz and 5.2 GHz covering all azimuth angles simultaneously. As these two cylindrical AFSS screens can work independently from each other when they are loaded in the same antenna system, hence, the size of antenna system are reduced greatly by using this way. Therefore, this kind of antenna presents a viable candidate to realize further miniaturization and multifunction of modern communication systems.

Secondly, to obtain a high gain of beam switching antenna, a new approach has been introduced. This high-gain antenna is composed of an omnidirectional monopole antenna, a hexagon FSS screen, and six metallic sheets that surround the monopole antenna. The beam-switching antenna is divided into six equal portions by six metallic sheets, which are employed here to improve the gain of the antenna. Therefore, by changing the states of pin-diodes in different column combinations of the hexagon FSS screen, this proposed antenna has realized a single-beam switching in six directions and multiple beams at 5.2 GHz in the azimuth plane with low voltage (2.15 V). From the experimental results, the proposed antenna with a high gain (11.54 dBi) effectively operates at 5.2 GHz. The maximum gain of the antenna enhancement of 7 dB has been achieved when the six metallic sheets are applied.

Thirdly, a novel technique has been proposed to achieve beam tilting antenna in this thesis. This has been realized by integrating an array of negative refractive index metamaterial (NRIM) to deflect the direction of the maximum beam. The proposed beam tilting antenna includes a double-feed DRA and a  $1 \times 4$  NRIM array. The measured radiation patterns results have demonstrated that the main beam can be tilted in the  $xoz$ -plane from  $-38^\circ$  to  $+38^\circ$  over a band of 5 to 5.5 GHz band by using the NRIM array. Therefore, the proposed beam-tilting antenna presents a viable candidate for WLAN applications.

Fourthly, in order to achieved multi beam directions in both elevation and azimuth planes, a three-layer quasi-Yagi antenna has been proposed at 5.2 GHz. There are four elements of the quasi-Yagi antenna and eight pin-diodes as switches inserted in the middle layer. The top and bottom layers include the parasitic elements, into which pin-diodes are inserted. By switching the pin-diodes ON and OFF in the different layers, the antenna can realize beam switching in azimuth plane and beam tilting in the elevation plane.

## 7.2 Future works

In this thesis, some research work has been done in radiation reconfigurable antennas based on active frequency selective surfaces, metamaterials and quasi-yagi antenna. However, not fully covered in this limited work, there are still some problems to be expanded, which can be used as future research directions, mainly including the following topics.

Firstly, working bandwidth of beam scanning antenna still have a room for further improvement, which is determined by the frequency range of the central feeding antenna and the operating bandwidth of AFSS. Broadband omnidirectional antenna technology is more mature, which means that the working bandwidth of the beam scanning antenna mainly depends on AFSS's bandwidth. Therefore, how to further improve AFSS frequency adjustment range is an interesting issue to be investigated in this area..

Secondly, in this thesis, the radiation patterns of antennas can scan freely in the azimuth plane. Therefore, an interesting future research topic would be to propose some particular method to make radiation patterns sweep freely in both elevation plane and azimuth plane.

Thirdly, due to limited time, the voltage controlling circuit was not developed and designed in this thesis. Applying the voltage controlling circuit can not only effectively avoid the error caused by the manual voltage control, but also make the operation more convenient and improve the efficiency of the antenna test. Hence, how to design a proper voltage controlling circuit is an important task in future work.

## 8 RÉSUMÉ

Ce chapitre résume le travail de recherche effectué dans le cadre de ma thèse, en commençant par présenter le contexte et les motivations de mon projet de recherche. Ensuite, les concept de nouvel antennes reconfigurable sont introduits. Les objectifs des travaux sont proposés. l'organisation de cette thèse est établie et les contributions de ma thèse sont répertoriées. Enfin, la conclusion et les travaux futurs sont présentés.

### 8.1 Contexte et motivation

Les systèmes de communication sans fil sont devenus l'un des domaines les plus dynamiques. La nouvelle génération de communications mobiles, LAN sans fil, système de positionnement par satellite, une variété de radars militaires et civils sont devenus de plus en plus importants dans nos vies quotidiennes. Antenne comme l'un des éléments importants dans le système de communication sans fil, ses caractéristiques de fonctionnement affectent directement les performances du système [1-2]. Le développement rapide des systèmes de communication sans fil modernes a mis en avant des exigences plus élevées telles que multifonction, haute capacité et bande ultra-large qui conduisent directement à un nombre croissant de sous-systèmes sur la même plateforme tandis que le nombre d'antennes augmente également. En conséquence, il existe plusieurs problèmes tels qu'un grand volume, un coût élevé et une compatibilité électromagnétique. Comme les performances des antennes traditionnelles sont fixées dans de nombreuses applications qui sont de plus en plus difficiles à satisfaire à ces exigences, une variété de nouvelles antennes sont progressivement développées. L'antenne reconfigurable représenter une excellent solution et, qui non seulement répondent aux exigences de développement des communications sans fil, mais a également une structure simple et une petite taille [3-4].

L'antenne reconfigurable se réfère à toute structure de rayonnement contrôlée au moyen d'approches électriques ou mécaniques pour changer une ou plusieurs de ses caractéristiques de fonctionnement fondamentales. Le principe clé de la conception d'antennes reconfigurables repose sur la théorie des antennes conventionnelles. Leurs caractéristiques de rayonnement désirées sont décalées en ajustant la structure du radiateur, en contrôlant la distribution du

courant ou en modifiant les paramètres électriques de l'antenne [5]. Les antennes reconfigurables sont capables d'ajouter indépendamment leur fréquence de fonctionnement, leur bande passante, leur polarisation ou leur diagramme de rayonnement afin de s'adapter aux besoins d'exploitation de leur environnement [6].

Selon les performances de reconstruction, les antennes reconfigurables peuvent être classées en antennes reconfigurables en fréquence, en antennes reconfigurables en polarisation, en antennes reconfigurables à diagramme de rayonnement variable et en antennes reconfigurables à multi-performances [7]. Les antennes reconfigurables en fréquence ont la capacité de syntoniser la bande de fréquence de travail, ce qui permet de filtrer les signaux interférents, ou d'accorder l'antenne pour tenir compte des nouveaux environnements [8-11]. Pour les antennes reconfigurables en polarisation, la polarisation de l'antenne peut être reconfigurée pour séparer les signaux désirés et filtrer les signaux indésirables [12-14]. De plus, les antennes reconfigurables à diagramme de rayonnement variable peuvent changer la direction du faisceau principal pour envoyer efficacement les signaux dans une direction désirée [15-16]. Ces antennes peuvent réduire considérablement les signaux interférents et améliorer la capacité du système. Les antennes reconfigurables à performances multiples sont deux ou trois types d'antennes à performances variables, telles que les antennes reconfigurables en fréquence et en diagramme de rayonnement, les antennes reconfigurables en fréquence et en polarisation, les antennes reconfigurables en polarisation et en fréquence [17-19]. Dans cette thèse, nous concentrons nos recherches principales sur les antennes reconfigurables à diagramme de rayonnement.

Les antennes reconfigurables à rayonnement peuvent apporter les améliorations suivantes aux performances globales des systèmes de communication modernes. Premièrement, en utilisant l'antenne reconfigurable à diagramme de rayonnement, on peut aligner la direction de rayonnement principale de l'antenne avec la direction de signal utile pour améliorer le rapport signal sur bruit, améliorer les performances du système et réduire la consommation d'énergie [7]. Deuxièmement, parce que la technologie multi-entrée multi-sortie (MIMO) a été capable d'augmenter la capacité du système, elle sera principalement utilisée dans les systèmes de communication 5G. Les systèmes MIMO doivent intégrer plusieurs antennes dans un espace limité, d'où la nécessité d'un faible couplage entre les éléments d'antenne. La technologie des antennes reconfigurable en diagramme de rayonnement peut effectivement réduire le couplage entre les éléments d'antenne dans le système MIMO [20-21]. Troisièmement, afin de répondre

aux exigences de miniaturisation et de multifonctions dans les systèmes de communication modernes, de plus en plus de dispositifs électroniques sont intégrés dans une plate-forme unique. Bien que cette méthode puisse améliorer considérablement la qualité de la communication, elle peut également entraîner de graves problèmes d'interférences. Les antennes reconfigurables à diagramme de rayonnement peuvent réduire les interférences provenant des rayonnements indésirables afin d'améliorer les performances des systèmes de communication [22].

En résumé, les antennes reconfigurables à diagramme de rayonnement peuvent réduire la taille, le coût et la complexité de conception du système de communication sans fil, ce qui améliore grandement la performance globale des systèmes de communication. Les avantages exceptionnels de ces antennes pour les systèmes de communication modernes nous ont motivés à établir une recherche complète dans ce domaine. Par conséquent, ce projet vise à concevoir, analyser et fabriquer de nouvelles antennes reconfigurables à diagramme de rayonnement pour les systèmes de communication modernes.

## 8.2 Antenne reconfigurable en diagramme de rayonnement

Ces dernières années, de plus en plus de chercheurs concentrent leurs intérêts sur les antennes reconfigurables en diagramme de rayonnement. L'une des méthodes les plus traditionnelles pour concevoir des antennes reconfigurables en diagramme de rayonnement est les réseaux à déphasage [23-24], qui consistent à changer la phase du déphaseur pour contrôler le diagramme de rayonnement. Cependant, les réseaux à déphasage ont un réseau d'alimentation très complexe, ce qui entraîne des problèmes de coût élevé et de conception. Comparé à un réseau à déphasage, les antennes reconfigurables à diagramme de rayonnement présentent une structure simple et une conception relativement facile, ce qui attire l'attention de plusieurs chercheurs. Selon les différentes méthodes de mise en œuvre, des antennes reconfigurables à diagramme de rayonnement peuvent être classées selon leur commande: mécanique, électrique, optique, à base de matériaux avancés tels que les métamatériaux.

### 8.2.1 Méthode de contrôle mécanique

La commande mécanique est obtenue en repositionnant et en déplaçant l'antenne pour atteindre les caractéristiques souhaitées. Cependant, l'approche mécanique est critiquée par son installation

et sa lenteur, et le système est complexe [25-27]. Dans [26], Hai Liang Zhu et al. a proposé une antenne reconfigurable à diagramme de rayonnement qui est composée d'une métasurface semi-circulaire planaire placée directement au sommet d'une antenne planaire circulaire, illustrée à la Fig. 8.1. En tournant la métasurface autour du centre de l'antenne patch, le faisceau de l'antenne peut être dirigé continuellement. La direction du faisceau principal de l'antenne est dirigée à un angle de  $32^\circ$  par rapport à la direction de l'axe de visée. Dans [27], Jorge R. Costa et al. ont conçu une antenne de faisceau orientable composée d'une lentille diélectrique qui pivote devant une seule source d'alimentation à gain modéré stationnaire, représentée à la Fig. 8.2. Cette antenne peut diriger le faisceau principal en élévation et en azimut mécaniquement.

### 8.2.2 Méthode de contrôle électrique

Les méthodes de commande électrique pour concevoir des antennes reconfigurables utilisent des composants de commutation RF et des dispositifs à réactance variable. Les commutateurs RF peuvent être utilisés pour connecter / déconnecter une partie de la structure de l'antenne ou pour modifier la distribution du courant afin d'obtenir différentes performances de l'antenne. Les composants de commutation micro-ondes comprennent principalement des diodes pin et des commutateurs RF-MEMS (systèmes micro-électromécaniques à radiofréquence). Pour les dispositifs à réactance variable, il s'agit principalement de diodes varactor. Dans la littérature, de nombreuses antennes reconfigurables à diagramme de rayonnement sont contrôlées par des diodes pin [28-34]. Ces diodes ont une faible perte d'insertion, une vitesse de commutation rapide et une faible tension de polarisation continue. Ils peuvent contrôler de forte signal en hyperfréquence. Dans [29], Tamer Aboufoul et al. ont proposé un modèle planaire compact-reconfigurable en incorporant quatre commutateurs à diode et deux éléments parasites, montré dans la Fig. 8.3. Les diagrammes de rayonnement de cette antenne pourraient être modifiés d'un modèle presque omnidirectionnel à un modèle directif. Dans [31], M.S. Alam et al. ont conçu une antenne planaire dirigée par faisceau, qui comprend un disque circulaire central entouré de quatre tronçons microruban coniques contrôlés par des diodes pin, montré dans la Fig. 8.4. En utilisant les diodes pin, les stubs changent leur statut de mode mis à la terre au mode ouvert pour fournir une reconfigurabilité de modèle dans quatre directions.

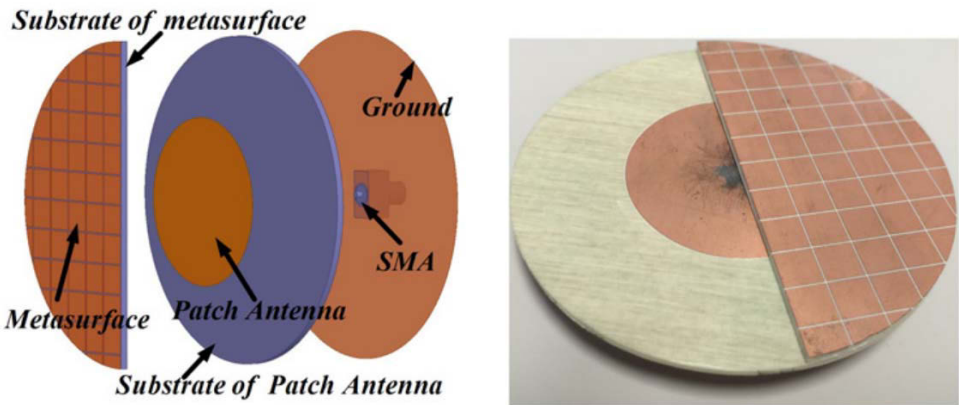


Figure 8.1 Antenne reconfigurable à structure mécanique utilisant la métasurface [26].



Figure 8.2 Une antenne de lentille orientable à faisceau compact [27].

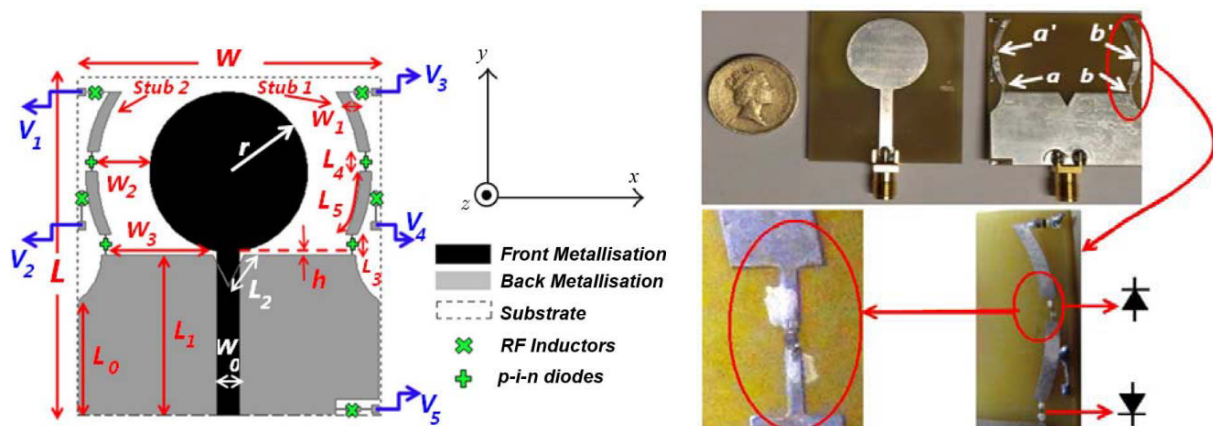
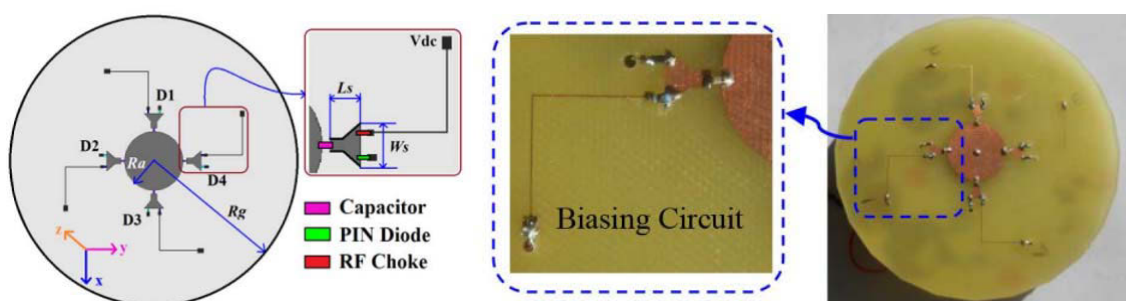
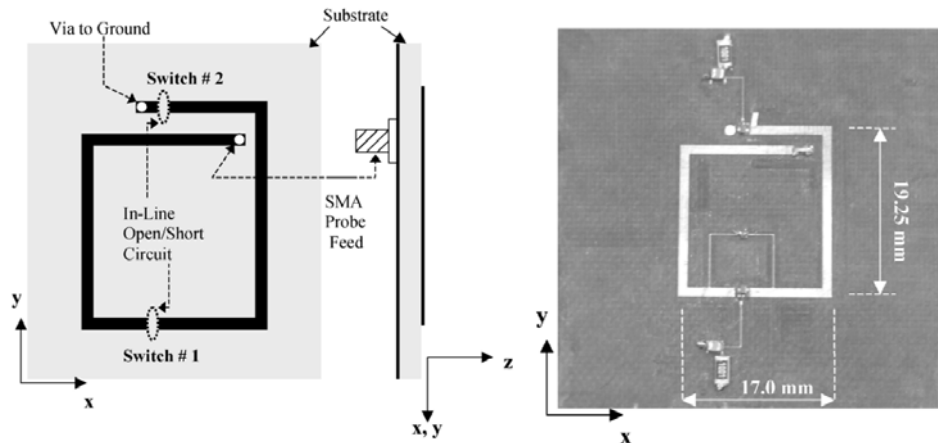


Figure 8.3 Un modèle plan compact-reconfigurable [29].

Les commutateurs RF-MEMS représentent aussi des dispositifs RF pour la communication. Dès 1998, E. R. Brown a proposé l'utilisation d'interrupteurs RF-MEMS pour concevoir une antenne reconfigurable [35]. De plus en plus, des études ont été rapportées [36-41]. L'un des principaux avantages des commutateurs RF-MEMS réside dans leur bonne isolation et leur propriété à faible perte. Ils peuvent être utilisés à haute fréquence avec une bonne linéarité. Cependant, l'inconvénient des commutateurs MEMS est leur réponse qui est plus lente que les diodes pin et leur tension de polarisation est plus élevée que celle des diodes pin [20]. Dans [36], Greg H. Huff et al. ont conçu une antenne microruban reconfigurable le diagramme rayonnement avec des commutateurs de système micro-électromécanique (MEMS). Deux commutateurs MEMS ont été utilisés pour reconfigurer les diagrammes de rayonnement d'une antenne microruban rectangulaire et spirale l'antenne est montrée à la figure. Les résultats simulés et le prototype sont montrés à la Fig. 8.5. L'antenne est montrée à la Fig. 8.6 est une antenne spirale rectangulaire reconfigurable avec un ensemble de commutateurs RF-MEMS, qui a été alimentée via un câble coaxial. La structure se compose de cinq sections qui sont connectées avec quatre commutateurs RF-MEMS. Sur la base de l'état des RF-MEMS intégrés, l'antenne peut changer la direction de son faisceau de rayonnement [37].



**Figure 8.4** Antenne planaire orientable par faisceau utilisant un disque circulaire et des stubs effilés contrôlés par quatre broches [31].



**Figure 8.5** Antennes microruban spirales reconfigurables à motif de rayonnement avec commutateurs RF MEMS [36].

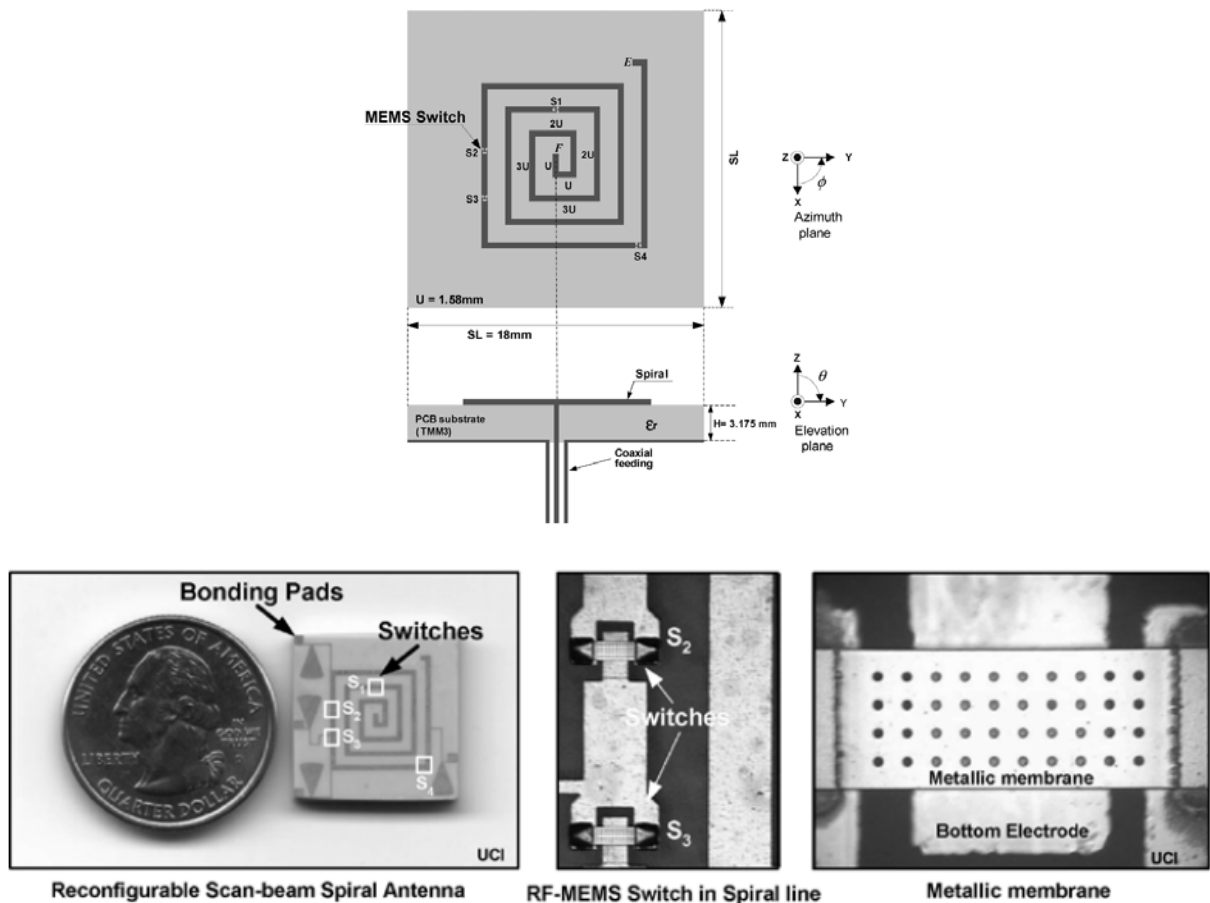


**Figure 8.6** Un diagramme de rayonnement reconfigurable antenne à spirale de faisceau de balayage [37].

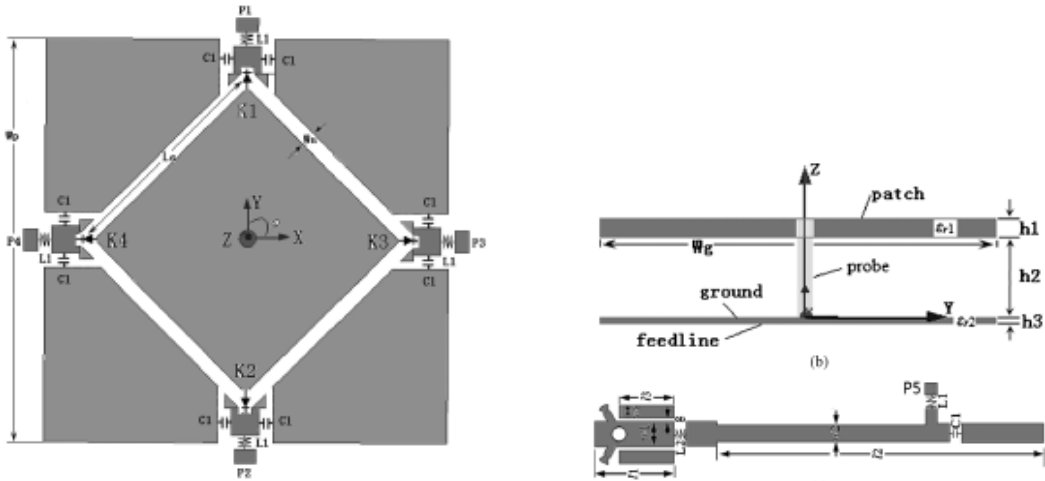


**Figure 8.7** Antenne reconfigurable à diagramme de rayonnement avec diode varactor [42].

Les diodes varactor sont des dispositifs micro-onde semi-conducteurs couramment utilisés, la capacité entre les deux pôles change avec le changement de tension de polarisation CC. Les diodes varactor peuvent être utilisées pour ajuster en continu la fréquence de fonctionnement des antennes et peuvent également être utilisées pour obtenir des performances de rayonnement d'antenne réglables en continu [42-45]. L'antenne représentée sur la Fig. 8.7 a été publiée dans la référence [42], il s'agit d'un type d'antennes reconfigurables à diagramme de rayonnement basé sur un modèle de réseau d'antennes à deux éléments. Les deux dipôles du réseau ont été pliés pour former un carré et les phases des dipôles magnétiques ont été ajustées par les diodes varactor chargées. Les diagrammes de rayonnement de cette antenne ont été reconfigurés dans deux plans orthogonaux.

### 8.2.3 Méthode de contrôle optique

Troisièmement, les antennes reconfigurables à commande optique sont basées principalement sur des commutateurs photoconducteurs. Lorsque la lumière laser illuminé l'interrupteur photoconducteur, l'interrupteur est activé. Par rapport aux dispositifs de commutation à micro-ondes traditionnels, les commutateurs photoconducteurs ne nécessitent pas de fil de polarisation CC supplémentaire, ce qui réduit les effets de rayonnement sur l'antenne. Et ils n'ont pas besoin de considérer l'isolation entre la tension de polarisation continue positive et négative, ce qui réduit la complexité de la structure d'antenne. Cependant, les plus grands défis de cette technologie reconfigurable sont l'intégration et la consommation d'énergie car la génération laser

nécessite des diodes laser et des fibres optiques. Les commutateurs photoconducteurs sont couramment utilisés pour concevoir des antennes reconfigurables en fréquence [46-50]. C. J. Panagamuwa et al. ont conçu une antenne reconfigurable en fréquence et en faisceau utilisant des commutateurs phototconducteurs, qui est représenté à la Fig. 8.8. À partir de cela, nous trouvons que deux commutateurs photo en silicium ont été placés sur de petits espaces dans les deux bras dipolaires équidistants de l'alimentation centrale. La lumière provenant de deux diodes laser infrarouges canalisées à travers des câbles à fibres optiques a été appliquée aux commutateurs. Avec les bandes dans le dipôle ponté, l'antenne résonne à une fréquence inférieure. Par conséquent, la longueur des deux bras de l'antenne a été contrôlée efficacement en utilisant un laser pour contrôler les commutateurs photoconducteurs, reconfigurabilité du fréquence et celle du faisceau a été atteinte [47].

#### 8.2.4 Changer les propriétés de la méthode matérielle

La modification des propriétés des matériaux est une autre méthode intéressante pour concevoir une antenne reconfigurable en diagramme de rayonnement et en fréquence [51-53]. Les cristaux liquides (LC), les matériaux ferroélectriques et ferromagnétiques sont une sorte de ces matériaux, qui ont été utilisés comme moyens de reconfiguration. En appliquant une tension continue ou un champ magnétique sur ces matériaux, les propriétés électriques de ceux-ci sont modifiées, ce qui conduit à modifier la réponse EM de la structure. Dans [51] et [52], une antenne à balayage de faisceau à fréquence fixe a été conçue en utilisant un substrat ferroélectrique, représentée à la Fig. 8.9. En changeant la tension de polarisation continue sur le substrat, la permittivité du matériau ferroélectrique a été modifiée. Par conséquent, la constante de phase électrique de l'onde de propagation a été modifiée et la direction du faisceau principal a pu être modifiée. Cependant, un niveau de polarisation croisée plus élevé dans le plomb ferromagnétique ne s'applique pas largement en tant que résonateurs dans les applications d'antenne.

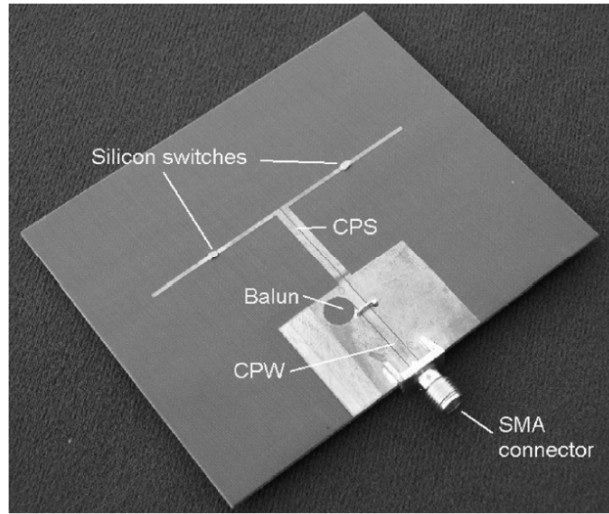


**Figure 8.8** Photographie de l'antenne reconfigurable en fréquence et en diagrammes de rayonnement à l'aide de commutateurs photoconducteurs [47].

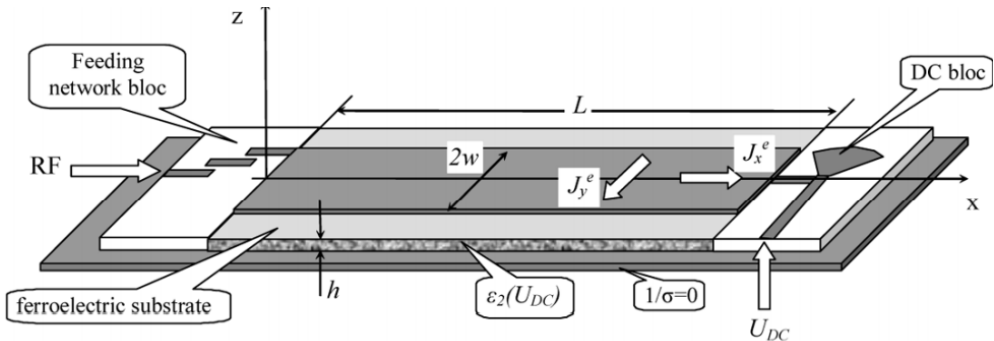


**Figure 8.9** Géométrie de base de l'antenne de balayage à base de substrat ferroélectrique [52].

### 8.2.5 Utilisation des métamatériaux

Au cours des dernières années, les métamatériaux ont de plus en plus attiré l'attention des chercheurs [54-56]. Selon la manière dont ils traitent les ondes électromagnétiques incidentes, les métamatériaux peuvent être réalisés sous forme de structures à bande interdite électromagnétique (EBG), de conducteur magnétique artificiel (AMC), de surface à haute impédance (HIS) et de surface sélective de fréquence (FSS). Ils sont constitués d'un réseau d'éléments périodiques disposés en un, deux ou trois dimensions. De nombreux métamatériaux de ce type ont été utilisés pour concevoir des antennes reconfigurables à diagramme de rayonnement en raison de leurs performances spécifiques aux ondes électromagnétiques [57-75].

Dans [58], M.A. Habib et al. ont conçu une antenne à commutation de faisceaux basée sur des structures périodiques à bande interdite électromagnétique (EBG). Cette antenne fonctionnait à 1.8 GHz avec un gain de 10 dBi. Et elle a commuté six faisceaux différents avec  $60^\circ$  de largeur de faisceau couvrant  $360^\circ$  dans le plan d'azimut, qui est montré à la Fig. 8.10. À partir de la Fig. 8.11, une antenne reconfigurable à motif avec quatre commutateurs à circuit ouvert sur une surface à haute impédance (HIS) a été proposée dans la référence [63]. En commutant différentes combinaisons d'interrupteurs, la direction du faisceau a été atteinte. D'après les références [64-75], la conception de l'antenne reconfigurable à diagramme de rayonnement utilise des surfaces sélectives en fréquence (FSS). Dans [69], Arezou Edalati et al. ont proposé une antenne reconfigurable en utilisant un FSS cylindrique actif qui est représentée à la Fig. 8.12. La structure FSS est constituée de bandes discontinues métalliques avec des diodes PIN dans leurs discontinuités. Un réseau dipôle coaxial couplé électromagnétiquement omnidirectionnel (ECCD) a été entouré par une FSS cylindrique. En contrôlant l'état des diodes dans la FSS, un diagramme de rayonnement directif balayait tout le plan azimutal. Dans la référence [73], Liang Zhang et al. ont conçu un système d'antenne dirigeable par faisceau utilisant des surfaces à sélectivité de fréquence activés (AFSS), qui est représenté à la Fig. 8.13. Les varactors ont été montés sur cette AFSS pour obtenir un réglage continu. La bande de réflexion change avec la tension inverse ajoutée sur les diodes varactor en continu. Le faisceau de cette antenne pourrait balayer dans le plan d'azimut entier à la fois pour les modes à un faisceau et les modes à double faisceau.

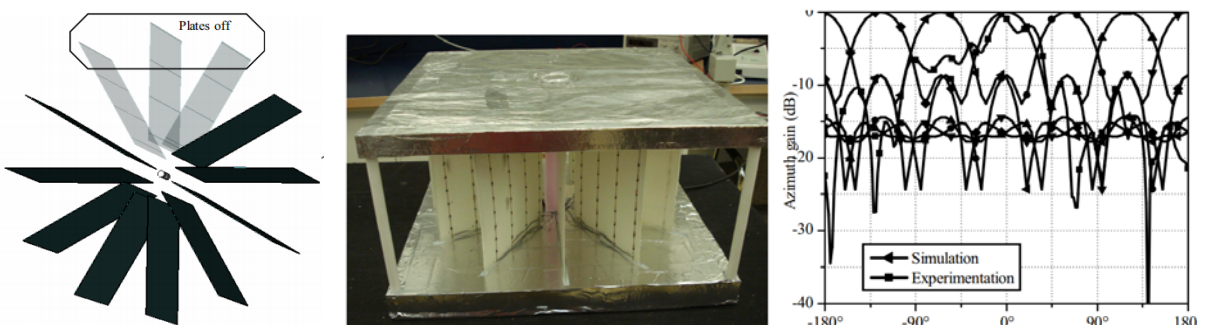


**Figure 8.10** Antenne de faisceau commutable basée sur la bande interdite électromagnétique (EBG) [58].

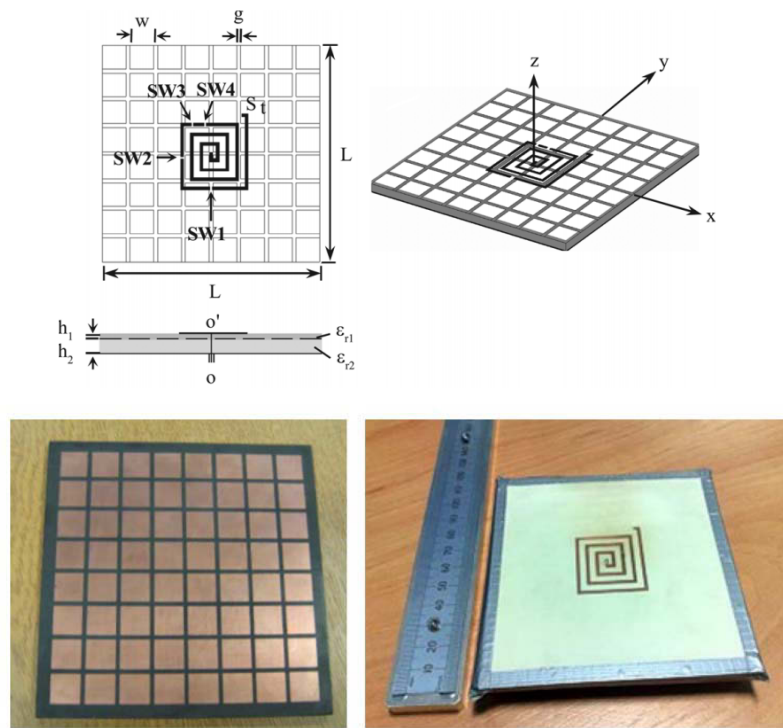


**Figure 8.11** Antenne reconfigurable en diagramme de rayonnement utilisant une surface à haute impédance (HIS) [63].

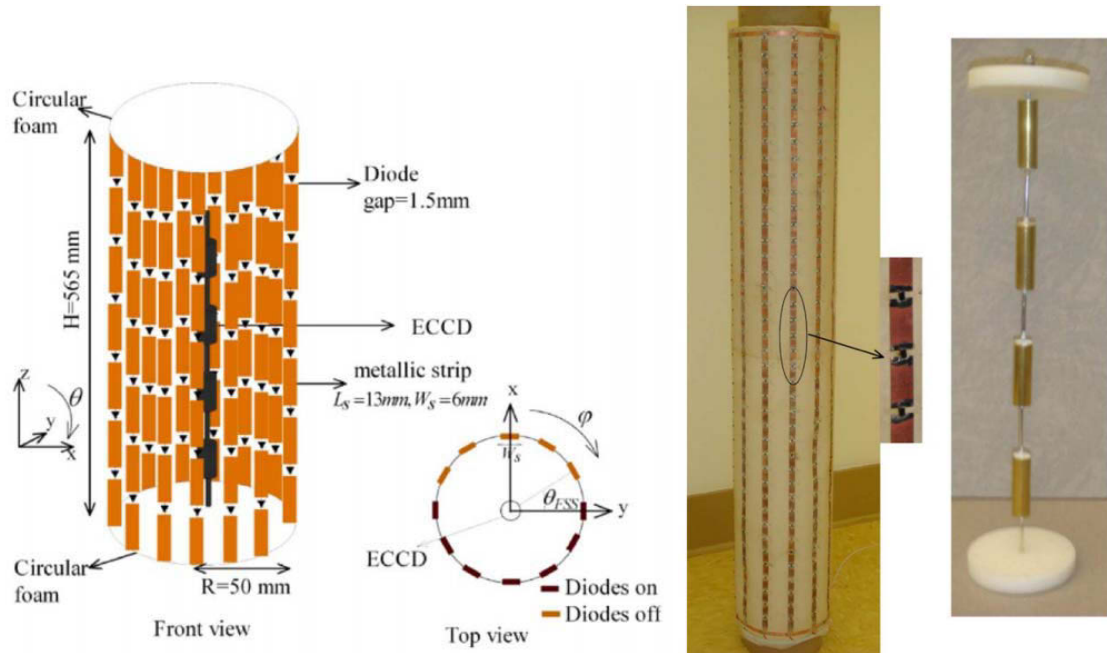


**Figure 8.12** Une antenne reconfigurable en diagramme de rayonnement basée sur la surface sélective de fréquence (FSS) [69].

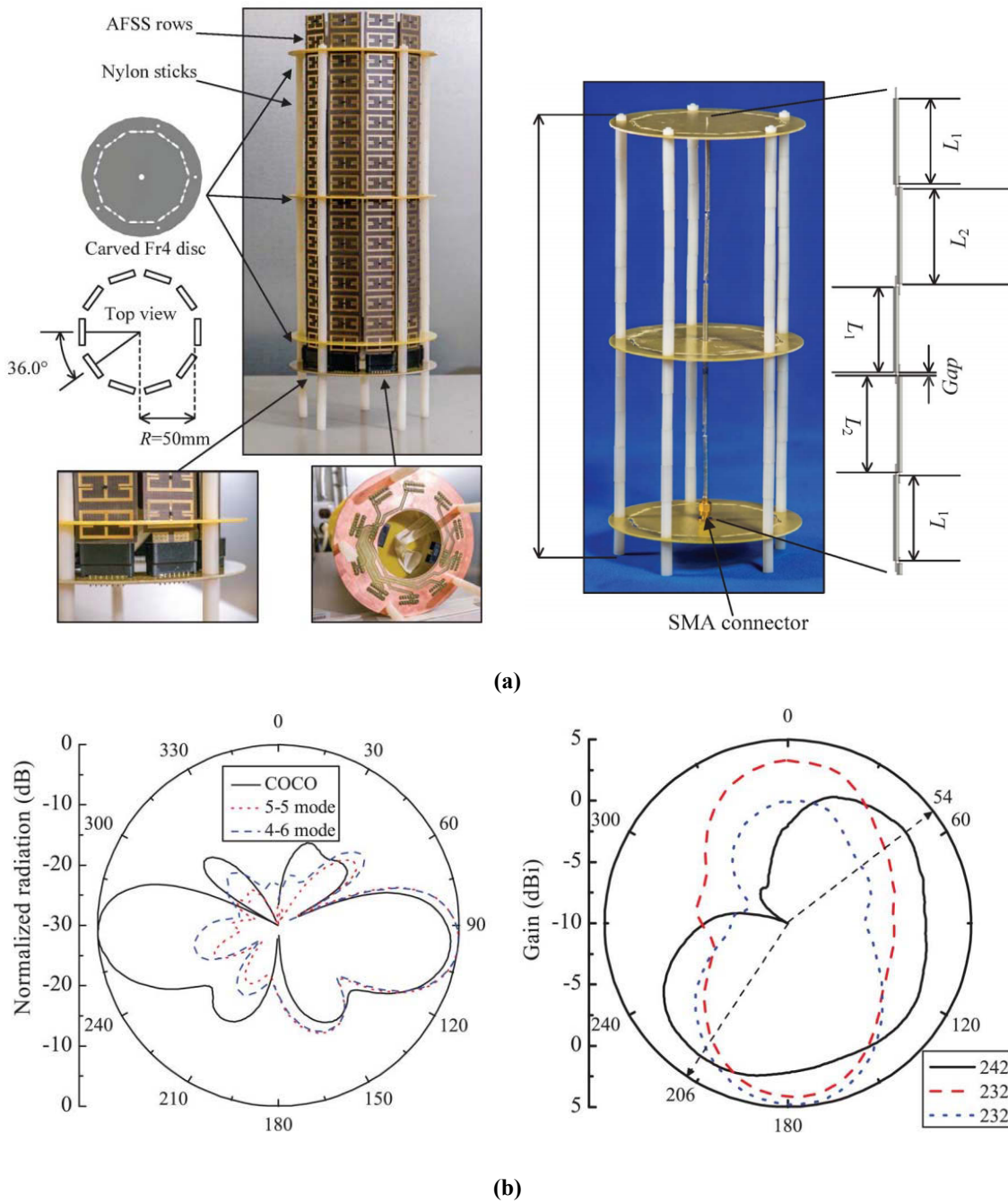


**Figure 8.13** Antennes orientables à diagramme de rayonnement basé sur l'AFSS [73], (a) Structure de l'antenne et installation. (b) Schémas de rayonnement des modes à faisceau unique et des modes à double faisceau.

**Tableau 8.1 Comparaison de différentes approches reconfigurables.**

Méthodes de conception	Avantages	Désavantages
<b>Mécanique</b>	Pilotage continu, faible perte d'insertion	Installation à basse vitesse et système complexe
<b>Pin-diode</b>	Vitesse rapide, faible coût	Plus de pertes d'insertion, l'isolement en réduisant la fréquence croissante, besoin de concevoir le circuit de polarisation en courant continu
<b>RF-MEMS</b>	Isolation élevée, faibles pertes d'insertion, faible consommation d'énergie	Vitesse lente, haute tension de polarisation, coût élevé
<b>Varactor</b>	Réglable en continu, faibles pertes d'insertion, faible consommation d'énergie	Nécessite une tension de polarisation stable
<b>Commutateurs photoconducteurs</b>	Ne nécessite pas de fils de polarisation CC supplémentaires	Coût élevé et intégration difficile
<b>Changer les propriétés du matériau</b>	Plus de liberté de conception	Tension de polarisation élevée, plus de pertes, polarisation croisée élevée
<b>Utiliser le métamatériaux</b>	Vitesse rapide, petite taille, plus de liberté de conception, faible consommation d'énergie	Nécessité de concevoir le circuit de polarisation en courant continu

En résumé, les approches de reconfiguration mentionnées ci-dessus ont été comparées dans Tab. 8-1. Sur la base des données répertoriées dans ce tableau, on peut conclure que la mise en œuvre de la structure de reconfiguration à base de métamatériaux propose de meilleures performances en termes de perte, de vitesse, de consommation d'énergie et de liberté de conception.

### 8.3 Surfaces Sélectives en Fréquence

Les surfaces sélectives en fréquence (FSS) sont des structures périodiques bidimensionnelles ou tridimensionnelles, qui se composent habituellement d'un réseau infini de rubans métalliques ou d'un réseau d'ouvertures dans une feuille métallique sur un substrat diélectrique. Les FSSs ont initialement été développés comme une sorte de filtre spatial en raison de leurs réponses aux ondes électromagnétiques (EM). Les FSSs peuvent transmettre presque toutes les ondes électromagnétiques sur une largeur de bande spécifique tout en réfléchissant presque toute l'énergie à travers une autre largeur de bande de fréquence. Selon les caractéristiques du filtre, les FSS peuvent être divisés en quatre types: passe-bas, passe-haut, coupe bande et passe bande. Les structures de base et leur réponse en fréquence sont représentées à la Fig. 8.14. La couleur orange de la figure montre le matériau métallique. À partir de la Fig. 8.14, la grille métallique fournit des caractéristiques de filtre passe-haut sur le champ électromagnétique et les patchs fournissent des caractéristiques de filtre passe-bas, tandis que le métal et l'ouverture FSS ont respectivement des caractéristiques de filtrage passe bande et coupe bande [76-78].

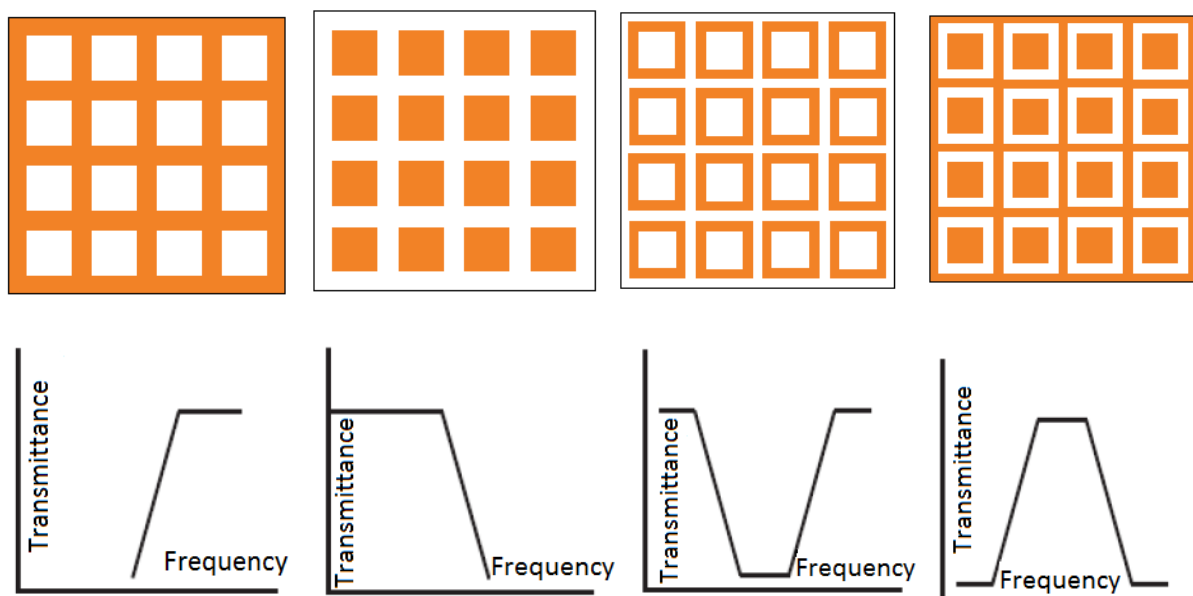


Figure 8.14 Les structures de base et leur réponse en fréquence.

Il existe de nombreuses formes différentes d'éléments FSS. Généralement, ces éléments peuvent être classés en quatre grandes catégories: les éléments centraux, les éléments en boucle, les éléments intérieurs solides et les éléments combinés, illustrés à la Fig. 8.15 [7]. Le premier

groupe est les éléments connectés au centre; certains éléments typiques du premier groupe sont l'élément droit, l'élément à trois pattes, l'élément d'ancrage, la croix de Jérusalem. Le deuxième groupe est constitué d'éléments en boucle, dont les éléments typiques comprennent les éléments chargés à trois ou quatre pattes, les boucles carrées et hexagonales. Le troisième groupe est constitué d'éléments intérieurs solides qui comprennent généralement un carré, un hexagone, un cercle et un triangle. Le quatrième groupe est constitué d'éléments de combinaison qui sont construits en combinant les trois autres membres du groupe. En adaptant ou en combinant d'autres éléments, les différents types d'éléments de combinaison sont conçus pour répondre aux exigences de l'application souhaitée.

#### 8.4 Applications des surfaces sélectives en fréquence

Le premier prototype de FSS en tant que surface à réflecteur partielle a été signalée en 1919 par Marconi et Franklin. Cependant, jusqu'au milieu des années 1960, les FSSs ont fait l'objet d'études approfondies théoriques et expérimentales et ont été largement utilisées dans de nombreux domaines [76].

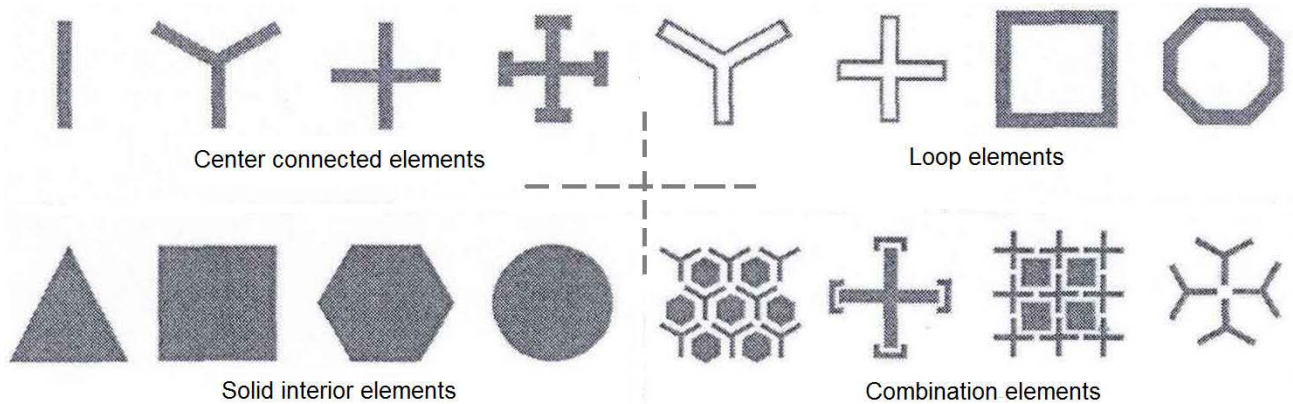
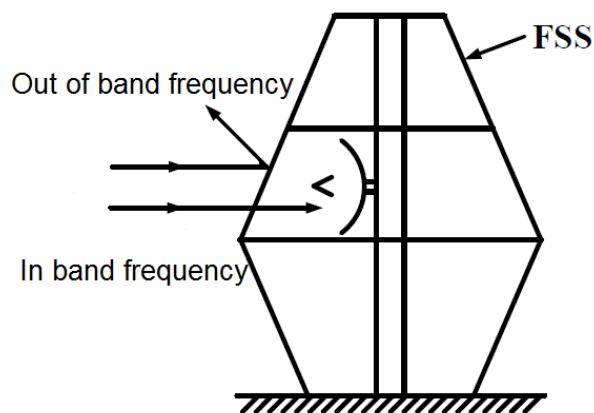


Figure 8.15 Les éléments typiques des FSSs.

Un exemple d'applications FSS est le blindage sur la porte d'un four à micro-ondes qui permet de voir la nourriture à l'intérieur tout en empêchant le rayonnement provenant des ondes électromagnétiques du four à micro-ondes, car le blindage est fait de FSS. Les FSSs reflètent l'énergie des micro-ondes et permettent à la lumière visible de passer à travers. En outre, il existe de nombreux applications des FSSs : civiles, les systèmes anticollision pour les véhicules

autonomes, les dispositifs de blindage électromagnétique dans les lieux publics tels que les hôpitaux et les aéroports, les systèmes de navigation robotiques, structures de bande interdite de cristaux photoniques, etc.

Une autre application importante est que les FSSs peuvent être utilisés pour des applications militaire, à titre d'exemple en cite les radômes ; ces derniers peuvent diminuer la section efficace radar (RCS) des antennes de communication et les cacher de l'ennemi. Les radomes fonctionnent en ne laissant passer que les fréquences opérationnelles et rejettent les autres fréquences qui se trouvent en dehors de cette bande [76], le diagramme schématique illustré à la Fig. 8.16.



**Figure 8.16** Schéma de principe du radôme.

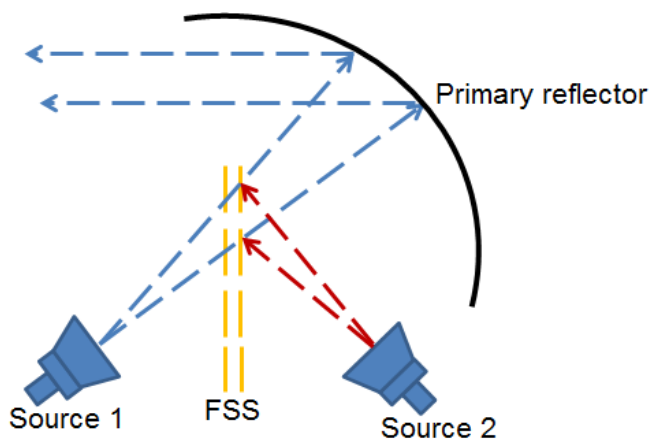


**Figure 8.17** Diagramme schématique du FSS en tant que sous-réflecteur dans les systèmes d'antennes.

Il existe une autre application très typique dans le domaine des antennes à hyperfréquences. Afin d'améliorer l'efficacité d'utilisation des antennes, les FSSs ont également été utilisés comme

sous-réflecteurs dans les systèmes d'antennes pour assurer un fonctionnement multifréquences [76]. Comme le montre la Fig. 8.17, les FSSs sont conçues comme des sous-réflecteurs placés entre deux sources de fréquence différentes dans un système d'antenne à réflecteur. La FSS est transparente pour l'alimentation 1 dans la première bande de fonctionnement, alors qu'elle fonctionne comme réflecteur secondaire dans la deuxième bande de fréquence de travail pour l'alimentation 2. Par conséquent, en utilisant un seul réflecteur principal à deux fréquences de fonctionnement différentes, non seulement la taille et le coût des systèmes d'antennes ont été réduits mais aussi l'efficacité des antennes a été améliorée [76].

## 8.5 Les objectifs de recherche

L'objectif principal de la recherche était de mettre au point une antenne reconfigurable compacte, petite et à faible coût, capable de configurer la direction du faisceau principal dans les plans d'azimut et d élévation sans affecter sa performance. Dans le processus de conception, le nombre d'éléments actifs a été maintenu au minimum afin de réduire le coût de l'antenne et d'améliorer également les performances de rayonnement, telles que l'amélioration du gain.

## 8.6 Organisation de la thèse

Cette thèse est divisée en 8 chapitres incluant le résumé et la référence. Le contenu des chapitres de la thèse sont énumérés ci-dessous.

Le chapitre 1 présente d'abord les travaux précédents et la motivation pour la recherche sur les antennes reconfigurables en diagramme de rayonnement. L'état de l'art sur les antennes reconfigurables en diagramme de rayonnement est également présenté. De plus, les approches de reconfiguration les plus couramment utilisées sont également décrites et comparées dans ce chapitre.

Suite au survol de la littérature, des études approfondies sur les surfaces sélectives en fréquence sont présentées au chapitre 2.

Le chapitre 3 décrit une antenne de balayage de faisceau bibande compacte constituée de deux surfaces sélectives en fréquence active cylindriques indépendantes (AFSS) et d'une antenne monopôle omnidirectionnelle à double bande. Les cellules unitaires des deux écrans AFSS

proposés sont conçues. Les caractéristiques de transmission et de réflexion de la cellule unitaire des deux AFSS sont également étudiées, respectivement, à leur propre fréquence de fonctionnement. Ensuite, le mécanisme d'exploitation de l'antenne à commutation bibande et les études paramétriques sont présentés et discutés dans cette partie. Enfin, les résultats de simulation et de mesure de la conception proposée sont indiqués, ce qui indique qu'elle peut effectivement effectuer un balayage de faisceau à 2.45 GHz et 5.2 GHz couvrant simultanément tous les angles d'azimut. La taille du système d'antenne proposé peut être considérablement réduite en utilisant cette méthode.

Le chapitre 4 présente une antenne à commutation de faisceaux avec un gain élevé et un contrôle flexible des faisceau basés sur une structure FSS. Cette antenne à gain élevé proposée est composée d'une antenne monopôle omnidirectionnelle en tant que source rayonnante entourée d'un écran FSS hexagonal et de six feuilles métalliques. La conception de la cellule FSS utilisée dans ce concept est présentée dans cette partie. Et les caractéristiques de transmission et de réflexion de la cellule unitaire du FSS sont également étudiées à 5.2 GHz. Ensuite, le mécanisme de fonctionnement de cette antenne à balayage de faisceau à gain élevé et des études paramétriques sont décrits et discutés. Enfin, les résultats de simulation et de mesure de la conception proposée sont représentés. En commutant les états des diodes pin dans l'écran FSS hexagone, l'antenne proposée non seulement balaye six directions avec un gain élevé dans le plan azimutal, mais aussi peut fonctionner de manière flexible à plusieurs modes de faisceaux, y compris le mode de deux faisceaux et trois faisceau avec une faible puissance à 5.2 GHz. De plus, les résultats montrent que le gain maximal de cette antenne proposée a augmenté de 7 dB lorsque les six feuilles métalliques ont été appliquées.

Le chapitre 5 décrit une antenne à inclinaison de faisceau avec un chargement en métamatériaux à indice de réfraction négatif (NRIM). L'antenne proposée est composée d'une antenne à résonateur diélectrique à double alimentation (DRA) et d'une matrice NRIM  $1 \times 4$  qui sont fixées au-dessus et au milieu du DRA. La cellule unité NRIM et l'antenne résonateur diélectrique à double alimentation sont conçues. Ensuite, la théorie des antennes à inclinaison de faisceau est analysée et les résultats expérimentaux sont présentés dans cette partie. À partir des résultats obtenus, en conclut que cette antenne peut orienter le faisceau principal de  $\pm 38^\circ$  dans le plan xoz sur la bande 5-5.5 GHz. Dans la bande de fréquences de fonctionnement, le coefficient de

réflexion est supérieur à -10 dB. De plus, les résultats mesurés sont en bon accord avec les résultats simulés.

Le chapitre 6 présente une antenne quasi-yagi reconfigurable à trois couches. Cette conception a permis d'obtenir des directions à faisceaux multiples dans les plans d'élévation et d'azimut à 5.2 GHz. Il y a quatre éléments de l'antenne quasi-Yagi et huit diodes pin que les commutateurs insérés dans la couche intermédiaire. Les couches supérieure et inférieure comprennent les éléments parasites qui sont insérés dans des diodes pin. En commandant les diodes pin dans la couche médiane, l'antenne peut réaliser une commutation de faisceau dans un plan azimutal dans quatre directions. De plus, l'inclinaison du faisceau dans le plan d'élévation est obtenue en activant les diodes pin dans les couches supérieure et inférieure pour reconfigurer les longueurs des éléments parasites. La performance est très avantageuse pour la communication sans fil moderne.

Le chapitre 7 présente un résumé de cet accomplissement du travail effectué dans le cadre de ma thèse. Les travaux futurs dans le domaine de recherche proposé sont inclus dans ce chapitre.

Un résumé de thèse en français est également présenté au chapitre 8.

## 8.7 Travaux futurs

Dans cette thèse, des travaux de recherche ont été menés sur des antennes reconfigurables en diagramme rayonnement à partir de surfaces sélectives de fréquences reconfigurables, de métamatériaux et d'antennes quasi-yagi. Cependant, pas entièrement couvert dans ce travail limité, il y a encore de nombreux problèmes à développer, qui peuvent être utilisés comme orientations de recherche futures, notamment en incluant les paragraphes suivants.

Premièrement, la largeur de bande de travail de l'antenne à balayage de faisceau peut encore être améliorée, ce qui est déterminé par la gamme de fréquences de l'antenne centrale et la bande passante d'exploitation de l'AFSS. La technologie d'antenne omnidirectionnelle à large bande est plus mature, ce qui signifie que la largeur de bande de travail de l'antenne à balayage de faisceau dépend principalement de la bande passante de l'AFSS. Par conséquent, comment améliorer davantage la plage de fréquence AFSS est une autre piste intéressante dans ce domaine.

Deuxièmement, dans cette thèse, les diagrammes de rayonnement des antennes peuvent balayer librement dans le plan azimutal. Par conséquent, un autre sujet de recherche intéressant est de proposer une méthode particulière pour balayer librement les diagrammes de rayonnement dans les plans d'élévation et d'azimut.

Troisièmement, en raison du temps limité, nous n'avons pas conçu le circuit de contrôle de tension dans cette thèse. L'application du circuit de commande de tension peut efficacement éviter l'erreur causée par la tension de commande manuelle, mais peut également rendre l'opération plus commode et améliorer l'efficacité du test d'antenne. Par conséquent, la conception d'une unité de contrôle de tension est un travail important dans les travaux futurs.



## **9 REFERENCES**

- [1] K. Chang. RF and microwave wireless systems, New York: Wiley, 2000.
- [2] J.R. Golio. RF and microwave handbook. New York: CRC Press, 2001.
- [3] D. Schaubetal, Frequency-Agile Polarization Diverse Microstrip Antennas and Frequency Scanned Arrays, US Patent 4, Jan.4, 1983, Vol. 2, pp.367-474.
- [4] Y. Yashchyshyn, Reconfigurable Antennas: the State of the Art. International Journal of Electronics and Telecommunications, 56(3), pp. 319-326.
- [5] Jennifer T. Bernhard, Reconfigurable Antennas, Morgan & Claypool Publishers, 2007.
- [6] C. Sulakshana and L. Anjaneyulu, "Reconfigurable antennas with frequency, polarization, and pattern diversities for multi-radio wireless applications," International Journal of Microwave and Wireless Technologies, vol. 9, no. 1, pp. 121–132, 2017.
- [7] Mahmoud Niroo-Jazi, Nimble Radiation-Pattern Antennas Using Agile Frequency Selective Surfaces, Thesis, 2012.
- [8] S. Yang, C. Zhang, H. K. Pan, A. E. Fathy and V. K. Nair, "Frequency-reconfigurable antennas for multiradio wireless platforms," IEEE Microwave Magazine, vol. 10, no. 1, pp. 66-83, Feb. 2009.
- [9] H. A. Majid, M. K. A. Rahim, M. R. Hamid and M. F. Ismail, "A Compact Frequency-Reconfigurable Narrowband Microstrip Slot Antenna," IEEE Antennas and Wireless Propagation Letters, vol. 11, pp. 616-619, 2012.
- [10] Tong Li, Huiqing Zhai, Xin Wang, Long Li, Changhong Liang, "Frequency-Reconfigurable Bow-Tie Antenna for Bluetooth WiMAX and WLAN Applications", Antennas and Wireless Propagation Letters IEEE, vol. 14, pp. 171-174, 2015, ISSN 1536-1225.
- [11] Yunfei Cao, S. W. Cheung, X. L. Sun, T. I. Yuk, "Frequency-reconfigurable monopole antenna with wide tuning range for cognitive radio", Microwave and Optical Technology Letters, vol. 56, pp. 145, 2014.

- [12] K. Boyon, P. Bo, S. Nikolaou, K. Young-Sik, et al., "A Novel Single-Feed Circular Microstrip Antenna With Reconfigurable Polarization Capability," IEEE Transn. On Ant. and Propag., Vol. 56 (No. 3), p. p. 630-638, 2008.
- [13] F. Ferrero, C. Luxey, R. Staraj, G. Jacquemod, et al., "A Novel Quad-Polarization Agile Patch Antenna," IEEE Transn. on Ant. and Propag., Vol. 57 (No. 5), p. p.1563-1567, 2009.
- [14] S. W. Cheung, C. F. Zhou, Q. L. Li and T. I. Yuk, "A simple polarization-reconfigurable antenna," 2016 10th European Conference on Antennas and Propagation (EuCAP), Davos, 2016, pp. 1-4.
- [15] S. Lim and H. Ling, "Design of Electrically Small, Pattern Reconfigurable Yagi Antenna," Elec. Lett., Vol. 43 (No. 24), p. p. 1326-1327, 2007.
- [16] W. Sung-Jung and M. Tzyh-Ghuang, "A Wideband Slotted Bow-Tie Antenna With Reconfigurable CPW-to-Slotline Transition for Pattern Diversity," IEEE Transn. On Ant. and Propag., Vol. 56 (No. 2), p. p. 327-334, 2008.
- [17] Symeon Nikolaou et al., "Pattern and frequency reconfigurable annular slot antenna using PIN diodes," IEEE Transactions on Antennas and Propagation, vol. 54, no. 2, pp. 439-448, Feb. 2006.
- [18] P. Y. Qin, Y. J. Guo, Y. Cai, E. Dutkiewicz and C. H. Liang, "A Reconfigurable Antenna With Frequency and Polarization Agility," IEEE Antennas and Wireless Propagation Letters, vol. 10, pp. 1373-1376, 2011.
- [19] FAKHARIAN, M. M., REZAEI, P., OROUJI, A. A. Polarization and radiation pattern reconfigurability of a planar monopole-fed loop antenna for GPS application. Radioengineering, vol. 25, no. 4, p. 680–686, 2016.
- [20] C. G. Christodoulou, Y. Tawk, S. A. Lane, and S. R. Erwin, Reconfigurable antennas for wireless and space applications. Proceedings of the IEEE, vol. 100, no. 7, 2012, pp. 2250-2261.
- [21] J. D. Boerman and J. T. Bernhard, "Performance Study of Pattern Reconfigurable Antennas in MIMO Communication Systems," IEEE Transactions on Antennas and Propagation, vol. 56, no. 1, pp. 231-236, Jan. 2008.

- [22] M. Jusoh, T. Sabapathy, M. F. Jamlos, M. R. Kamarudin, "Reconfigurable four-parasitic-elements patch antenna for high-gain beam switching application", IEEE Antennas Wireless Propag. Lett., vol. 13, pp. 79-82, 2014.
- [23] T. A. Denidni, G. Y. Delisle, "A nonlinear algorithm for output power maximization of an indoor adaptive phased array", IEEE Trans. Electromagn. Compat., vol. 37, no. 2, pp. 201-209, May 1995.
- [24] T. A. Denidni, D. McNeil, G. Y. Delisle, "Experimental investigations of a new adaptive dual-antenna array for handset applications", IEEE Trans. Veh. Technol., vol. 52, no. 6, pp. 1417-1423, Nov. 2003.
- [25] G. Washington, Hwan-Sik Yoon, M. Angelino and W. H. Theunissen, "Design, modeling, and optimization of mechanically reconfigurable aperture antennas," IEEE Transactions on Antennas and Propagation, vol. 50, no. 5, pp. 628-637, May 2002.
- [26] H. L. Zhu, S. W. Cheung and T. I. Yuk, "Mechanically pattern reconfigurable antenna using metasurface," IET Microwaves, Antennas & Propagation, vol. 9, no. 12, pp. 1331-1336, 9 17 2015.
- [27] J. R. Costa, E. B. Lima, and C. A. Fernandes, "Compact beam-steerable lens antenna for 60-GHz wireless communications," IEEE Trans. Antennas Propag., vol. 57, no. 10, pp. 2926–2933, Oct. 2009
- [28] T. Guo, W. Leng, A. Wang, J. Li and Q. Zhang, "A Novel Planar Parasitic Array Antenna With Frequency- and Pattern-Reconfigurable Characteristics," IEEE Antennas and Wireless Propagation Letters, vol. 13, pp. 1569-1572, 2014.
- [29] T. Aboufoul, C. Parini, X. Chen and A. Alomainy, "Pattern-Reconfigurable Planar Circular Ultra-Wideband Monopole Antenna," IEEE Transactions on Antennas and Propagation, vol. 61, no. 10, pp. 4973-4980, Oct. 2013.
- [30] P. K. Li, Z. H. Shao, Q. Wang and Y. J. Cheng, "Frequency- and Pattern-Reconfigurable Antenna for Multistandard Wireless Applications," IEEE Antennas and Wireless Propagation Letters, vol. 14, pp. 333-336, 2015.

- [31] M. S. Alam and A. M. Abbosh, "Beam-Steerable Planar Antenna Using Circular Disc and Four PIN-Controlled Tapered Stubs for WiMAX and WLAN Applications," IEEE Antennas and Wireless Propagation Letters, vol. 15, pp. 980-983, 2016.
- [32] L. Zhong, J. S. Hong and H. C. Zhou, "A Novel Pattern-Reconfigurable Cylindrical Dielectric Resonator Antenna With Enhanced Gain," IEEE Antennas and Wireless Propagation Letters, vol. 15, pp. 1253-1256, Dec. 2016.
- [33] W. S. Kang, J. A. Park, and Y. J. Yoon, Simple reconfigurable antenna with radiation pattern. Electronics Letters, vol. 44, no. 3, pp. 182-186, 2008.
- [34] P. Y. Qin, Y. J. Guo, A. R. Weily and C. H. Liang, "A Pattern Reconfigurable U-Slot Antenna and Its Applications in MIMO Systems," in IEEE Transactions on Antennas and Propagation, vol. 60, no. 2, pp. 516-528, Feb. 2012.
- [35] E. R. Brown, RF-MEMS switches for reconfigurable integrated circuits. IEEE Transactions on Microwave Theory and Techniques, vol. 46, no. 112, pp. 1868-1880, 1998.
- [36] G. H. Huff and J. T. Bernhard, "Integration of packaged RF MEMS switches with radiation pattern reconfigurable square spiral microstrip antennas," IEEE Transactions on Antennas and Propagation, vol. 54, no. 2, pp. 464-469, Feb. 2006.
- [37] Chang won Jung, Ming-jer Lee, G. P. Li and F. De Flaviis, "Reconfigurable scan-beam single-arm spiral antenna integrated with RF-MEMS switches," IEEE Transactions on Antennas and Propagation, vol. 54, no. 2, pp. 455-463, Feb. 2006.
- [38] B. A. Cetiner, H. Jafarkhani, J. Y. Qian, H. J. Yoo, A. Grau, and F. De Flaviis, Multifunctional reconfigurable MEMS integrated antennas for adaptive MIMO systems. IEEE Communications Magazine, vol. 42, no. 12, pp. 62-70, 2004.
- [39] L. Petit, L. Dussopt, and J. Laheurte, MEMS-switched parasitic-antenna array for radiation pattern diversity. IEEE Transactions on Antennas and Propagation, vol. 54, no. 9, pp. 2624-2631, 2006.
- [40] X. Yang, B. Wang, S. H. Yeung, Q. Xue, and F. M. Kim, Circularly polarized reconfigurable crossed-yagi patch antenna. IEEE Antennas and Propagation Magazine, vol. 53, no. 5, pp. 65-80, 2011.

- [41] A. Sundaram, M. Maddela, R. Ramadoss and L. M. Feldner, "MEMS-Based Electronically Steerable Antenna Array Fabricated Using PCB Technology," *Journal of Microelectromechanical Systems*, vol. 17, no. 2, pp. 356-362, April 2008.
- [42] Y. Bai, S. Xiao, C. Liu, X. Shuai, and B. Wang, Design of pattern reconfigurable antennas based on a two—element dipole array model. *IEEE Transactions on Antennas and Propagation*, vol.61, no. 9, pp. 4867-4871, 2013.
- [43] R. L. Li, V. F. Fusco, and R. Cahill, Pattern shaping using a reactively loaded wire loop antenna. *IEE Proceedings-Microwaves Antennas and Propagation*, vol. 148, no. 3, pp. 203-208, 2001.
- [44] H. Iizuka, P. S. Hall, S. Sugiura, and K. Sato, Varactor-loaded H-shaped antenna with radiation pattern control. *IEEE Transactions on Antennas and Propagation*, vol. 56, no. 9, pp.2833-2840, 2008.
- [45] S. Chen, A. Hirata, T. Ohira, and N. C. Karmakar, Fast beamforming of electronically steerable parasitic array radiator antennas: theory and experiment. *IEEE Transactions on Antennas and Propagation*, vol. 52, no. 7, 2004, pp. 1819-1832.
- [46] V. Sathi, N. Ehteshami, and J. Nourinia, Optically tuned frequency-reconfigurable microstrip antenna. *IEEE Antennas and Wireless Propagation Letters*, vol. 11, 2012, pp. 1018-1020.
- [47] C. J. Panagamuwa, A. Chauraya, and J. C. Vardaxoglou, Frequency and beam reconfigurable antenna using photoconductive switches,*IEEE Trans. Antennas Propag.*, vol. 54, no. 2, pp. 449–454, Feb. 2006.
- [48] Y. Tawk, J. Costantine, S. Hemmady, G. Balakrishnan, K. Avery, and C. G. Christodoulou, Demonstration of a cognitive radio front end using an optically pumped reconfigurable antenna system (OPRAS). *IEEE Transactions on Antennas and Propagation*, vol. 60, no. 22, 2012, pp.1075-1083.
- [49] Y. Tawk, A. R. Albrecht, S. Hemmady, G. Balakrishnan, and C. G. Christodoulou, Optically pumped frequency reconfigurable antenna design, *IEEE Antennas Wireless Propag. Lett.*, vol. 9, pp. 280–283, 2010.
- [50] P. G. Jin, L. D. Zhang, and L. R. Li, Optically controlled reconfigurable antenna for cognitive radio applications. *Electronics Letters*, vol. 47, no. 17, 2011, pp. 920-948.

- [51] G. Lovat, P. Burghignoli, and S. Celozzi, A tunable ferroelectric antenna for fixed-frequency scanning applications. IEEE Antennas and Wireless Propagation Letters, vol. 5, 2006, pp.353-356.
- [52] Y. Yashchyshyn, and J. W. Modelska, Rigorous analysis and investigations of the scan antennas on a ferroelectric substrate. IEEE Transactions on Microwave Theory and Techniques, vol. 53, no. 2, 2005, pp. 427-438.
- [53] M. F. Iskander, Z. Q. Yun, Z. J. Zhang, R. Jensen, and S. Redd, Design of a low-cost 2-D beam-steering antenna using ferroelectric material and the CTS technology. IEEE Transactions on Microwave Theory and Techniques, vol. 49, no. 5, 2001, pp. 1000-1003.
- [54] D. R. Smith, J. B. Pendry, M. C. K. Wiltshire, Metamaterials and Negative Refractive Index, Science, pp: 788-792, 06 Aug 2004.
- [55] Ari Sihvola, Metamaterials in electromagnetics, Metamaterials, Volume 1, Issue 1, Pages 2-11, 2007.
- [56] Christophe Caloz, Tatsuo Itoh, Electromagnetic Metamaterials: Transmission Line Theory and Microwave Applications, John Wiley & Sons, 2005.
- [57] G. Poilasne, P. Pouliquen, K. Mahdjoubi, L. Desclos and C. Terret, "Active metallic photonic band-gap materials (MPBG): experimental results on beam shaper," IEEE Transactions on Antennas and Propagation, vol. 48, no. 1, pp. 117-119, Jan 2000.
- [58] M. A. Habib, M. N. Jazi, A. Djaiz, M. Nedil and T. A. Denidni, "Switched-beam antenna based on EBG periodic structures," 2009 IEEE MTT-S International Microwave Symposium Digest, Boston, MA, 2009, pp. 813-816.
- [59] H. Boutayeb, T. A. Denidni, K. Mahdjoubi, A. C. Tarot, A. R. Sebak and L. Talbi, "Analysis and design of a cylindrical EBG-based directive antenna," IEEE Transactions on Antennas and Propagation, vol. 54, no. 1, pp. 211-219, Jan. 2006.
- [60] W. S. Zhao, X. C. Wang and J. Hu, "Frequency- and beam-reconfigurable THz Fabry-Perot antenna based on hybrid Cu-graphene HIS," 2015 IEEE MTT-S International Microwave Workshop Series on Advanced Materials and Processes for RF and THz Applications (IMWS-AMP), Suzhou, 2015, pp. 1-3.

- [61] M. Li, S. Xiao and B. Wang, "Compact, low-profile, HIS-based pattern-reconfigurable antenna for wide-angle scanning," The 8th European Conference on Antennas and Propagation (EuCAP 2014), The Hague, 2014, pp. 1541-1544.
- [62] M. Li, S. Q. Xiao, Z. Wang and B. Z. Wang, "Compact Surface-Wave Assisted Beam-Steerable Antenna Based on HIS," IEEE Transactions on Antennas and Propagation, vol. 62, no. 7, pp. 3511-3519, July 2014.
- [63] P. Deo, A. Mehta, D. Mirshekar-Syahkal and H. Nakano, "An HIS-Based Spiral Antenna for Pattern Reconfigurable Applications," IEEE Antennas and Wireless Propagation Letters, vol. 8, pp. 196-199, 2009.
- [64] C. Gu et al., "Frequency-Agile Beam-Switchable Antenna," IEEE Transactions on Antennas and Propagation, vol. 65, no. 8, pp. 3819-3826, Aug. 2017.
- [65] C. Gu et al., "3-D Coverage Beam-Scanning Antenna Using Feed Array and Active Frequency-Selective Surface," IEEE Transactions on Antennas and Propagation, vol. 65, no. 11, pp. 5862-5870, Nov. 2017.
- [66] C. Gu et al., "Dual-Band Electronically Beam-Switched Antenna Using Slot Active Frequency Selective Surface," IEEE Transactions on Antennas and Propagation, vol. 65, no. 3, pp. 1393-1398, March 2017.
- [67] A. Edalati and T. A. Denidni, "Frequency Selective Surfaces for Beam-Switching Applications," IEEE Transactions on Antennas and Propagation, vol. 61, no. 1, pp. 195-200, Jan. 2013.
- [68] M. Niroo-Jazi and T. A. Denidni, "Electronically Sweeping-Beam Antenna Using a New Cylindrical Frequency-Selective Surface," IEEE Transactions on Antennas and Propagation, vol. 61, no. 2, pp. 666-676, Feb. 2013.
- [69] A. Edalati and T. A. Denidni, "High-Gain Reconfigurable Sectoral Antenna Using an Active Cylindrical FSS Structure," IEEE Transactions on Antennas and Propagation, vol. 59, no. 7, pp. 2464-2472, July 2011.
- [70] B. Liang, B. Sanz-Izquierdo, E. A. Parker and J. C. Batchelor, "Cylindrical Slot FSS Configuration for Beam-Switching Applications," IEEE Transactions on Antennas and Propagation, vol. 63, no. 1, pp. 166-173, Jan. 2015.

- [71] M. N. Jazi and T. A. Denidni, "Frequency Selective Surfaces and Their Applications for Nimble-Radiation Pattern Antennas," *IEEE Transactions on Antennas and Propagation*, vol. 58, no. 7, pp. 2227-2237, July 2010.
- [72] H. Boutayeb, P. R. Watson, W. Lu and T. Wu, "Beam Switching Dual Polarized Antenna Array With Reconfigurable Radial Waveguide Power Dividers," *IEEE Transactions on Antennas and Propagation*, vol. 65, no. 4, pp. 1807-1814, April 2017.
- [73] L. Zhang, Q. Wu and T. A. Denidni, "Electronically Radiation Pattern Steerable Antennas Using Active Frequency Selective Surfaces," *IEEE Transactions on Antennas and Propagation*, vol. 61, no. 12, pp. 6000-6007, Dec. 2013.
- [74] I. Y. Tarn and S. J. Chung, "A Novel Pattern Diversity Reflector Antenna Using Reconfigurable Frequency Selective Reflectors," *IEEE Transactions on Antennas and Propagation*, vol. 57, no. 10, pp. 3035-3042, Oct. 2009.
- [75] C. H. Ko, I. Y. Tarn and S. J. Chung, "A Compact Dual-Band Pattern Diversity Antenna by Dual-Band Reconfigurable Frequency-Selective Reflectors With a Minimum Number of Switches," *IEEE Transactions on Antennas and Propagation*, vol. 61, no. 2, pp. 646-654, Feb. 2013.
- [76] B. A. Munk, *Frequency Selective Surfaces: Theory and Design*. New York, NY, USA: Wiley, 2000.
- [77] B. A. Munk, *Finite Antenna Arrays and FSS*, John Wiley & Sons, 2003.
- [78] T. K. Wu, *Frequency Selective Surface and Grid Array*, John Wiley & Sons, 1995.
- [79] A. Giere et al., "Tunable dielectrics for microwave applications," 2008 17th IEEE International Symposium on the Applications of Ferroelectrics, Santa Fe, NM, USA, 2008, pp. 1-2.
- [80] B. Schoenlinner, A. Abbaspour-Tamijani, L. C. Kempel and G. M. Rebeiz, "Switchable low-loss RF MEMS Ka-band frequency-selective surface," *IEEE Transactions on Microwave Theory and Techniques*, vol. 52, no. 11, pp. 2474-2481, Nov. 2004.
- [81] G. M. Coutts, R. R. Mansour and S. K. Chaudhuri, "Microelectromechanical Systems Tunable Frequency-Selective Surfaces and Electromagnetic-Bandgap Structures on Rigid-Flex

Substrates," IEEE Transactions on Microwave Theory and Techniques, vol. 56, no. 7, pp. 1737-1746, July 2008.

- [82] G. I. Kiani, K. L. Ford, L. G. Olsson, K. P. Esselle and C. J. Panagamuwa, "Switchable Frequency Selective Surface for Reconfigurable Electromagnetic Architecture of Buildings," IEEE Transactions on Antennas and Propagation, vol. 58, no. 2, pp. 581-584, Feb. 2010.
- [83] G. I. Kiani, K. P. Esselle, A. R. Weily and K. L. Ford, "Active frequency selective surface using PIN diodes," 2007 IEEE Antennas and Propagation Society International Symposium, Honolulu, HI, 2007, pp. 4525-4528.
- [84] M. Niroo-Jazi and T. A. Denidni, "Reconfigurable dual-band frequency selective surfaces using a new hybrid element," 2011 IEEE International Symposium on Antennas and Propagation (APSURSI), Spokane, WA, 2011, pp. 2673-2676.
- [85] C. Mias, "Varactor tunable frequency selective absorber," Electronics Letters, vol. 39, no. 14, pp. 1060-1062, 10 July 2003.
- [86] C. Mias, "Varactor-tunable frequency selective surface with resistive-lumped-element biasing grids," IEEE Microwave and Wireless Components Letters, vol. 15, no. 9, pp. 570-572, Sept. 2005.
- [87] C. Mias and J. H. Yap, "A Varactor-Tunable High Impedance Surface With a Resistive-Lumped-Element Biasing Grid," IEEE Transactions on Antennas and Propagation, vol. 55, no. 7, pp. 1955-1962, July 2007.
- [88] E. A. Parker and S. M. A. Hamdy, "Rings as elements for frequency selective surfaces," Electronics Letters, vol. 17, no. 17, pp. 612-614, August 20 1981.
- [89] E. A. Parker, S. M. A. Hamdy and R. J. Langley, "Arrays of concentric rings as frequency selective surfaces," in Electronics Letters, vol. 17, no. 23, pp. 880-881, November 12 1981.
- [90] S. M. A. Hamdy and E. A. Parker, "Comparison of modal analysis and equivalent circuit representation of E-plane arm of the jerusalem cross," Electronics Letters, vol. 18, no. 2, pp. 94-95, January 21 1982.
- [91] S. B. Savia and E. A. Parker, "Equivalent circuit model for superdense linear dipole FSS," IEE Proceedings - Microwaves, Antennas and Propagation, vol. 150, no. 1, pp. 37-42, Feb. 2003.

- [92] A. D. Chuprin, E. A. Parker and J. C. Batchelor, "Resonant frequencies of open and closed loop frequency selective surface arrays," *Electronics Letters*, vol. 36, no. 19, pp. 1601-1603, 14 Sep 2000.
- [93] Chich-Hsing Tsao and R. Mittra, "A spectral-iteration approach for analyzing scattering from frequency selective surfaces," *IEEE Transactions on Antennas and Propagation*, vol. 30, no. 2, pp. 303-308, Mar 1982.
- [94] J. F. Ma, R. Mittra and N. T. Huang, "Analysis of multiple FSS screens of unequal periodicity using an efficient cascading technique," *IEEE Transactions on Antennas and Propagation*, vol. 53, no. 4, pp. 1401-1414, April 2005.
- [95] E. A. Parker, A. D. Chuprin and R. J. Langley, "Finite element analysis of electromagnetic wave diffraction from buildings incorporating frequency selective walls," *IEE Proceedings - Microwaves, Antennas and Propagation*, vol. 146, no. 5, pp. 319-323, Oct 1999.
- [96] M. Lambea, M. A. Gonzalez, J. A. Encinar and J. Zapata, "Analysis of frequency selective surfaces with arbitrarily shaped apertures by finite element method and generalized scattering matrix," *IEEE Antennas and Propagation Society International Symposium. 1995 Digest*, Newport Beach, CA, USA, 1995, pp. 1644-1647 vol.3.
- [97] I. Bardi, R. Remski, D. Perry and Z. Cendes, "Plane wave scattering from frequency-selective surfaces by the finite-element method," *IEEE Transactions on Magnetics*, vol. 38, no. 2, pp. 641-644, Mar 2002.
- [98] E.P. Kosmidou, T.I. Kosmanis, T.D. Tsiboukis, "A comparative FDTD study of various PML configurations for the termination of nonlinear photonic bandgap waveguide structures", *Magnetics IEEE Transactions on*, vol. 39, pp. 1191-1194, 2003, ISSN 0018-9464.
- [99] V. S. Rao, V. V. Srinivasan, and S. Pal, "Generation of dual beams from spherical phased array antenna," *Electron. Lett.*, vol. 45, no. 9, pp. 441–442, Apr. 2009.
- [100] R. Harrington, "Reactively controlled directive arrays," *IEEE Trans. Antennas Propag.*, vol. 26, no. 3, pp. 390-395, May 1978.
- [101] Y. Y. Bai, S. Xiao, M. C. Tang, Z. F. Ding and B. Z. Wang, "Wide-Angle Scanning Phased Array With Pattern Reconfigurable Elements," *IEEE Transactions on Antennas and Propagation*, vol. 59, no. 11, pp. 4071-4076, Nov. 2011.

- [102] S. V. S. Nair and M. J. Ammann, “Reconfigurable antenna with elevation and azimuth beam switching”, IEEE Antennas Wireless Propag. Lett., vol. 9, pp. 367-370, Apr. 2010.
- [103] S.-J. Shi and W.-P. Ding, “Radiation pattern reconfigurable microstrip antenna for WIMAX applications”, Electron. Lett., vol. 51, no. 9, pp. 662-664, Apr. 2015.
- [104] A. Rathore, R. Nilavalan, H.F. AbuTarboush, and T. Peter, “Compact dual-band (2.4/5.2GHz) monopole antenna for WLAN applications,” Proceedings of the IWAT 2010, pp. 1–4, Mar. 2010.
- [105] Microsemi, GMP4201-GML4701 surface mount PIN &Limiter Diodes. 2009-01-22. [Online]. Available:[http://www.microsemi.com/index.php?option=com\\_docman&task=doc\\_download&gid=8724](http://www.microsemi.com/index.php?option=com_docman&task=doc_download&gid=8724)
- [106] A. Alexiou and M. Haardt, “Smart antenna technologies for future wireless systems: Trends and challenges,” IEEE Commun. Mag., vol. 42, no. 9, pp. 90–97, Sep. 2004.
- [107] K.-H. Li, M. A. Ingram, and E. O. Rausch, “Multibeam antennas for indoor wireless communications,” IEEE Trans. Commun., vol. 50, no. 2, pp. 192–194, Feb. 2002.
- [108] A. Dadgarpour, M. S. Sorkherizi, T. A. Denidni and A. A. Kishk, “Passive Beam Switching and Dual-Beam Radiation Slot Antenna Loaded With ENZ Medium and Excited Through Ridge Gap Waveguide at Millimeter-Waves,” IEEE Trans. Antennas Propag., vol. 65, no. 1, pp. 92-102, Jan. 2017.
- [109] M. Chryssomallis, “Smart antennas,” IEEE Antennas Propag. Mag., vol. 42, pp. 129–136, 2000.
- [110] D. Pujara, A. Modi, N. Pisharody and J. Mehta, “Predicting the Performance of Pyramidal and Corrugated Horn Antennas Using ANFIS,” IEEE Antennas Wireless Propag. Lett., vol. 13, pp. 293-296, 2014.
- [111] A. Y. Modi, C. A. Balanis, C. R. Birtcher and H. N. Shaman, “Novel Design of Ultrabroadband Radar Cross Section Reduction Surfaces Using Artificial Magnetic Conductors,” IEEE Trans. Antennas Propag., vol. 65, no. 10, pp. 5406-5417, Oct. 2017.
- [112] A. Y. Modi, C. A. Balanis and C. Birtcher, “Novel technique for enhancing RCS reduction bandwidth of checkerboard surfaces,” 2017 IEEE International Symposium on Antennas and

Propagation & USNC/URSI National Radio Science Meeting, San Diego, CA, 2017, pp. 1911-1912.

- [113] A. Y. Modi, C. A. Balanis and C. Birtcher, "AMC cells for broadband RCS reduction checkerboard surfaces," 2017 IEEE International Symposium on Antennas and Propagation & USNC/URSI National Radio Science Meeting, San Diego, CA, 2017, pp. 1915-1916.
- [114] M. J. Al-Hasan, T. A. Denidni and A. R. Sebak, "Millimeter-Wave Compact EBG Structure for Mutual Coupling Reduction Applications," IEEE Trans. Antennas Propag., vol. 63, no. 2, pp. 823-828, Feb. 2015.
- [115] H. Farahani, M. Veysi, M. Kamyab, A. Tadjalli, "Mutual coupling reduction in patch antenna arrays using a UC-EBG superstrate", IEEE Antennas Wireless Propag. Lett., vol. 9, pp. 57-59, Jan. 2010.
- [116] M. J. Al-Hasan, T. A. Denidni and A. R. Sebak, "Millimeter-Wave EBG-Based Aperture-Coupled Dielectric Resonator Antenna," IEEE Trans. Antennas Propag., vol. 61, no. 8, pp. 4354-4357, Aug. 2013.
- [117] R. Mittra, C. H. Chan, and T. Cwik, "Techniques for analyzing frequency selective surfaces-a review," Proc. IEEE, vol. 76, no. 12, pp. 1593–1615, Dec. 1988.
- [118] H. X. Xu, G. M. Wang, Z. Tao and T. J. Cui, "High-directivity emissions with flexible beam numbers and beam directions using gradient-refractive-index fractal metamaterial", Sci. Rep., vol. 4, pp.5744, 2014.
- [119] A. Dadgarpour, B. Zarghooni, B. S. Virdee and T. A. Denidni, "Enhancement of tilted-beam in elevation plane for planar end-fire antennas using artificial dielectric medium", IEEE Trans. Antennas Propag., vol. 63, no. 10, pp. 4540-4545, Oct. 2015.
- [120] J. Ren, X. Yang, J.-Y. Yin and Y.-Z. Yin, "A novel antenna with reconfigurable patterns using H-shaped structures", IEEE Antennas Wireless Propag. Lett., vol. 14, pp. 915-918, Jan. 2015.
- [121] A. Dadgarpour, B. Zarghooni, B. S. Virdee and T. A. Denidni, "Beam tilting antenna using integrated metamaterial loading", IEEE Trans. Antennas Propag., vol. 62, no. 5, pp. 2874-2879, May 2014.

- [122] A. Dadgarpour, B. Zarghooni, B. S. Virdee and T. A. Denidni, “Beam deflection using gradient refractive index media for 60 GHz end-fire antenna”, IEEE Trans. Antennas Propag., vol. 63, no. 8, pp. 3768-3774, Aug. 2015.
- [123] J. P. Turpin, Q. Wu, D. H. Werner, B. Martin, M. Bray and E. Lier, “Low Cost and Broadband Dual-Polarization Metamaterial Lens for Directivity Enhancement,” IEEE Trans. Antennas Propag., vol. 60, no. 12, pp. 5717-5726, Dec. 2012.
- [124] S. Kosulnikov, D. Filonov, S. Glybovski, P. Belov, S. Tretyakov and C. Simovski, “Wire-Medium Hyperlens for Enhancing Radiation From Subwavelength Dipole Sources,” IEEE Trans. Antennas Propag., vol. 63, no. 11, pp. 4848-4856, Nov. 2015.
- [125] S. Ahdi Rezaeieh, M. A. Antoniades and A. M. Abbosh, “Bandwidth and Directivity Enhancement of Loop Antenna by Nonperiodic Distribution of Mu-Negative Metamaterial Unit Cells,” IEEE Trans. Antennas Propag., vol. 64, no. 8, pp. 3319-3329, Aug. 2016.
- [126] B. Zhou and T. J. Cui, “Directivity enhancement to Vivaldi antennas using compactly anisotropic zero-index metamaterials,” IEEE Antennas Wireless Propag. Lett., vol. 10, pp. 326-329, Apr. 2011.
- [127] L. Chen, Z.-Y. Lei and X.-W. Shi, “Meander-line based broadband artificial material for enhancing the gain of printed end fire antenna,” Progress In Electromagnetics Research,, vol. 151, pp. 55-63, 2015.
- [128] X. Chen, H.-F. Ma, X.-Y. Zou, W.-X. Jiang, T.-J. Cui, “Three-dimensional broadband and high-directivity lens antenna made of metamaterials”, J. Appl. Phys., vol. 110, no. 4, pp. 044904-044904-8, 2011.
- [129] M. Sun, Z. N. Chen, and X. Qing, “Gain enhancement of 60-GHz antipodal tapered slot antenna using zero-index metamaterial,” IEEE Trans. Antennas Propag., vol. 61, no. 4, pp. 1741-1746, Jun. 2013.
- [130] R. W. Ziolkowski, “Design, fabrication, and testing of double negative metamaterials,” IEEE Trans. Antennas Propag., vol. 51, no. 7, pp. 1516-1529, July 2003.
- [131] S. J. Shi and W. P. Ding, ‘Radiation pattern reconfigurable microstrip antenna for WiMAX application’, Electron. Lett., 2015, 51, (9), pp. 662-664

- [132] S. K. Raj Joseph, J. Fahlbusch and J. Schoebel, ‘A beam switching three layer reconfigurable antenna’, 2012 The 7th German Microwave Conference, Ilmenau, 2012, pp. 1-4.
- [133] J. Huang, ‘Planar microstrip yagi array antenna’, Antennas and Propagation Society International Symposium, 1989. AP-S. Digest, 1989, 2, pp. 894–897